2017

Specification of Stem Cells and Niche During Hair Follicle Morphogenesis

Tamara Ouspenskaia
The Rockefeller University

SPECIFICATION OF STEM CELLS AND NICHE DURING HAIR FOLLICLE MORPHOGENESIS

A Thesis Presented to the Faculty of

The Rockefeller University

in Partial Fulfillment of the Requirements for

the degree of Doctor of Philosophy

by

Tamara Ouspenskaia

June 2017

SPECIFICATION OF STEM CELLS AND NICHE DURING HAIR FOLLICLE MORPHOGENESIS

Tamara Ouspenskaia, Ph. D.

The Rockefeller University 2017

Adult stem cell (SC) behavior is tightly coordinated by the signals received from the “niche” - the microenvironment that the SCs reside in. Little is known about the role of the niche in SC specification during organ morphogenesis. In particular, the question of whether the niche exists prior to SC specification or whether it is recruited after SC establishment in a developing tissue remains largely unanswered. In addition, the signals responsible for the specification and regulation of SCs during morphogenesis remain unexplored.

To answer these questions, I focused my analysis on the earliest stages of hair follicle (HF) morphogenesis. Using immunofluorescence and live imaging, I found that in developing HFs, basal cell divisions are asymmetric and perpendicular to the basement membrane. These divisions result in differential levels of WNT signaling in the daughter cells, with basal cells remaining WNT^{high}, and suprabasal cells becoming WNT^{low}. Using *in utero* lentiviral transduction and genetic mouse models, I created mosaic epidermis with gain- or loss-of-function for WNT signaling to demonstrate that juxtaposition of WNT^{low} and WNT^{high} cells is sufficient to confer SOX9+ cell fate to the WNT^{low} cells. This suggested that the

perpendicular asymmetric divisions that I observed in the developing HFs produce the WNT gradient, necessary for the establishment of SOX9+ cells.

To further investigate the mechanism behind SOX9+ cell specification, I investigated the signaling patterns of SHH, previously suggested to regulate Sox9 expression. Interestingly, while Shh was expressed exclusively by the WNT^{high} basal cells, SHH signaling was primarily detected in the suprabasal SOX9+ cells. By inducing the expression of lentivirus-delivered Shh at different stages in morphogenesis, I found that the levels of WNT signaling dictate the responsiveness to SHH. When WNT signaling is low or moderate, cells respond to SHH, resulting in the inhibition of WNT signaling. However, WNT^{high} cells are resistant to SHH signaling. Thus, in the suprabasal SOX9+ daughters, SHH acts to repress WNT signaling, further boosting the levels of SOX9, while due to high levels of WNT signaling in the basal daughters, they are unable to respond to SHH and remain SOX9-negative.

Finally, using Shh-CreER lineage-tracing, I demonstrated that the earliest asymmetric cell divisions of the WNT^{high}, Shh+ cells produce SOX9+ cells that eventually contribute to the adult stem cell pool. Interestingly, SOX9+ cells are produced only during the early asymmetric cell divisions, while the same Shh+ cells later give rise to various differentiated lineages of the developing HF.

Thus, in developing HFs, asymmetric cell divisions produce a WNT^{low} SOX9+ SC daughter and a WNT^{high} “niche” cell daughter that produces SHH, necessary to suppress WNT signaling and expand the SOX9+ SCs.

ACKNOWLEDGMENTS

First of all, I would like to thank my mentor and graduate advisor, Elaine Fuchs. My gratitude goes back to my first year in the graduate program, when Elaine allowed me to join her lab for my thesis research. Despite my initial interest in pursuing a cancer-related project, seeing my fascination with developmental biology, Elaine allowed me to instead focus on the mechanisms regulating hair follicle morphogenesis. I really appreciated the freedom Elaine has given me to explore various research directions during my time in her lab, while gently nudging me forward. Finally, I would like to thank Elaine for everything she has taught me about crafting a manuscript, linking my findings together, and putting them in a broad perspective.

I am also grateful to many Fuchs lab members whom I have had a pleasure to interact with during my graduate studies. I would like to thank Slobodan Beronja, my rotation mentor, who shared his vast knowledge, skills, passion and enthusiasm for science with me. I would like to thank Irina Matos, who has seen me progress through my graduate studies, encouraged me along the way, and helped me in crystallizing my ideas, understanding my results, and finally preparing the manuscript. A huge thank you also goes to Aaron Mertz for his live imaging, analysis, and late nights working on the manuscript, as well as for being such a strong supporter of women in science – I will never forget the time he ran after a seminar organizer, defending me. I also thank Vincent Fiore

for contributing his integrin signaling expertise to my project, and for various interesting discussions that we have had.

I would also like to thank the graduate students in the lab with whom I have overlapped that have encouraged me, celebrated with me, and comforted me – Kenneth Lay, Evan Heller, Amma Asare, Chiung-Ying Chang, Cynthia Alexander and Rene Adam.

In addition, I am grateful to all the staff in the lab, who make it run smoothly and help out so much. First of all, Ellen Wong, my bay mate, who helped me finish experiments, procure reagents and chocolate, and who has supported me all these years. I am also grateful to Maria Nikolova, for managing the lab, placing orders, taking care of repairs, and maintaining my Russian. I would like to thank June Racelis for teaching me how to perform *in situ* hybridizations, and Sophia Chai for her help with lentivirus preparation. I also want to thank Lisa Polak, John Levorse, Megan Sribour, Sacha Hacker, Nicole Stokes, Dan Oristian, and Angelie Aldeguer for taking care of the mouse colony, setting up matings, injecting lentivirus, treating with tamoxifen, getting genotyping samples ready, performing surgeries, and all other aspects of my research involving mice.

I would like to acknowledge the graduate program and the Dean's office for supporting my research and studies, providing housing, on-campus childcare, and student budget. I would like to thank the research facilities at the Rockefeller University, in particular, the Flow Cytometry Research Center and the Bio-

imaging Resource Center for their support. I am also grateful to my faculty advisory committee – Jennifer Zallen, Hironori Funabiki and Marc Tessier-Lavigne – for their useful suggestions and recommendations pertaining both to my research and my career.

Finally and most importantly, I would like to thank my parents who have always believed in me; and my husband Sol, and my children Valerie and Max for their support, understanding and patience.

TABLE OF CONTENTS

LIST OF FIGURES

CHAPTER 1: INTRODUCTION

Adult tissues are maintained and repaired by resident stem cells (SCs), which are capable of long-lived self-renewal and differentiation into one or more cell types. Depending on the state and the function of the organ, SCs can remain quiescent for prolonged periods of time, or undergo activation and expansion to replenish the SC pool or to produce transit-amplifying cells, which will undergo additional rounds of division to give rise to differentiated cells – the functional units of a given organ.

SC behavior depends on the signals received from their "niche", which is defined as the local tissue microenvironment that maintains and regulates SC function (Morrison and Spradling, 2008; Schofield, 1978). The niche is typically composed of heterologous cell types, but can also include transit-amplifying cells (TACs) as well as differentiated cells that have descended from the SCs (Hsu et al., 2014b; Hsu et al., 2011). Additionally, SCs can also signal back to their progeny to regulate their fate and function (Pardo-Saganta et al., 2015). The signaling crosstalk between the niche and the SCs in various adult tissues has been the focus of intensive research.

The developmental origins of SCs are less well understood. Organ morphogenesis generally involves rapid, but well-orchestrated, cell proliferation to produce enough building blocks that will fulfill the function of a given organ. At the same time, at some point during this process, a distinct pool of cells – the stem cells - needs to be set apart that will maintain the organ throughout the life

time of the organism. The mechanisms regulating tissue resident SC specification during organ morphogenesis remain largely obscure. In addition, given the dependence of SCs on their niche for maintenance and regulation in adulthood, the importance of the niche for SC specification is a fascinating question. Is the niche set up first to be subsequently populated by SCs or are the SCs specified first and then recruit specific cell types from their microenvironment to form the niche for their maintenance and regulation?

Epidermis and the hair follicles (HFs) provide an excellent model to study the behavior and regulation of SCs. While the mechanisms involved in the regulation of SC quiescence and activation, as well as SC fate, are becoming increasingly well understood, the origins of HFSCs remain largely unknown.

In this chapter, I will provide a brief overview of our current understanding of the role of the niche in SC regulation in adult tissues, with a particular focus on the HF. I will then discuss what is known about the mechanisms of SC specification during morphogenesis of various tissues. Finally, I will describe the signaling pathways and known regulators that have been implicated in the induction and coordination of HF morphogenesis and SC specification.

Stem cell identity

SCs are defined by their capacity for long-term self-renewal and ability to give rise to one or multiple types of differentiated cells within a given tissue. Thus, every SC division has the potential to be symmetric – giving rise to two

SCs or two differentiating cells, or asymmetric – giving rise a to SC and a differentiating cell. The choice between a symmetric and an asymmetric cell division can be governed by both cell intrinsic and cell extrinsic factors. Cell intrinsic mechanisms involve asymmetric partitioning of cellular components to one daughter cell, but not the other, thus affecting their fates differentially. Alternatively, daughter cells can be positioned in different extracellular environments following the division, such that the environment will determine the fate of each daughter cell (Knoblich, 2008). Defects in self-renewal mechanisms can cause developmental defects or contribute to cancer initiation and progression.

SC identity and function depend on the expression of a core set of genes, which vary depending on the tissue. Their expression is regulated by epigenetic marks on the chromatin, which in turn depend on the signals received from the microenvironment. SC identity can be conferred to a non-SC by turning on the expression of these "core signature genes" – often transcription factors (TFs). One example is the generation of induced pluripotent stem cells (iPSCs), where forced expression of four pioneer transcription factors (Sox2, Klf4, Oct3/4, and c-Myc) is sufficient to convert a differentiated fibroblast into an iPSC (Takahashi and Yamanaka, 2006).

This cell fate reprogramming depends on the ability of the pioneer factors to bind to "closed" chromatin (as defined by lack of DNAse I hypersensitivity and

epigenetic marks) and to turn on the expression of other genes important for SC identity (Iwafuchi-Doi and Zaret, 2014).

SC reprogramming can also occur *in vivo*, and usually involves TACs or even differentiated cells reverting back to SC fate. This reprogramming is achieved by signals sent out from the SC niche in response to tissue damage or SC niche vacancy, and will be discussed next.

Stem cell regulation by the niche

Schofield was the first to propose and define the term “niche” in the context of the microenvironment that regulates the behavior of hematopoietic SCs. In particular, he described several attributes that a SC niche should possess, such as control of SC proliferation and quiescence, integration of signals reflecting tissue and organismal state, and conferral of SC features on daughter cells depending on their location following cell division – inside or outside of the niche (Schofield, 1978).

Since then, SC niches have been described for a variety of organs, although new microenvironment components of each specific niche continue to be elucidated. The best understood SC-niche models are the male and female germ line stem cells (GSCs) in the fly *Drosophila*. Male GSC niche consists of the somatic hub cells at the testis tip. Female GSCs reside at the very tip of the ovary, in physical contact with the somatic cap cells, which act as the GSC niche and are critical for the maintenance of the GSCs (Fuller and Spradling, 2007; Xie

and Spradling, 2000). Although *Drosophila* male and female GSC niches consist of heterologous cell types, recent findings in the hematopoietic system, HFs and in the intestine have shown that SC progeny can also contribute to the SC niche and regulate SC function (Hsu et al., 2011; Sato et al., 2011; Scadden, 2014).

Drosophila GSC niche is also able to confer stemness to TA cells that have left the niche and embarked on the path to differentiation (Brawley and Matunis, 2004). The ability of the niche to induce stemness in cells that have already left the niche has also been demonstrated in various mammalian organs, such as the intestine (van Es et al., 2012), the lung (Tata et al., 2013), and the HF (Rompolas et al., 2013).

Hair follicle stem cells

HFSCs reside in a niche called “the bulge” (Cotsarelis et al., 1990). The bulge has been identified as the location of HFSCs based on their slow cycling properties. This was first demonstrated using tritiated thymidine ([^{3}H]TdR), where mice are repeatedly treated with [^{3}H]TdR over several days such that the majority of their cells becomes labeled and then chased for several weeks. During the chase period, fast-cycling cells dilute the label, while slow-cycling cells remain labeled. Based on these observations, the slow-cycling population within HFs was mapped to the bulge region (Cotsarelis et al., 1990). It took several more years to demonstrate that these slow-cycling cells within the bulge region possess the properties of SCs. This was achieved by adapting the pulse-chase

strategy using tetracycline-inducible histone, tagged with GFP (H2BGFP) (Tumbar et al., 2004). Labeled cells were then purified and subjected to the ultimate test, where they were able to reconstitute entire HFs in nude mice (Blanpain et al., 2004).

Therefore, although HFSCs are more quiescent than other cells within the HFs, their proliferation and exit form the niche can be triggered upon the HF entry into the growth phase of the hair cycle (anagen). Once activated, HFSCs give rise to cells within the outer root sheath (ORS), which reside within the basal layer of HFs. The ORS cells continue to proliferate and produce TACs, which constitute the matrix. The matrix cells undergo additional rounds of proliferation and proceed to differentiate into seven lineages that fulfill the role of producing the hair, and supporting its growth (Blanpain and Fuchs, 2006; Greco et al., 2009; Hsu et al., 2011) (Figure 1-1).

As matrix cells exhaust their proliferative capacity, hair growth stops and the HF enters a destructive phase (catagen). During catagen, the lower two-thirds of the mature HF undergo apoptosis and degenerate. The bulge region containing SCs is spared, as well as the cells within the ORS. The cells in the upper ORS form the new bulge, while the cells within the lower ORS form the hair germ (Hsu et al., 2011). Upon completion of catagen, the HF enters a resting phase (telogen). Telogen phase becomes progressively longer as mice age.

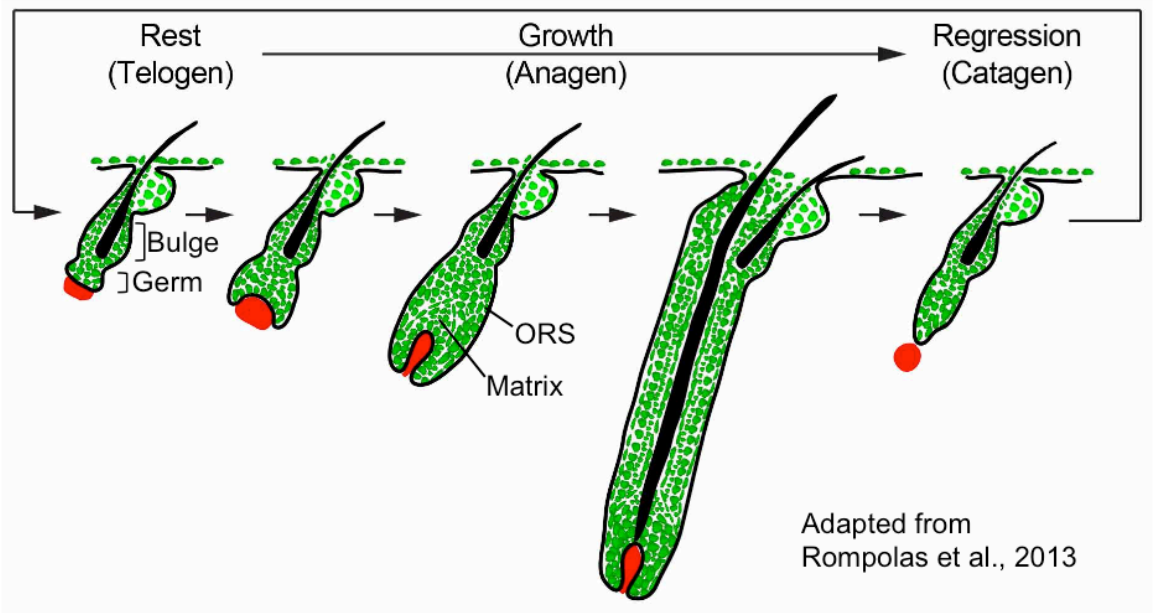

Figure 1-1. Hair follicle cycle. HFSCs are located in the bulge and remain quiescent as long as the HF is in telogen. Upon entry into the growth phase of the hair cycle (anagen), HFSCs in the bulge as well as in the germ become activated and give rise to the outer root sheath (ORS) cells, located within the basal layer of HFs. ORS cells proliferate and give rise to the transit-amplifying cells in the matrix. The matrix undergoes further proliferation and gives rise to several differentiated lineages within the HF. Eventually, the HF enters the regression phase (catagen), during which the lower part of the HF undergoes apoptosis, leaving behind the bulge and the hair germ, which will fuel subsequent hair cycles.

Eventually, a new round of anagen initiates, with the activation of the cells within the hair germ, followed by the activation of several cells within the new bulge. The hair cycle then repeats (Figure 1-1).

Maintaining hair follicle stem cell identity

HFSC identity is maintained by a set of transcription factors, loss of which results in the failure of HFSCs to maintain their fate and differentiate. One example is LHX2, loss of which results in HFSC differentiation into sebocytes (Folgueras et al., 2013). Another example is SOX9, loss of which results in HFSC differentiation into the epidermal cells (Kadaja et al., 2014). Additionally, loss of SOX9 in embryonic epidermis results in the failure to establish the SC pool during HF morphogenesis (Nowak et al., 2008; Vidal et al., 2005).

Apart from maintaining SC identity in vivo, HFSCs can be isolated and cultured *in vitro*, then grafted back onto a nude mouse along with freshly isolated newborn dermal fibroblasts to regenerate entire HFs (Blanpain et al., 2004; Lichti et al., 1993; Weinberg et al., 1993). Additionally, HFSCs can participate in wound repair, where they adopt the epidermal fate and regenerate the epidermis (Taylor et al., 2000; Tumbar et al., 2004). Therefore, HFSCs need to maintain their stemness in culture while at the same have the flexibility to change their fate “on demand” in response to changes in the environment, when tissue damage needs to be repaired.

It has been recently demonstrated that SOX9 is necessary for the maintenance of HFSC fate both in vivo and in vitro due to its unique ability to act as a pioneer transcription factor (Adam et al., 2015; Nowak et al., 2008; Vidal et al., 2005). The critical role of SOX9 in establishing and maintaining HFSC identity was demonstrated by analyzing its binding patterns to the chromatin of HFSCs in vivo, in vitro and upon wounding. SOX9 was found to bind within the super-enhancers of multiple genes, essential for proper HFSC function (including Lhx2, Tcf3, Tcf4, Nfatc1, and others). Although the expression of these genes is normally confined to the HF, such that they are Polycomb-repressed in the interfollicular epidermis (IFE), induction of SOX9 expression in the adult IFE was sufficient to induce their expression in the IFE, demonstrating that SOX9 is a true pioneer transcription factor, able to induce chromatin remodeling and removal of inhibitory marks (Adam et al., 2015).

The ability of SOX9 to induce the expression of other key HFSC transcription factors in the IFE and in culture, and to maintain HFSC fate in various circumstances suggests that it is the combination of internal factors (such expression of SOX9) and the microenvironment that dictates the state and function of HFSCs. Previous studies have suggested that when HFSCs are laser-ablated in vivo, it is in fact possible to convert non-SC epithelial cells to HFSC fate, by triggering their mobilization and migration into the unoccupied niche (Rompolas et al., 2013). This finding further underlies the critical role of the niche in specifying and maintaining HFSCs in adult HFs.

Hair follicle stem cell niche microenvironment

The HFSC niche is composed primarily of dermal fibroblasts that become a permanent appendage of the adult HF during its morphogenesis and constitute the dermal papilla (DP). Several factors produced by the DP have been suggested to participate in HFSC activation, such as FGFs, TGFβ2, and BMP inhibitors (Sostdc1, Bambi, and Noggin) (Greco et al., 2009; Oshimori and Fuchs, 2012; Rendl et al., 2005; Rendl et al., 2008; Rosenquist and Martin, 1996). At the same time, BMP4 produced by the DP contributes to maintaining HFSC quiescence (Plikus et al., 2008). Interestingly, DP ablation experiments have shown it to be dispensable for HFSC quiescence, but required for HFSC activation (Rompolas et al., 2012).

HFSCs also receive regulatory signals from other cellular types that are in proximity to the HFSCs and can be considered a part of their regulatory niche. For example, activation of HFSCs during anagen is accompanied by angiogenesis, and inhibiting angiogenesis results in delayed anagen induction (Mecklenburg et al., 2000; Yano et al., 2001). This suggests that vascularization is necessary for proper activation of HFSCs during anagen. Another possible component of the HFSC niche are neurons that innervate the upper bulge. Nerves produce SHH that signals to the upper bulge and may guide their behavior during wounding (Brownell et al., 2011). Additionally, neuropeptides substance P and nerve growth factor (NGF) can be produced by the nerves in stressful conditions to halt proliferation and induce catagen (Peters et al., 2006).

Finally, subcutaneous fat also produces signals that can both activate and inhibit HFSCs. For example, mature cutaneous adipocytes produce BMP2 to inhibit HFSC activation and anagen entry (Plikus et al., 2008). Interestingly, immature adipocytes produce platelet-derived growth factor alpha (PDGFA) to activate HFSCs via PDGF signaling in the DP (Festa et al., 2011).

Apart from the heterologous non-epithelial cell types, differentiated progeny of HFSCs also contribute to the regulation of HFSC quiescence (Hsu et al., 2011) and activation (Hsu et al., 2014b) and can be considered part of the niche. The suprabasal layer of the bulge, marked by keratin 6, produces BMP6 and FGF18 (Hsu et al., 2011) that keeps HFSCs quiescent. Additionally, upon onset of anagen, TACs that have descended from HFSCs start expressing Shh, which signals to HFSCs to induce their proliferation (Hsu et al., 2014b).

Apart from the evidence above, the importance of the HFSC niche in maintaining and regulating HFSCs is highlighted by laser ablation experiments, which have shown that the DP is essential for HFSC activation in telogen, but may be dispensable for the maintenance of quiescence (Rompolas et al., 2012). At the same time, HFSC grafts only give rise to hair when coupled with purified neonatal dermal fibroblasts, further underlining the importance of the signals emanating from the dermis (Lichti et al., 1993; Weinberg et al., 1993). Finally, the niche is sufficient to convert non-SC epithelial cells to SC fate, by triggering their mobilization and migration into the unoccupied niche upon HFSC ablation (Rompolas et al., 2013).

Ectodermal appendage morphogenesis

Teeth, nails, several eccrine glands (mammary, sweat, salivary, and lacrimal glands), and hair are all derivatives of the ectoderm (Pispa and Thesleff, 2003). Despite their functional diversity, they share several common features in development. Ectodermal appendage morphogenesis initiates through a crosstalk between the epithelial cells and the mesenchymal cells, resulting in the formation of placodes – aggregates of epithelial cells that mark the location of the future ectodermal appendage. Formation of epithelial placodes is accompanied by the condensation of mesenchymal cells underneath and formation of the dermal papilla.

Initial hair placode formation occurs via centripetal migration of basal skin cells into the site of the future hair placode, and cell compaction. Cell proliferation does not play a major role in this process (Ahtiainen et al., 2014). Similar observations have been made during early feather formation, where little proliferation is occurring both in the feather epidermis and the underlying dermis undergoing condensation (Wessells, 1965). Finally, mammary placode formation and initial stages of morphogenesis do not involve proliferation. After initial specification, mammary rudiment growth lags behind that of the rest of the body. However, in the last days of pregnancy the relations are reversed, and the mammary gland rudiment undergoes a burst of growth and proliferation (Balinsky, 1950).

After initial specification and condensation, subsequent appendage morphogenesis depends on the continuous crosstalk between the epidermis and the mesenchyme. The signaling molecules from the WNT, TGFβ, hedgehog (Hh), and FGF families are used reiteratively at different stages of ectodermal organogenesis to produce the final shape and function of the tissue.

Signaling pathways in hair follicle morphogenesis

WNT signaling

Hair follicle morphogenesis initiates at E14, with the specification of hair placodes. From tissue recombination experiments, where mesenchyme and epithelium of different species, body regions or developmental time points were paired, the outcome was mostly dictated by the identity of the mesenchyme (Bereiter-Hahn et al., 1984; Sengel, 1976). Although the first signal remains elusive, several lines of evidence suggest that it is a member of the WNT family of ligands and will be discussed below.

There are 19 genes encoding members of the WNT family (Clevers and Nusse, 2012). Wnt3a, Wnt4, Wnt5a, Wnt6, Wnt10a, Wnt10b, Wnt11, Wnt16 are expressed in the embryonic skin at various stages of morphogenesis (Fu and Hsu, 2012; Huelsken et al., 2001; Reddy et al., 2001). Wnt3a, Wnt4, and Wnt6 are expressed throughout the epidermis, Wnt10a and Wnt10b are upregulated in the placode upon specification, Wnt16 is downregulated in placodes, while Wnt5a and Wnt11 are expressed by the dermal condensates.

WNT signaling can trigger a canonical and a non-canonical signaling cascade. The canonical cascade (Figure 1-2) involves the ligand binding to a heterodimeric complex, which consists of a Frizzled (Fz) and a Low-density lipoprotein receptor-related protein 5 or 6 (LRP5/6). There are 10 mammalian Fz receptors. WNT ligand binding to the Fz receptors is promiscuous, with several WNTs capable of binding the same Fz receptor, and vice versa (Janda et al., 2012). In the absence of the WNT ligand, β-catenin is sequestered by a degradation complex, which is held together by scaffolding proteins Axin and APC. In this complex, β-catenin is phosphorylated by CK1 and GSK3 and targeted for proteasomal degradation by β-TrCP. Upon WNT ligand binding to Fz/LRP complex, Axin is phosphorylated by the receptor complex, which destabilizes the degradation complex and allows β-catenin accumulation in the cytoplasm and entry into the nucleus. Although β-catenin does not bind the chromatin directly, upon entry in the nucleus, β-catenin interacts with transcription factors in the TCF/LEF family, which includes LEF1, TCF1, TCF3, and TCF4 and regulates gene expression (Behrens et al., 1996; Molenaar et al., 1996). WNT/β-catenin-dependent gene expression is highly context and tissue dependent. One of the most consistently WNT-activated genes is Axin2. Axin2-based reporters are widely used as a proxy for WNT signaling as well as for lineage-tracing of WNT-responsive cells (Lustig et al., 2002a). Additionally, several WNT reporters have been generated where reporter transcription is downstream of a minimal promoter and an enhancer containing several copies of

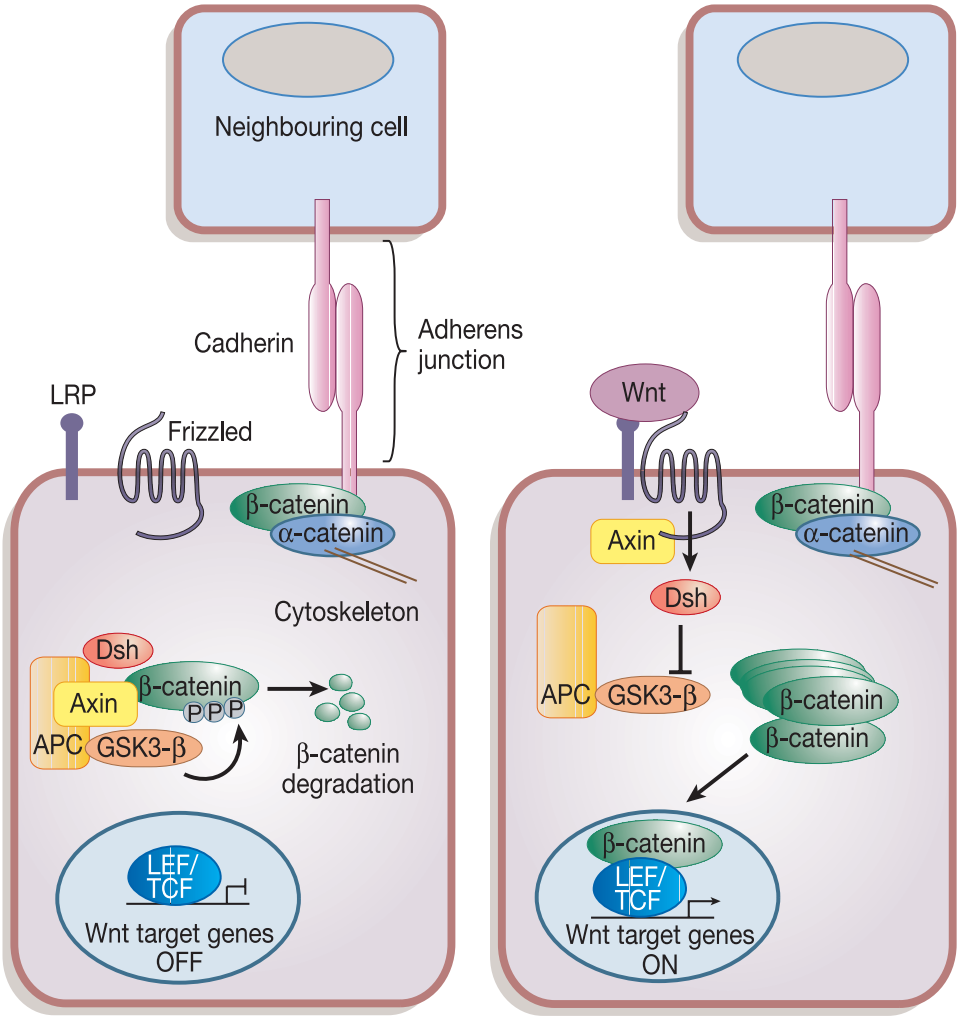

With permission from (Reya and Clevers, 2005)

Figure 1-2. Canonical WNT signaling. In the absence of WNT signaling (left panel), β-catenin is sequestered in the cytosol in a complex with axin, APC and GSK3, where is phosphorylated and targeted for degradation. Upon WNT ligand binding (right panel), the degradation complex is disassembled and β-catenin is stabilized. β-catenin translocates to the nucleus where it interacts with TCF/LEF transcription factors, thus regulating gene expression.

LEF/TCF-binding sites, such as TOPGAL and BATGAL (DasGupta and Fuchs, 1999; Maretto et al., 2003).

Based on these reporters as well as nuclear β-catenin and LEF1 expression, WNT signaling is active in the upper dermis of developing skin as early as E12.5 – prior to HF morphogenesis. Starting at E13.5-E14, WNT reporter activity increases in the nascent hair placodes and underlying dermal condensates (DasGupta and Fuchs, 1999; Zhang et al., 2009; Zhou et al., 1995).

Several secreted proteins that work through different mechanisms negatively regulate the canonical WNT signaling pathway. For example, Frizzled-related proteins (sFRPs) and WNT inhibitory protein (WIF) bind WNT ligands and prevent their interaction with the WNT receptors (Bovolenta et al., 2008). On the other hand, proteins of the Dickkopf (DKK) family antagonize WNT signaling by binding LRP5/6 (Glinka et al., 1998). APCDD1 is another example of a WNT signaling antagonist. APCDD1 is a membrane-bound glycoprotein, which inhibits WNT signaling by binding both WNT ligand and LRP receptor (Shimomura et al., 2010).

Non-canonical WNT signaling pathways also proceed through WNT ligand binding to Fz receptors, however in this case, ligand binding to the receptor does not result in β-catenin stabilization and induction of TCF/LEF-dependent transcription. The best-characterized non-canonical WNT signaling pathway is the planar cell polarity (PCP) pathway. In this case, Fz receptor activation results in the downstream activation of small GTPases RAC1 and RHOA, as well as

JNK, which control various aspects of cytoskeleton and can also affect transcription. The PCP pathway regulates cellular polarity and affects various morphogenetic processes, such as gastrulation and neural tube closure to name a few (Gomez-Orte et al., 2013).

Both canonical and non-canonical WNT signaling branches are involved in coordinating HF morphogenesis. Several lines of evidence suggest that canonical WNT signaling is the first signaling pathway absolutely required for the specification of HFs as well as other ectodermally-derived skin appendages. Keratin 14 promoter-driven epidermis-specific overexpression of Dkk1 or knockout of β-catenin completely abolish HF specification (Andl et al., 2002; Huelsken et al., 2001). Conversely, hyperactivation of WNT signaling by epidermis-specific expression of a non-degradable, constitutively active form of β-catenin results in ectopic HF formation (Gat et al., 1998).

Additionally, modulating the intensity of WNT signaling has been proposed to regulate the spacing and patterning of the developing HFs. For example, overexpressing variable levels of Dkk2 in the epidermis affects the density of specified HFs, with the density of specified HFs correlating to the level of transgene expression (Sick et al., 2006).

On the other hand, the non-canonical WNT/PCP signaling branch has been implicated in HF polarity. PCP signaling components Vangl2 and Celsr1 are critical for proper HF angling during HF morphogenesis (Devenport and Fuchs, 2008). Additionally, epidermis-specific deletion of Fz6 results in generation of

whorls and tufts of hair on the mouse skin, resembling Fz loss-of-function phenotypes in the *Drosophila* wing (Guo et al., 2004; Vinson et al., 1989). Interestingly, Wnt5a and Wnt11, two WNT ligands expressed by the dermal condensate shortly after hair placode specification, are known to preferentially activate non-canonical WNT signaling. Wnt5a and Wnt11 are involved in the regulation of convergent extension in lower vertebrates, while Wnt5a has also been shown to regulate PCP in mice during cochlear development (Heisenberg et al., 2000; Moon et al., 1993; Qian et al., 2007). It remains unknown whether Wnt5a and Wnt11 signal through the non-canonical WNT/PCP pathway to regulate HF polarity.

SHH and BMP signaling

While WNT signaling is considered to be the first signal required for HF specification, several additional signaling pathways take part in regulating various aspects of HF morphogenesis.

Sonic hedgehog (SHH) signaling is downstream of WNT signaling. SHH is one of three mammalian hedgehog proteins, the other two being Indian and Desert hedgehog. In vertebrates, SHH is secreted and signals by binding to the receptor patched (PTCH1). Upon SHH interaction with PTCH1, smoothened (SMO) is released from PTCH1 inhibition and activates glioma-associated oncogene (GLI) family of transcription factors GLI1-GLI3 (Ingham and McMahon, 2001). GLI1 acts exclusively as a transcription activator, while GLI2 and GLI3 can

be post-transcriptionally processed by cleavage and phosphorylation to act both as transcription activators and repressors (Koebernick and Pieler, 2002). GLI1 is not required to initiate SHH signaling, and is itself a direct downstream transcriptional target of SHH. Therefore, GLI1 promoter has been used to generate SHH reporters (Bai et al., 2002b).

Shh expression becomes upregulated in the hair placode shortly after specification. Based on Gli1-LacZ reporter activity, SHH signals both to the epidermal placode, as well as to the dermal condensate (Jamora et al., 2003; St-Jacques et al., 1998). Apart from a variety of developmental phenotypes in various organs, Shh knockout embryos also fail to develop HFs, which become arrested shortly after specification, and do not invaginate into the dermis (St-Jacques et al., 1998). The defects in HF morphogenesis have been attributed to the failure to recruit the dermal condensate, as well as decreased proliferation in the hair placode (St-Jacques et al., 1998; Woo et al., 2012). Additionally, SHH regulates the expression of noggin in the dermal condensate, which feeds back to the developing hair follicle to further boost the expression of Shh, as well as to repress BMP signaling (Woo et al., 2012).

Bone morphogenetic proteins (BMP) belong to the transforming growth factor β (TGFβ) superfamily, which consists of at least 30 genes in mammals, including 3 TGFβ isoforms, 4 activin β chains, nodal, 10 BMPs and 11 growth and differentiation factors (GDFs). TGFβ signaling proceeds through the ligand binding to a heterotetrameric receptor complex, which consists of type I and type

II receptors, with a conserved intracellular Ser-Thr kinase domain. Upon ligand binding, the type II receptor phosphorylates and activates the type I receptor, which enables the recruitment and phosphorylation of receptor-activated SMADs (R-SMADs). SMAD C-terminal phosphorylation by the receptor complex allows R-SMADs to form a complex with SMAD4. SMAD complexes accumulate in the nucleus, where they can bind and regulate the expression of target genes (Schmierer and Hill, 2007).

The signaling of TGFβ ligands can be counteracted by several soluble factors, which bind the TGFβ ligands and prevent them from interacting with the receptors. Most are BMP antagonists, such as chordin, noggin, sclerostin, and members of the Cerberus family (Balemans and Van Hul, 2002). Additional inhibitors include follistatin, which inhibits activin signaling, but can also bind BMPs and GDF8 (Thompson et al., 2005).

BMPs are expressed in a tissue specific manner, with diverse biological functions in different tissues. During HF morphogenesis, BMP2 is expressed in the developing hair placode, while BMP4 is expressed in the underlying dermal condensate. BMP signaling has various roles at different stages of HF morphogenesis. During HF specification, BMP signaling is thought to be involved in HF patterning, where it acts by antagonizing the HF fate. To counteract the inhibitory effects of BMP signaling, noggin is produced by the dermal condensate in a SHH-dependent manner (Botchkarev et al., 1999; Woo et al., 2012). Noggin knockout embryos have less HFs specified, and those specified are delayed in

their morphogenesis (Botchkarev et al., 1999). Additionally, BMP inhibition by noggin is necessary for Lef1 expression in the developing HFs (Botchkarev et al., 1999; Jamora et al., 2003).

WNT-SHH crosstalk in *Drosophila*

Some of the earliest examples of the crosstalk between WNT (*wingless* in *Drosophila*) and hedgehog (HH) signaling pathways come from work in the *Drosophila* embryo, in particular, in the context of intrasegmental patterning during morphogenesis. Insect bodies are composed of segments, which give rise to particular structures and patterns according to their position. The *Drosophila* body plan is established at the blastoderm stage of embryonic development. The blastoderm is a single-layer epithelium covering the *Drosophila* embryo (Ingham, 1988). By the time the blastoderm is formed, transcripts of *wingless* (*wg*) and *engrailed* (*en*) accumulate in fourteen stripes along the anterior-posterior axis of the embryo, and are expressed at each side of the border between segments (Akam, 1987; Ingham, 1988; Lee et al., 1992). Subsequently, the *en*+ domain expresses *hh. Hh* and *wg* act in concert to maintain each other's expression (Lee et al., 1992; Tabata et al., 1992).

Stem cell specification during organ morphogenesis

As I have previously discussed, adult SC identity and function are determined by a core set of genes that are expressed in tissue-specific manner.

SC niches are critical for the maintenance of the SC fate and regulation of SC function, but can also confer stemness to TACs and even differentiated cells when they are returned to the niche upon SC depletion or if vacancies arise.

The mechanisms governing the specification of SCs during organ morphogenesis are more obscure. What mechanisms trigger or restrict the expression of the core genes that are necessary and sufficient for SC identity and function? When during morphogenesis are SCs specified? Given the importance of the niche in the maintenance and regulation of adult SCs, what is the role of the niche in SC specification? Answering these questions is important as it might give us cues on how to recapitulate these processes *in vitro* in order to derive functional SCs for regenerative medicine.

In the majority of described models, SC establishment relies on signals emanating from a pre-established niche. In *Drosophila* gonads, the SC niche acts as a signaling center to recruit and maintain germ SCs from among a small population of undifferentiated primordial germ cells (PGCs) (Dansereau and Lasko, 2008). PGCs outside of the niche directly enter cyst (females) or gonialblast (males) differentiation pathways (Bhat and Schedl, 1997; Song et al., 2002; Zhu and Xie, 2003). In the developing intestine, cells expressing SC marker Lgr5 are initially present throughout the epithelium. They become confined to the crypt base as the villus buckles, thereby concentrating differentiation signals within the upper tip region (Shyer et al., 2015). Finally, hematopoietic stem cells (HSCs) are specified from the dorsal aorta endothelial

cells, which receive signals from vascular smooth muscle cells (Clements and Traver, 2013). These examples, described in more details below, demonstrate that SC specification during morphogenesis generally depends on the signals received from heterologous cell types that constitute the niche at that point in development.

Drosophila germ stem cell specification

The mechanisms involved in the specification, maintenance and differentiation of *Drosophila* germline stem cells (GSCs) lay the foundation of our understanding of SC regulation and clearly show the importance of the niche in the process. In the female, the core of the GSC niche consists of 5-7 somatic cap cells that form adherens junctions with 2-3 GSCs, physically anchoring them to the anterior of each germarium (Spradling et al., 1997; Xie and Spradling, 2000). The female GSC niche additionally consists of the terminal filament (TF) cells and the sheath cells, surrounding the ovariole (Spradling et al., 2001). In the male, the niche consists of approximately 12 somatic hub cells, which maintains 5-9 GSCs (Hardy et al., 1979; Le Bras and Van Doren, 2006).

Drosophila germline stem cells (GSCs) are derived from a population of primordial germ cells (PGCs), which are set aside from the somatic lineages early in the fly development. PGCs and the somatic gonadal precursors (SGPs) are specified at different locations, and come from different lineages, the SGPs of mesodermal origin, and PGCs coming from the embryonic posterior pole.

Therefore, the PGCs must migrate from the posterior of the embryo to meet the SGPs and form the embryonic gonad. The direction of PGC migration is determined by repulsive cues provided by two phospholipid phosphatases Wunen and Wunen2 (Renault et al., 2004; Zhang et al., 1997), as well as by attractive signals produced by SGPs, including Hedgehog as well as products of HMG-CoA reductase (Deshpande et al., 2001; Van Doren et al., 1998).

Once PGCs migrate and adhere to the gonadal precursors, they migrate anteriorly to form a gonad. The SGPs then ensheath the PGCs, thus forming the niche. The ensheathing process requires the expression of the adhesion molecule E-Cadherin and another transmembrane protein Fear-of-Intimacy, expressed by the SGPs (Jenkins et al., 2003; Van Doren et al., 2003). The adhesion with and ensheathing of the PGCs by the SGPs essentially completes the formation of the GSC niche. The PGCs that did not establish adherens junctions with the mesoderm and thus did not enter the niche fail to maintain PGC status and differentiate (Song et al., 2002).

Apart from the physical adhesion and ensheathing that are required for the maintenance of GSCs in undifferentiated state, additional signaling pathways play an important role in this process, which differ slightly between males and females. In the female, Dpp signaling is the primary GSC maintenance pathway. Dpp, the *Drosophila* homolog of BMP2, is produced by the somatic niche and signals nonautonomously over the short range to repress GSC cytoblast differentiation. Dpp maintains GSC fate by repressing the expression of an RNA-

binding protein *bag of marbles (bam)* (Song et al., 2004). Bam forms a protein complex with Bgcn, another RNA-binding protein, and together they act to downregulate several important SC maintenance factors, such as Nanos (Nos), E-cadherin, germline Piwi, microRNAs, and Dpp signaling (Perinthottathil and Kim, 2011). Dpp signaling is required throughout embryonic and larval development to repress PGC differentiation and to maintain their potential to become GSCs (Zhu and Xie, 2003). Dpp signaling also plays a role in male GSC maintenance, and represses the expression of *Bam* (Kawase et al., 2004). However, in the male, Bam is not required for differentiation, and overexpression of Dpp is not sufficient to block differentiation (Schulz et al., 2004).

In the male germline, the Jak-Stat pathway is the main determinant of GSC identity. In this case, the hub cells express Upd – a short-range signal that signals to GSCs via the Domeless receptor and Hopscotch (Kiger et al., 2001; Tulina and Matunis, 2001). Jak-Stat pathway activation results in the phosphorylation of Stat92E transcription factor, which activates the expression of genes necessary for GSC state (Bausek, 2013). Importantly, during testis morphogenesis, after gonad coalescence, all PGCs maintain activated Stat92E. However, active Jak-Stat signaling becomes restricted to the PGCs directly attached to the hub cells, while PGCs further away from the hub have low levels of phosphorylated Stat92E and initiate differentiation (Sheng et al., 2009).

While Dpp and Jak-Stat signaling pathways are mostly unidirectional from the niche to the GSCs, it is worth noting that GSCs can also signal to their niche.

For example, in the female, Notch signaling plays an important role in the maintenance of GSCs and control of GSC numbers. In this case, Notch ligands are expressed by the GSCs and signal to the cap cells. Delta overexpression in the germline causes expansion of the cap cells, which consequently increases vacancies in the niche, resulting in more GSCs (Ward et al., 2006).

In summary, specification of GSCs in *Drosophila* testis and ovaries depends on the signals produced by the pre-established niche. In the case of female germline development, cap cells express Dpp, which signals to the PGCs to maintain them in undifferentiated state, allowing them to adopt GSC fate. In the case of testis development, the hub cells express Upd, which signals to the adjacent PGCs, allowing them to become GSCs and preventing their differentiation.

Intestinal stem cell specification

Intestinal SCs (ISCs) are among the best-studied epithelial SC populations in mammals. In adult, ISCs reside in the intestinal crypt, and are identified by the expression of Lgr5 (Barker et al., 2007). ISCs are tightly regulated by their niche, which consists of heterologous cell types, as well as Paneth cells, which are descendants of the ISCs (Barker, 2014). Despite the recent progress in our understanding of adult ISC regulation, little is known about the origins of ISCs.

The development of the small intestine varies slightly among vertebrates. In the chick, the sequential differentiation of the smooth muscle layers of the gut

restricts the expansion of the growing endoderm and mesenchyme, causing the epithelium to fold into longitudinal ridges, followed by a zigzag pattern, and lastly individual villi (Shyer et al., 2013). In the mouse, villi emerge at embryonic day (E) 14.5 directly from a smooth lumen. In this model, the contribution of the smooth muscle to villi formation is less well defined. Inhibition of muscle differentiation via treatment with platelet-derived growth factor (PDGF) receptor kinase inhibitor AG1295 or a calcineurin inhibitor tacrolimus (FK-506) impairs villi formation, suggesting that smooth muscles contribute to villi formation (Fukuda et al., 1998; Kurahashi et al., 2008; Shyer et al., 2013). However, both drugs can exert additional functions that could contribute to villi formation impairment. For example, mesenchymal cells that cluster within villi also express *Pdgfra*, and thus can also affect villi formation (Karlsson et al., 2000). An alternative mechanism of villi formation in the mouse gut suggests a Turing-based model (Walton et al., 2016). In this case, hedgehog ligands produced by the epithelium signal to the mesenchyme and induce mesenchymal cell cluster formation. These mesenchymal clusters subsequently express BMP ligands and receptors. Modulating BMP signaling affects the villi pattern in a manner consistent with Turing activator/inhibitor model (Walton et al., 2016). Regardless of the model, villification occurs well before the appearance of the intestinal crypts, and the specification of various epithelial cell types that populate them, which take place postnatally.

To determine when ISCs first emerge in the developing gut, studies have relied on the *Lgr5*$^{GFP\text{-}IRES\text{-}CreER}$ knock-in mice (Barker et al., 2007). At E12.5, GFP signal can be found throughout the epithelium of the small intestine. Afterwards, it becomes progressively restricted to the space between villi as they form (Shyer et al., 2015). Interestingly, Paneth cells are not present in the developing gut until P15-P21, where they intermingle between GFP+ cells (Kim et al., 2012), suggesting that restriction of GFP+ cells to the intervilli regions is largely independent of the signals received from Paneth cells.

In the mouse, villi formation is accompanied by the formation of a mesenchymal condensate at the villus tip, also known as villus cluster (Karlsson et al., 2000). In the chick, bending of the epithelium induces increased local concentration of Hh signaling within the villus cluster, which results in a local increase of BMP signaling and inhibition of proliferation at the villi tips (Shyer et al., 2015). In the adult ISC niche, BMP has been shown to inhibit ISC self-renewal by antagonizing WNT signaling (He et al., 2004). Thus, increased BMP signaling at the villi tips during villi morphogenesis might potentially inhibit WNT signaling and ISC fate, restricting ISCs to the villi crypts. In support of this mechanism, blocking SHH or BMP signaling in cultured samples of E14 chick intestines increased proliferation and expanded the expression of Sox9 – a target of WNT signaling in the intestines (Shyer et al., 2015).

On the other hand, a study that has investigated the status of WNT signaling using TOP-GAL, Axin2-LacZ and nuclear β-catenin as reporters in

developing mouse intestines has found little evidence for WNT signaling in E14.5 mouse intestines, despite the broad expression patterns of *Lgr5-GFP* reported by Shyer et al (Kim et al., 2007; Shyer et al., 2015). Additionally, as intestinal morphogenesis progresses between E16 and birth, WNT signaling is restricted to villi, and excluded from intervillus regions. Interestingly, WNT signaling starts shifting to the intervillus spaces shortly after birth and is fully shifted to the intervillus spaces by post-natal day 3 (Kim et al., 2007). Therefore, whether WNT or additional signals are responsible for the expression of Lgr5-GFP and Sox9 in the epithelial cells lining the developing intestines remains to be determined.

Nevertheless, the available data suggest that during intestinal morphogenesis, the entire epithelial lumen has the potential to acquire ISC fate. Increased local concentration of SHH-BMP signaling in the villus clusters contributes to the inhibition of ISC fate at the villi tips, gradually restricting ISCs to the intervilli regions. This suggests a model where ISCs are passively restricted to the intervilli spaces, rather than actively specified by a niche.

Hair follicle stem cell specification

HFSC bulge niche becomes apparent when the HF undergoes the first round of growth and degeneration (catagen). At that point, the HFSCs are protected from catagen and remain in the bulge, where they become active again at the onset of the next hair cycle (Fuchs, 2007). However, a distinct population of quiescent cells within the upper ORS can be identified by pulse-chase

experiments as early as two days after birth, demonstrating that HFSCs are specified during embryogenesis, much earlier than the first telogen entry (Nowak et al., 2008). Already at that stage, HFSCs express several transcription factors that mark and regulate HFSC function during adult homeostasis, such as Lhx2, Sox9, Nfatc1, and Tcf3/4, but still lack other adult HFSC markers such as CD34 (Nowak et al., 2008).

Some of these transcription factors have also been shown critical for HFSC specification during HF morphogenesis. For example, epidermis-specific deletion of Lhx2 and Sox9 results in the failure to specify the early HFSC pool (Folgueras et al., 2013; Nowak et al., 2008). On the other hand, other transcription factors, such as Nfatc1, regulate HFSC function during adult homeostasis and their loss does not affect HFSC specification during morphogenesis, despite their expression during that stage (Horsley et al., 2008). Interestingly, Lhx2 and Sox9 are expressed in distinct populations of cells in the developing HFs right from the onset, where they can be detected by antibody staining at the placode level (Nowak et al., 2008; Rhee et al., 2006). At this stage of morphogenesis, Lhx2 is expressed by the basal cells of the hair placodes, while Sox9 largely marks the suprabasal cells. The mechanisms involved in establishing this early cellular heterogeneity within the developing hair placodes are currently unknown.

Given SOX9's role as a pioneer factor, expression of which is necessary and sufficient to maintain HFSC fate in vivo and in culture (Adam et al., 2015),

this raises an additional question of whether Sox9 expression in hair placodes marks a pool of cells that will later contribute to the adult SC pool in mature HFs. If this is the case, what are the mechanisms involved in their specification and control of their expansion and differentiation in the absence of the bulge – their niche?

CHAPTER 2: DETERMINANTS OF HETEROGENEITY DURING HAIR FOLLICLE MORPHOGENSIS

Organ morphogenesis requires several processes to occur in parallel or sequentially. During morphogenesis, a given organ must undergo the specification of the various cell types, which are the building blocks for that given tissue and will fulfill its functions. These cell types need be properly positioned and organized within the organ, such that the overall morphology of the organ is conducive to its proper function. Finally, in many organs, a restricted pool of SCs needs to be set apart to maintain the organ in homeostasis, replenish dying cells and participate in tissue repair.

The hair follicle is a useful model to study organogenesis, where organ morphology, cell type specification, and SC restriction occur during five days between initial hair placode formation at E14.5 and birth. Interestingly, cellular heterogeneity can be observed as early as at the placode stage, where the basal cells express high levels of P-cadherin and Lhx2, while the suprabasal cells express E-cadherin and Sox9 (Nowak et al., 2008; Rhee et al., 2006). How this heterogeneity is achieved so early in morphogenesis is unknown.

To address this question, I used a combination of mosaic lentiviral lineage tracing, fixed immunofluorescence and live imaging of cell divisions within the placodes and IFE, as well as mosaic genetic perturbations. I found that exclusively perpendicular divisions to the basement membrane within hair placodes set up the scene for differential fates of the daughter cells. The balance

of WNT and SHH signaling within the daughter cells subsequently determines their fates.

Results

Divisions within early hair placodes are perpendicular to the basement membrane and asymmetric

To address how cell type heterogeneity is established at the earliest stages of HF morphogenesis, I used in utero transduction to selectively infect the single layer of surface ectoderm of E9.5 embryos with lentivirus (LV), which by 24-48h, stably integrates into the host genome and is thereafter propagated to progeny. The progeny of the transduced cells will contribute to the IFE, the HFs, as well as other ectodermal appendages (Beronja et al., 2010).

I infected Rosa26-fl-STOP-fl-YFP (R26YFPfl/+) embryos with LV expressing an inducible CreER recombinase (LV-CreER) (Figure 2-1A). Low-dose tamoxifen at E15.5 activated CreER in isolated cells throughout the skin. The treated embryos were harvested 48 hours later, at E17.5, allowing for 1-2 cell divisions to take place following tamoxifen treatment. Several small YFP+ clones with P-cad^{hi} SOX9- basal and SOX9+ suprabasal cells were detected within hair placodes (Figure 2-1B). One way this type of pattern could be generated is by a basal cell undergoing a perpendicular division relative to the basement membrane, giving rise to a basal and a suprabasal cell (Figure 2-1C), which subsequently acquire different fates.

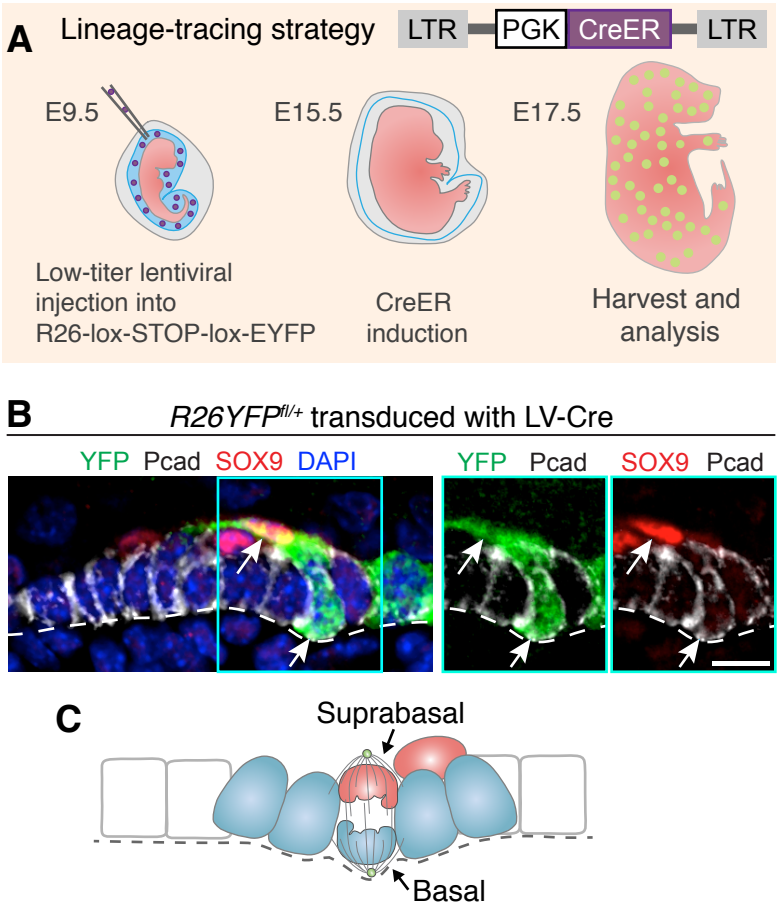

Figure 2-1. Short-term lineage-tracing in the epidermis. (A) Lineage-tracing strategy using lentiviral transduction of CreER. *Rosa26-lox-STOP-lox-EYFP* embryos were transduced with LV-CreER at E9.5. Pregnant dams were treated with tamoxifen at E15.5 and embryos were harvested at E17.5 and processed for immunofluorescence. **(B)** Lineage-traced clone in a placode. Arrows mark $Pcad^{hi}$ $SOX9^{-}$ basal and $SOX9^{+}$ suprabasal cells within a YFP^{+} clone. White dashed lines indicate basement membrane. **(C)** Schematic of perpendicular placode division that would give rise to a vertical clone as observed in (B).

To address how the LV-generated short-term lineage-tracing pattern observed above is generated, I investigated the first cell divisions that occur following placode formation. Immunolabeling for acetylated tubulin decorated the stable spindle microtubules and the cleavage furrow of mitotic cells, and P-cadherin (Pcad) distinguished placodes from interfollicular epidermis (IFE).

Unexpectedly, nearly all mitotic spindles within ($Pcad^{hi}$) hair placodes were oriented perpendicular (>45° angle) to the underlying basement membrane (Figure 2-2A). Quantitative analysis of an additional cleavage furrow marker, survivin, was suggestive of a perpendicular bias of late-stage mitotic division planes within these early stages of epithelial budding (Figure 2-2B). Hitherto overlooked, the nearly exclusive perpendicular angling further distinguished hair placodes from IFE, where such perpendicular spindles are fewer and have been linked to early steps involved in forming the skin barrier (Clayton et al., 2007; Lechler and Fuchs, 2005; Williams et al., 2014).

To ascertain whether perpendicular spindle orientations resolve into basal and suprabasal daughters, my collaborators Aaron Mertz and Irina Matos in the Fuchs lab developed a method to perform 4D video-microscopy on immobilized, ex utero E14.5 mouse embryos whose epidermis expressed a fluorescently tagged histone gene (Krt14–H2BGFP). Placodes were readily identified by their tight cell packing and hexagonal organization (Figure 2-2C). In total, we measured relative positions of daughters from 322 basal placode divisions.

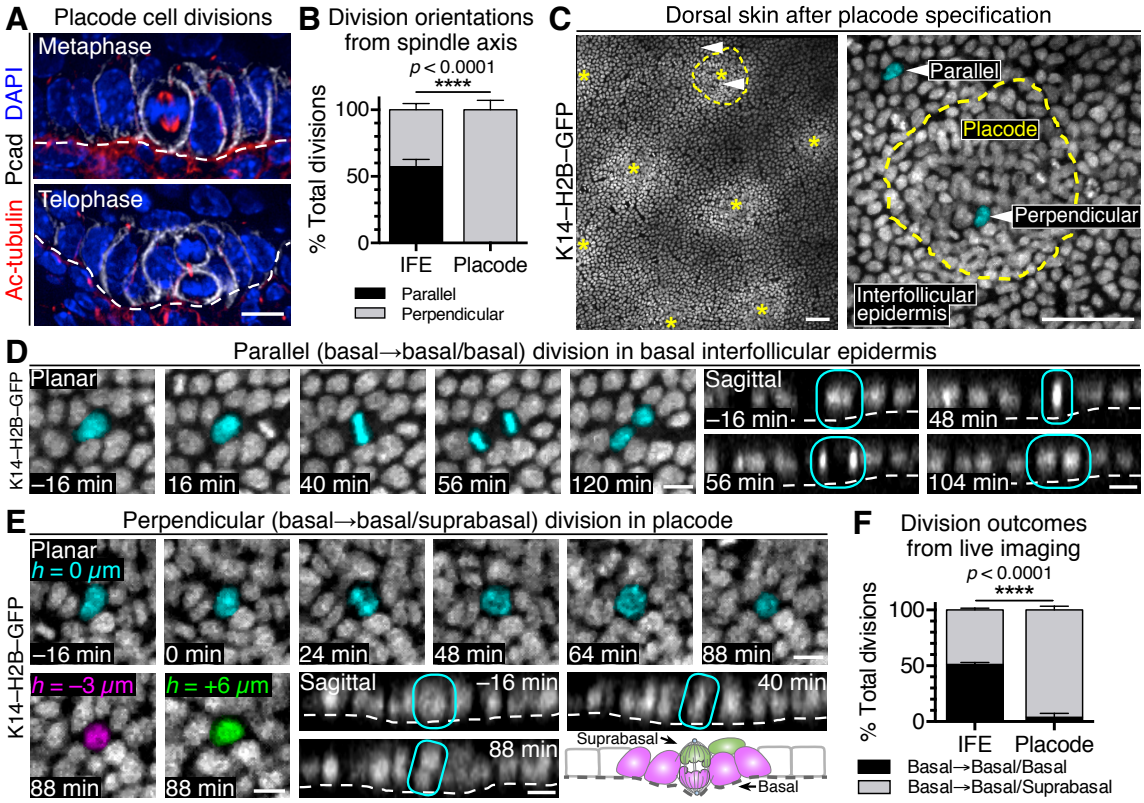

Figure 2-2. Cells divide perpendicularly in hair placodes. (A) Perpendicular divisions during metaphase (top) and telophase (bottom) in mouse hair placodes. **(B)** Quantification of parallel and perpendicular division orientation based on spindle axis of basal cells in IFE and placodes. Data are % ± standard deviation (SD) from pooled counts in *n*=3 embryos, 41 placodes, 187 IFE divisions. **(C)** E14.5 dorsal skin visualized by live imaging of K14–H2B–GFP embryos. (Left) Stitched image of placodes (asterisks) and IFE. (Right) Placode (yellow outline) surrounded by IFE. Arrows indicate examples of a parallel or perpendicular division, depicted in (D,E), respectively. **(D)** Time course from live imaging of parallel division in basal IFE. (Left) Planar views centered in basal plane with dividing cell pseudo-colored cyan. (Right) Sagittal views reconstructed from confocal stacks. Dividing cell circled in cyan. **(E)** Time course from live imaging of perpendicular division in placode. (Top) Planar views centered in basal plane at height 0μm, with dividing cell pseudo-colored cyan. (Bottom left) Planar views after mitosis indicating pseudo-colored basal daughter at –3μm (left, magenta) and suprabasal daughter at +6μm (right, green). (Bottom right) Sagittal views reconstructed from confocal stacks. Dividing cell circled in cyan. Schematic of perpendicular placode division. **(F)** Quantifications of division outcomes in IFE and placodes based on live imaging of placodes. Data are mean % ± SD from 322 divisions, *n*=3 embryos. All scales bars, 10μm, except (C), 50μm.

Parallel divisions were largely confined to IFE (Figure 2-2D). By contrast, divisions within placodes were nearly exclusively vertical, leaving one daughter at –3μm and one daughter at +6μm relative to the basal plane (Figure 2-2E). Together, these data showed that perpendicular spindle orientations within the hair placodes result in a basal daughter that remains attached to the basement membrane and a suprabasal daughter that is born unattached. The movies corroborated my spindle axis measurements and showed an equal proportion of parallel and perpendicular divisions in basal IFE, but almost exclusively perpendicular divisions in basal placodes (Figure 2-2F).

To determine when the heterogeneity first arises following the perpendicular divisions within early hair placodes, I performed whole-mount immunofluorescence of late-stage mitoses within placodes (Figure 2-3A). Imaging analysis and quantification revealed that basal daughters differentially inherited Pcad, indicating that these perpendicular divisions are asymmetric (Figure 2-3B,C).

Previous work in *Caenorhabditis elegans* and *Drosophila* has implicated the $G_{\alpha i}$–LGN/AGS3–NuMA–dynein/dynactin pathway in the regulation of asymmetric cell divisions. These proteins are asymmetrically distributed at the cell cortex during mitosis and govern spindle positioning (Knoblich, 2008; Siller and Doe, 2009). In chick neuroepithelium or during mammalian neurogenesis, LGN also regulates spindle orientation, promotes planar divisions, and is symmetrically inherited (Konno et al., 2008; Morin et al., 2007). However, in the

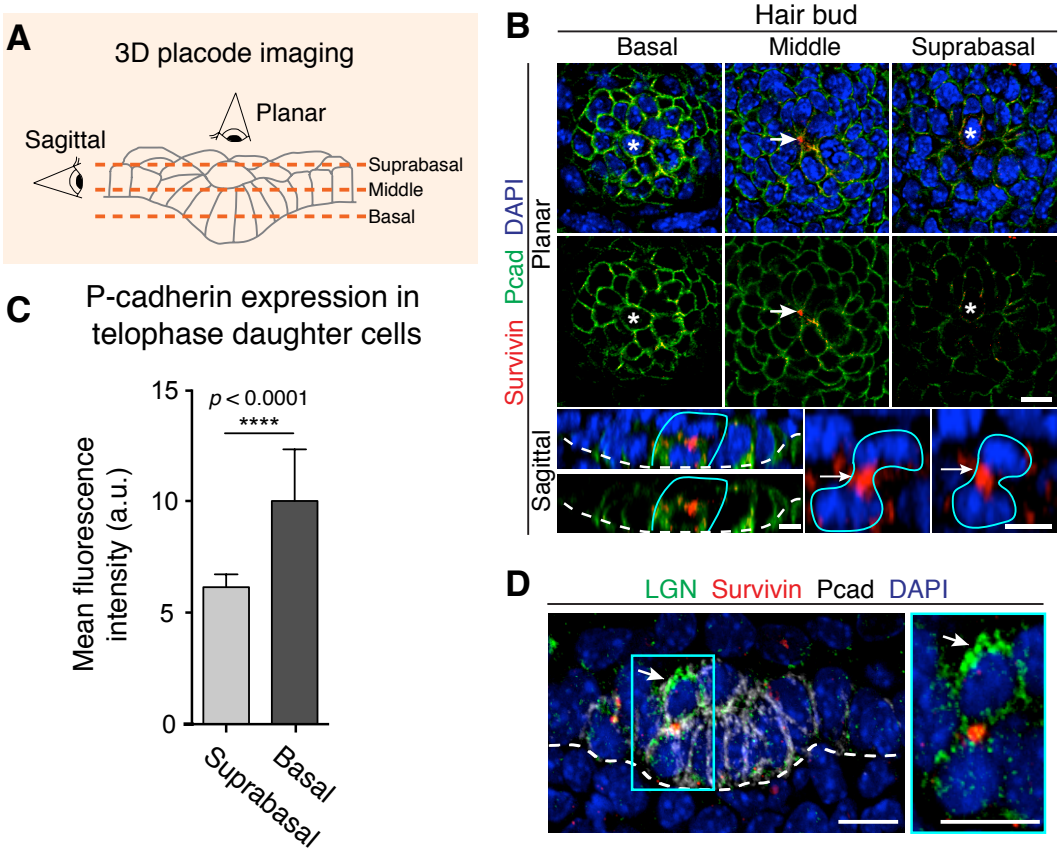

Figure 2-3. Perpendicular divisions within placodes are asymmetric.
(A) Schematic of epithelial bud imaging. Dashed lines mark imaging planes. **(B)** Planar and sagittal projections through hair placode, subjected to whole-mount IMF. Pcad enriched in basal cells. Vertical division (asterisk) marked by Survivin (arrows) to identify midbody of late-stage mitotic daughters (cyan lines). **(C)** Quantifications of Pcad IMF. Data (mean ± SD) are from 3 embryos (*n*=26 doublets). **(D)** Suprabasal enrichment of LGN (arrow) in the suprabasal cell in hair placode. White dashed lines indicate basement membrane. Tissues processed as indicated for immunofluorescence. All scale bars, 10μm, except lower-right sagittal views in (B), 5μm.

developing IFE, LGN is apically localized in dividing cells, and becomes asymmetrically inherited during mitosis. In the IFE, LGN binds to $G_{\alpha i}$, links mitotic spindles to the apical PAR3/aPKC complex, and promotes asymmetric divisions. Disruption of LGN using LV-delivered shRNAs caused spindle orientation defects during divisions of basal IFE cells, which negatively affects epidermis differentiation and leads to barrier defects of affected pups (Williams et al., 2011; Williams et al., 2014).

Similar to the IFE, LGN was also apically localized in perpendicular, late-stage mitotic placode cells, resulting in its asymmetric distribution to suprabasal daughters (Figure 2-3D). Together, this data suggest that the perpendicular divisions within early hair placodes are asymmetric.

Perpendicular divisions in hair placodes asymmetrically partition WNT signaling

WNT signaling is required for hair placode specification, and its levels are increased upon HF specification (Andl et al., 2002; DasGupta and Fuchs, 1999) (Figure 2-4).

However, the role of WNT signaling in establishing cellular heterogeneity within early hair placodes has not been explored. Therefore, I monitored the status of WNT signaling in the basal and suprabasal cells of developing hair placodes. Surprisingly, only basal LHX2+ daughters exhibited intense nuclear

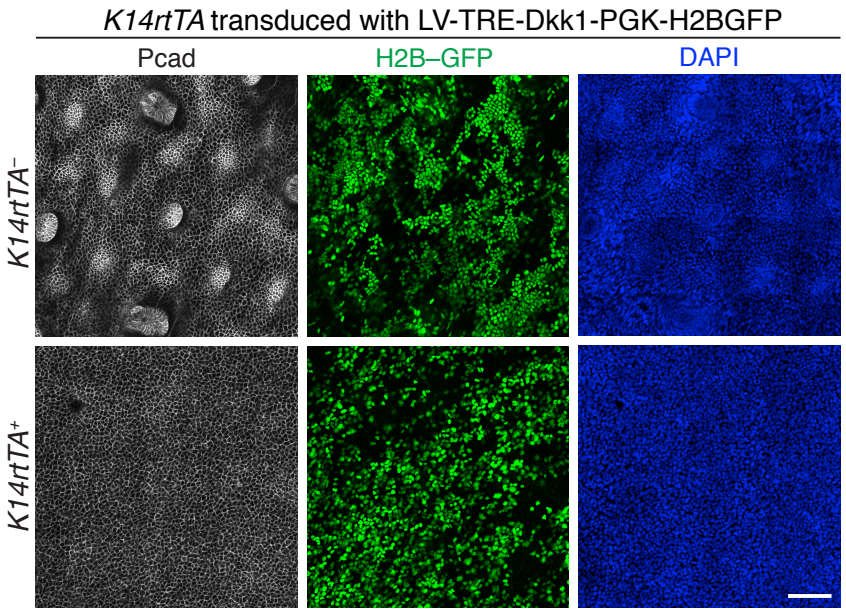

Figure 2-4. Inhibition of WNT signaling blocks hair placode formation. K14rtTA+ and K14rtTA- littermates were transduced with doxycycline-inducible Dkk1 lentivirus, which also expresses H2BGFP under a constitutive PGK promoter. Treatment with doxycycline resulted in Dkk1 overexpression, which blocked hair placode specification.

LEF1, a transcription factor that forms a complex with β-catenin necessary to propagate WNT signal to regulate transcription (Figure 2-5A). Additionally, genetic loss of Lef1 has been previously shown to inhibit HF morphogenesis (van Genderen et al., 1994).

To further address whether Lef1 expression patterns correlate with active WNT signaling, I determined the status of WNT signaling using in vivo WNT reporter activity. Strong activity of WNT reporter Axin2-LacZ (Lustig et al., 2002b) in basal $Pcad^{hi}$ LHX2+ cells confirmed that WNT signaling was high in the daughter cells that remained attached to underlying basement membrane, but decreased in the suprabasal SOX9+ cells (Figure 2-5A).

It has been demonstrated that activated focal adhesion kinase (FAK) has the ability to phosphorylate and inactivate GSK3β (Gao et al., 2015). GSK3β inhibition prevents the phosphorylation of β-catenin, leading to reduced degradation of β-catenin, thus mimicking WNT stimulation (Wu and Pan, 2010). In turn, FAK activity is dependent upon integrin signaling, which mediate adhesion between basal cells and the basement membrane (Parsons, 2003).

Interestingly, in work carried out by my collaborator Vincent Fiore in the Fuchs lab, activated FAK and β1-integrin concentrated on the basement membrane-associated side of WNT^{hi} basal placode cells (Figure 2-5B). This observation was in line with higher levels of WNT signaling in the basal cells of hair placodes, suggesting a possible role for β1-integrin-FAK signaling in stabilizing β-catenin and boosting WNT signaling.

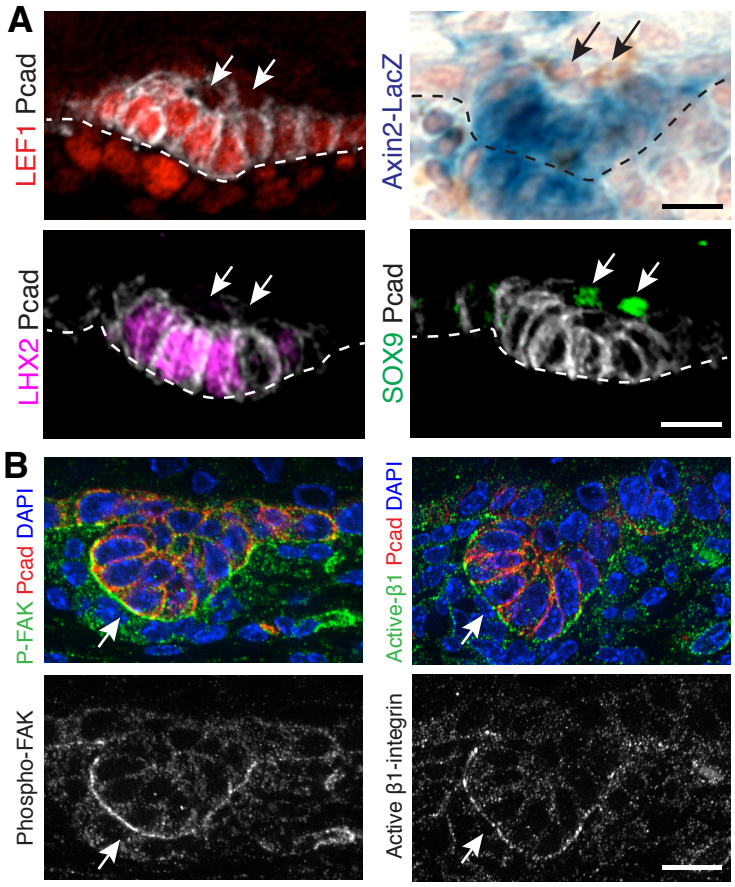

Figure 2-5. WNT signaling is asymmetrically partitioned to basal cells in placodes. (A) IMF or X-gal staining of WT placodes. Note enrichment of WNT-signaling in basal cells and absence of WNT-signaling in suprabasal cells (arrows). **(B)** Basal enrichment (arrows) of phospho-Tyr397 (P)-Focal Adhesion Kinase (FAK) and active β1-integrin in hair buds. White dashed lines indicate basement membrane. Tissues processed as indicated for IMF (Pcad, LEF1, SOX9, LHX2, P-FAK, Active β1-integrin) or X-gal (Axin2-LacZ). All scale bars, 10μm.

Differential WNT-signaling is Key for Coupling Asymmetric Fates to Asymmetric Cell Divisions

The striking difference in the levels of WNT signaling between basal and suprabasal cells within hair placodes suggested that the purpose of the perpendicular divisions within placodes is to release suprabasal daughters from the high-WNT-signaling environment of their parents. Thus, I hypothesized that super-activation of WNT-signaling should prevent SOX9+ cell specification. With my collaborator Irina Matos, I tested this possibility by mosaically ablating the gene encoding APC, a member of the AXIN-APC-GSK3β complex that sequesters and targets non-junctional β-catenin for phosphorylation and proteosome-mediated degradation (Azzolin et al., 2014; Li et al., 2012; Mendoza-Topaz et al., 2011).

Given the severity of conditionally ablating *Apc* in skin (Kuraguchi et al., 2006), we infected E9.5 $Apc^{fl/fl}$; $R26YFP^{fl/+}$ embryos with low-titer LV-Cre. Small mosaic patches of *Apc*-null-derived YFP^{+} epidermal cells exhibited robust WNT-signaling as evidenced by elevated nuclear β-catenin and LEF1 (Figure 2-6A,B). Notably, the *Apc*-null patches were $Pcad^{hi}$ and $LHX2^{+}$ and devoid of SOX9, indicating a skewing of fates relative to their wild-type counterparts (Figure 2-6B).

Within the basal plane, a halo of WT $SOX9^{+}$ cells surrounded the *Apc*-null patches (Figure 2-6B). Since the $SOX9^{+}$ halo was Apc^{WT} while $LHX2^{+}$ cells were *Apc*-null, halo cells could not have been generated by asymmetric cell divisions. Rather, the unifying feature between this mosaic, genetically altered skin and

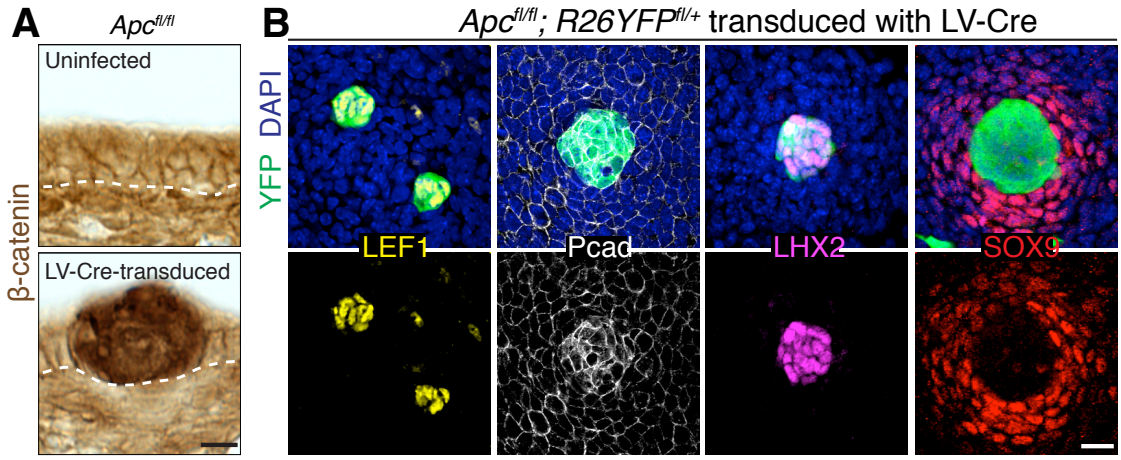

Figure 2-6. SOX9+ cells are associated with APC-null WNT^{high} regions of the epidermis. (A) Immunohistochemistry of *Apc*$^{fl/fl}$ epidermis uninfected (top) or LV-Cre-transduced (bottom), generating *Apc*-null regions with increased WNT activity, indicated by intense β-catenin signal. **(B)** Planar confocal IMF of *Apc*$^{fl/fl}$; *R26YFP*$^{fl/+}$ epidermis mosaic for LV-Cre. Note WNT-hyperactivated next to WNT-normal regions establish boundary for asymmetric cell fates. Tissues processed as indicated for immunohistochemistry (β-catenin) or immunofluorescence (LEF1, Pcad, LHX2, SOX9, YFP). Dashed lines in (A) indicate basement membrane.

native, asymmetrically dividing skin placodes was differential levels of WNT-signaling in LHX2^{+} versus SOX9^{+} neighbors.

To pursue the hypothesis that specification of SOX9^{+} cells is dependent on juxtaposing WNT^{lo} and WNT^{hi} cells, I tested the reverse, namely the consequences to asymmetric cell fates when mosaic clones null for the β-catenin gene (*Ctnnb1*) were juxtaposed with WT clones. For this experiment, I infected E9.5 *Ctnnb1*$^{fl/fl}$*; R26YFP*$^{fl/+}$ or *Ctnnb1*$^{fl/+}$*; R26YFP*$^{fl/+}$ embryos with LV-Cre, generating WT regions and regions that have lost β-catenin.

In WT patches, nuclear LEF1 was seen throughout IFE, even though it was higher in hair placodes. By contrast, *Ctnnb1*-null epidermal patches lacked not only β-catenin, but also nuclear LEF1 (Figure 2-7A). Loss of β-catenin has destabilized adherens junctions, which resulted in the overall reduction of junctional Pcad staining in the epidermis (Figure 2-7B). In highly transduced epidermal regions, basal placode markers LHX2 and high Pcad were not found in *Ctnnb1*-null regions, further underscoring the requirement of WNT-signaling for placode formation (Figure 2-7B). Nevertheless, I was able to find small patches of un-transduced WT cells that formed hair placodes. Notably, a halo of SOX9-expressing *Ctnnb1*-null epidermal cells surrounded these WT placodes. Analogous to the loss of APC experiments, based on the expression of YFP, these SOX9+ cells did not descend from the WT cells constituting the nascent

placodes. Instead, the close juxtaposition of β-catenin-null and WT cells was sufficient to induce the expression SOX9 in those cells.

Interestingly, as demonstrated by LV-Cre-mediated YFP^+ lineage tracing, these $SOX9^+$ cells remained in the epidermis and did not migrate into or contribute to HFs (Figure 2-7C).

Together, these gain- and loss-of-function studies provided compelling evidence that the key feature enabling $SOX9^+$ cell specification is juxtaposition of WNT^{hi} and WNT^{lo} signaling cells, regardless of the absolute levels of WNT signaling activity. I demonstrate here that SOX9+ cell specification can be achieved by juxtaposing APC-null WNT^{hi} cells with WT cells (in which case WT cells act as WNT^{lo}), or by juxtaposing β-catenin-null WNT^{null} cells with WT cells (in which case WT cells act as WNT^{hi}). In developing HFs, this juxtaposition appeared to be achieved through perpendicular asymmetric cell divisions, displacing the suprabasal daughter from the WNT^{hi} environment of its parent and linking asymmetric fates to asymmetric divisions. My findings show that if this condition is met by other means (e.g., through mosaic genetic mutation), asymmetric divisions are not needed to generate asymmetric fates. Thus, although WNT signaling is essential for hair placode specification, it is both dispensable for and also repressive of SOX9 expression.

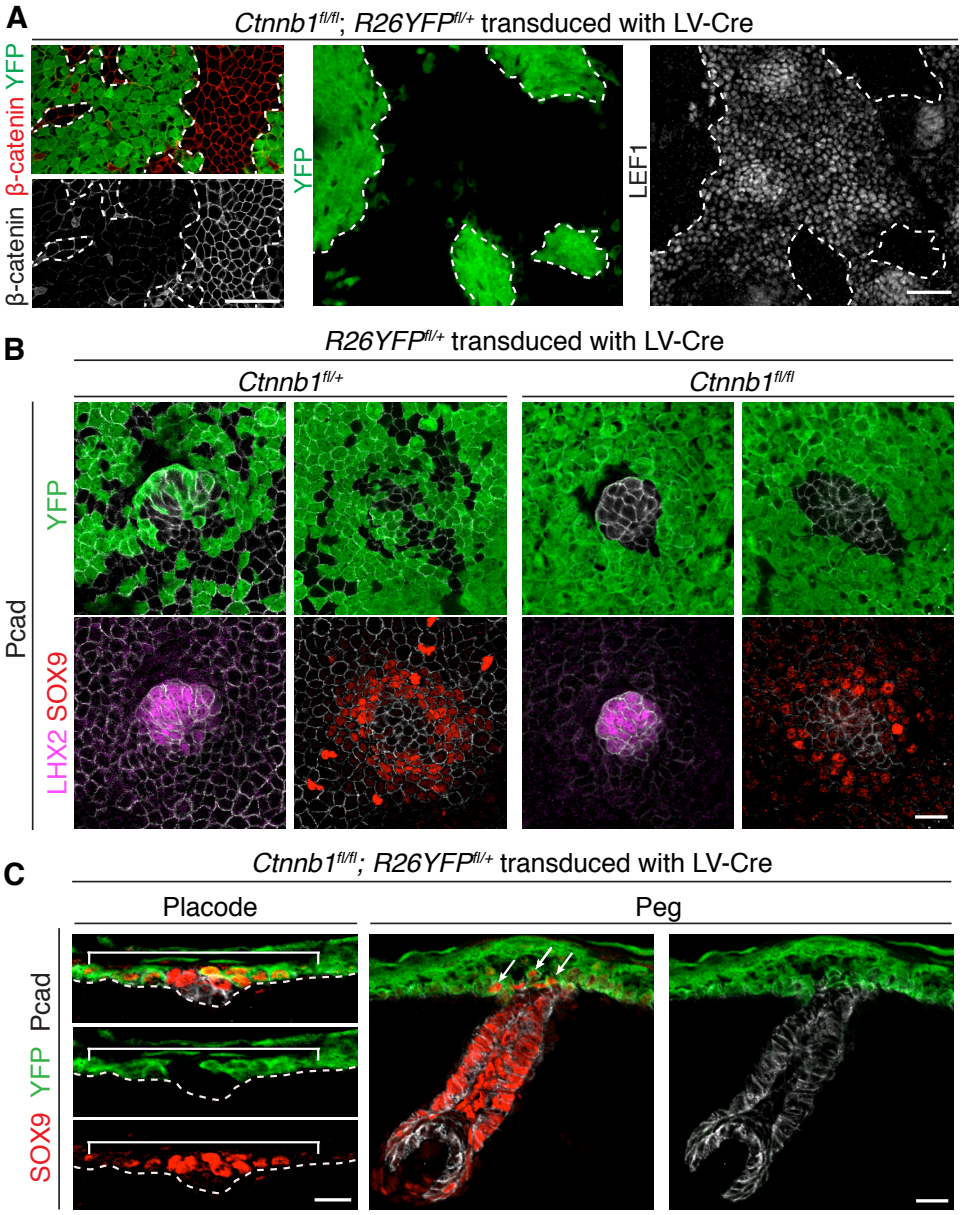

Figure 2-7. β-catenin-null cells acquire SOX9+ fate when juxtaposed next to WT cells. (A) Planar confocal IMF in *Ctnnb1*$^{fl/fl}$*; R26YFP*$^{fl/+}$ embryos transduced with LV-Cre. Note selective loss of LEF1 in IFE patches where β-catenin is absent. **(B)** Planar confocal IMF in *Ctnnb1*$^{fl/fl}$ (or $^{fl/+}$)*; R26YFP*$^{fl/+}$ embryos infected with high-titer LV-Cre to generate small regions of β-catenin^{+} untransduced cells surrounded by β-catenin^{-} transduced cells. **(C)** Sagittal IMF in placode (top) and peg (bottom) of *R26YFP*$^{fl/+}$*; Ctnnb1*$^{fl/fl}$ embryos transduced with LV-Cre. Bracket indicates SOX9^{+} IFE halo. Note YFP^{+} SOX9^{+} IFE cells do not contribute to mature HF. Dashed lines in (C) indicate basement membrane, in (A), borders between transduced and untransduced regions. Scale bars in (A), 50μm; in (B,C), 20μm.

SHH Produced by WNT^{hi} Placode Cells Promotes Symmetric Divisions of SOX9^{+} Cells But Cannot Signal Its Own Cells

My results thus far suggested that SOX9+ cell specification is dependent upon downregulating WNT signaling in the suprabasal cells of the hair placodes. However, if downregulation of WNT signaling was sufficient to specify SOX9+ cells, then all β-catenin-null cells would be SOX9+, yet SOX9+ cells cannot be entirely independent of WNT signaling, as *Ctnnb1*-null epidermal halos of SOX9+ cells were restricted to regions juxtaposed to (WNT-responding) WT placodes. One possibility consistent with these data is that adjacent WNT^{hi} cells generate a downstream effector, which reinforces SOX9+ cell specification and/or expansion. A good candidate was SHH, whose loss does not compromise WNT-signaling nor formation of epithelial buds (Jamora et al., 2003).

Using in situ hybridization, with help from June de la Cruz in the lab, I first verified that the basal WNT^{hi} placode cells are positive for *Shh* (Figure 2-8A). Next, I used Gli1-LacZ reporter to determine which cells are undergoing active SHH signaling (Bai et al., 2002b). As SHH is known to signal to the underlying dermal condensate (Woo et al., 2012), Gli1-LacZ reporter activity in these dermal cells was anticipated (Figure 2-8B). Within developing placodes and germs however, SOX9^{+} cells displayed stronger SHH-reporter activity than basal LEF1/WNT^{hi} cells. Comparing *Shh* expression and WNT and SHH reporter activities, three patterns emerged: 1) Basal hair bud cells produce *Shh* but show only high WNT-signaling and no SHH-signaling; 2) Suprabasal placode cells

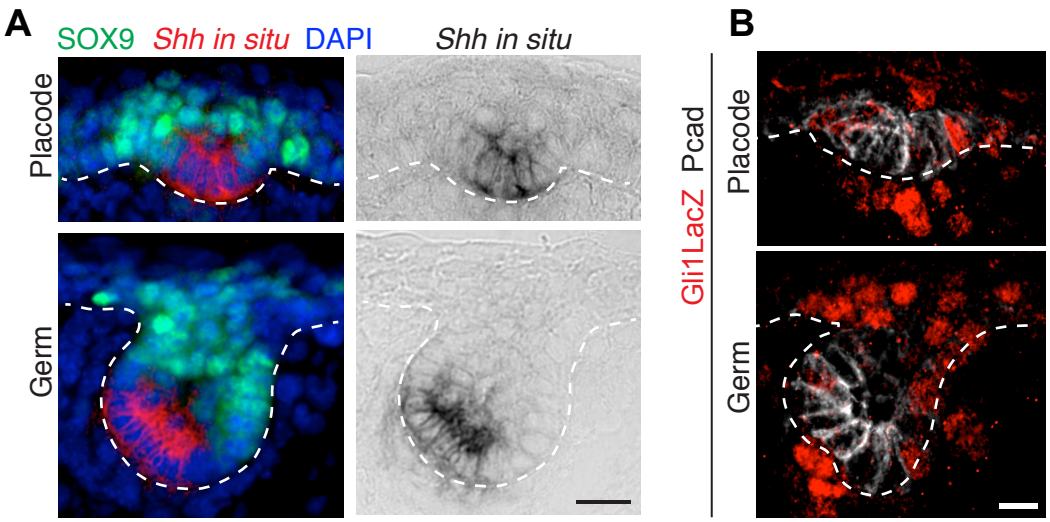

Figure 2-8. WNT^{high} cells express *Shh*, but display little SHH signaling. (A) Combined *Shh in situ* hybridization and SOX9 immunofluorescence (Left) or *Shh in situ* (Right) on sagittal sections of WT hair placode (top) and hair germ (bottom). Note *Shh* expressed by SOX9- basal HF cells. **(B)** Gli1LacZ/βgal immunofluorescence of sagittal sections of placode (top) and hair germ (bottom). Note low SHH-signaling (Gli1LacZ/βgal) in basal Pcad^{high} cells. White dashed lines indicate basement membrane. Scale bars, 10μm.

show low WNT-signaling but elevated SHH-signaling; and 3) Nascent dermal papilla cells exhibit both WNT- and SHH- signaling.

Based on these observations, I had two hypotheses: 1) SHH-producing cells are unable to undergo autocrine SHH signaling; 2) In developing hair buds, high WNT-signaling antagonizes SHH-signaling. To test these hypotheses, I engineered a mouse model that allowed us to activate *Shh* at different stages in epidermis development. I used a transgenic mouse model that constitutively expresses reverse tetracycline transactivator (rtTA) from the epidermis-specific keratin 14 promoter (K14rtTA). Upon treatment with doxycycline, rtTA is activated and can bind to Tet-Reponse Elements (TRE) to drive gene expression. These mice were crossed to Gli1-LacZ reporter mice to monitor SHH signaling. Additionally, I used a lentiviral construct harboring the cDNA for the N-terminal Shh, which does not need to be post-translationally processed, is not lipid-modified and is therefore readily soluble (Zeng et al., 2001). The expression of Shh was driven by a minimal CMV promoter preceded by tandem TRE elements. The LV also harbored a constitutively expressed PGK-H2BGFP cassette to label LV-transduced cells. I transduced E9.5 *K14rtTA; Gli1LacZ* embryos with LV-TRE-Shh-PGK-H2BGFP, which allowed us to visualize which cells were LV-transduced and to induce Shh expression at different points in development by switching them to doxycycline-containing food (Figure 2-9A).

When *Shh* was induced at E13.5 (prior to HF specification) and analyzed at E15.5, ectopic paracrine SHH-signaling occurred in the WT IFE cells

surrounding GFP$^+$ transduced *Shh*-expressing IFE cells (Figure 2-9B). Intriguingly, however, clear signs of autocrine SHH-signaling were also noted, as evidenced by dual presence of H2B–GFP and β-galactosidase. This clearly demonstrated that Shh-expressing cells are competent to undergo autocrine SHH signaling. Interestingly, SOX9 was elevated in regions of and surrounding the transduced GFP$^+$*Shh*^{hi} epidermal patches (Figure 2-9C). Scattered SOX10$^+$ epidermal melanocytes showed Ab cross-reactivity, providing an internal control. To determine if SHH signaling induces the expression of Sox9 alone, or further changes the fate of the SOX9+ cells, I repeated the experiment on the background of K17mRFP reporter mice. Ectopically specified SOX9$^+$ epidermal cells expressed the K17mRFP reporter, analogous to SOX9+ in WT hair placodes (Figure 2-9D).

Moreover, regions of ectopic *Shh* expression showed strong repression of nuclear LEF1, normally present throughout the epidermis (Figure 2-9E). Taken together, these findings suggest that, under conditions where WNT-signaling is normally present but not as high as during placode specification, SHH can signal in autocrine manner and repress WNT signaling.

To explore this antagonism further, I induced *Shh* at E15.5, i.e., at a stage after HF morphogenesis was initiated. Analyses at E17.5 showed that LEF1 expression in the established WNT^{hi} pocket cells of the HF was refractory to elevated *Shh*, and no signs of fate conversion were observed, as transduced cells failed to acquire SOX9+ state (Figure 2-9F).

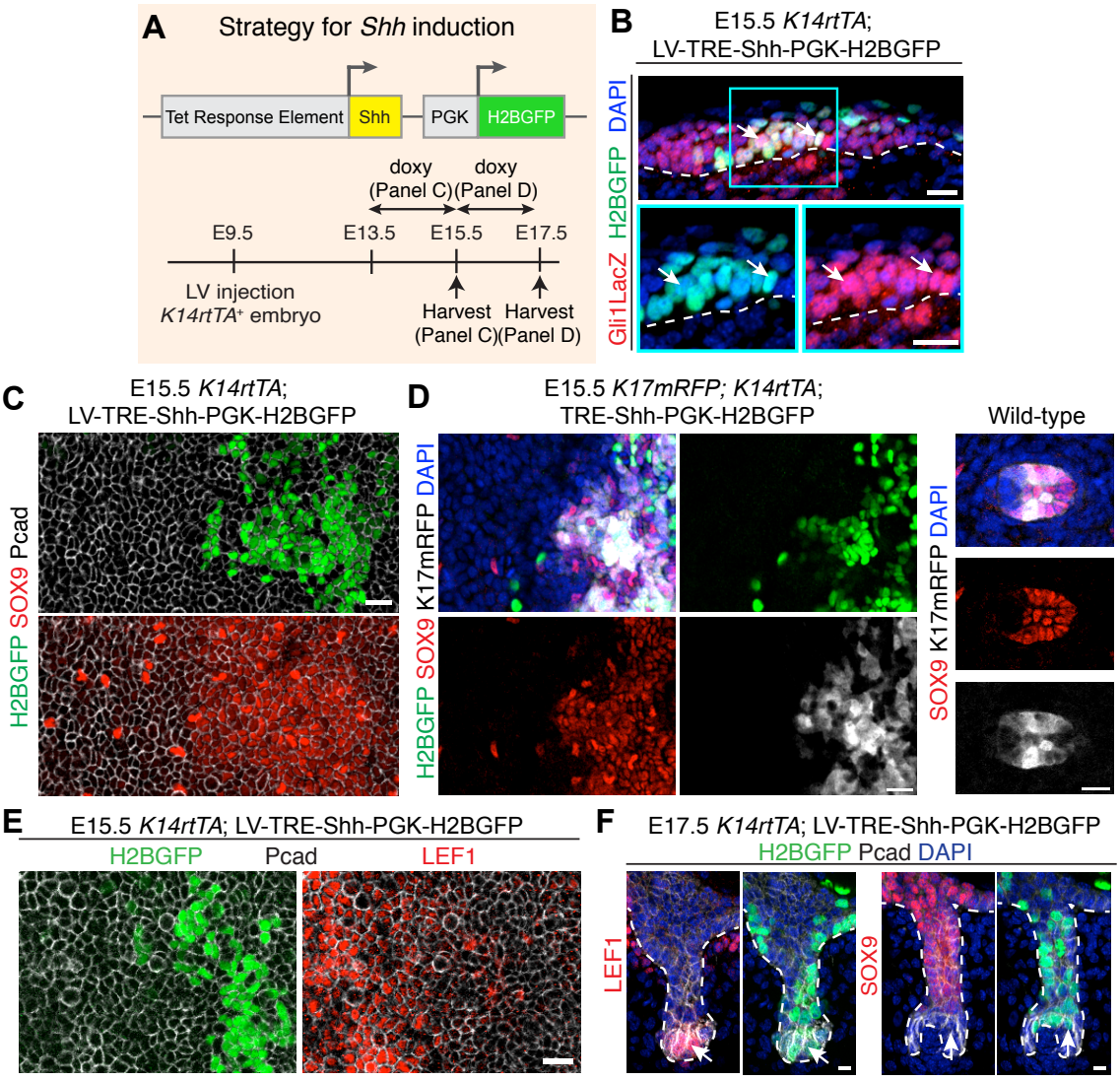

Figure 2-9. Ectopic SHH induces SOX9+ cell fate and inhibits WNT signaling. (A) Strategy for activating ectopic *Shh* in embryonic epidermis. **(B)** Immunofluorescence of sagittal sections of E15.5 *Gli1LacZ* epidermis transduced with LV-TRE-Shh, induced at E13.5, and immunolabeled for Gli1-LacZ. Boxed area is magnified. Arrows denote autocrine SHH-signaling. **(C-E)** Planar confocal IMF of E15.5 *K14rtTA* (C, E) or *K14rtTA*; *K17mRFP* (D) epidermis transduced with LV-TRE-Shh, induced at E13.5, and immunolabeled for SOX9 (C, D) or LEF1 (E). Note SOX9 and K17mRFP induction (C, D) and LEF1 inhibition (E) in transduced regions. **(F)** IMF of sagittal sections of E17.5 HFs transduced with LV-TRE-Shh, induced at E15.5. Note that once HFs start to mature, SHH-transduced pocket cells (arrows) do not show signs of LEF1 reduction or SOX9 induction.

Finally, if autocrine SHH-signaling is repressed by elevated WNT-signaling, then exclusive paracrine signaling should be observed when WNT-signaling is ectopically elevated. To test this hypothesis, I returned to our mosaic *Apc* loss-of-function model. First, Irina and I confirmed that *Shh* expression is dependent on elevated WNT signaling, such that only *Apc*-null cells expressed Shh (Figure 2-10A). Next, we purified WT and *Apc*-null cells from the transduced embryos and performed qRT-PCR. As expected, *Apc*-null cells expressed very high levels of WNT-target gene *Axin2* (Figure 2-10B). However, while these cells expressed high levels of *Shh*, they showed no signs of responding to it, as judged by failure to upregulate SHH target genes *Gli1* and *Ptch1*. Together, these results are consistent with the view that, in cells that do not experience high levels of WNT, autocrine or paracrine SHH signaling can occur and suppress WNT signaling. However, in WNT^{hi} cells expressing *Shh*, such as in WT hair placodes or in *Apc*-null regions, high WNT-signaling prevents autocrine signaling.

Given that the basal cells within hair placodes express high levels of *Shh*, but the suprabasal SOX9+ cells undergo higher levels of SHH signaling, I hypothesized that the role of SHH signaling within developing HFs is to suppress WNT signaling in the suprabasal daughter cells following the asymmetric perpendicular division. To understand the role of SHH signaling in asymmetric fate specification, I analyzed $SOX9^{+}$ and $LEF1^{+}$ populations in *Shh*-null hair buds. However, and in striking contrast to WT HFs, LEF1/WNT^{hi} cells were more

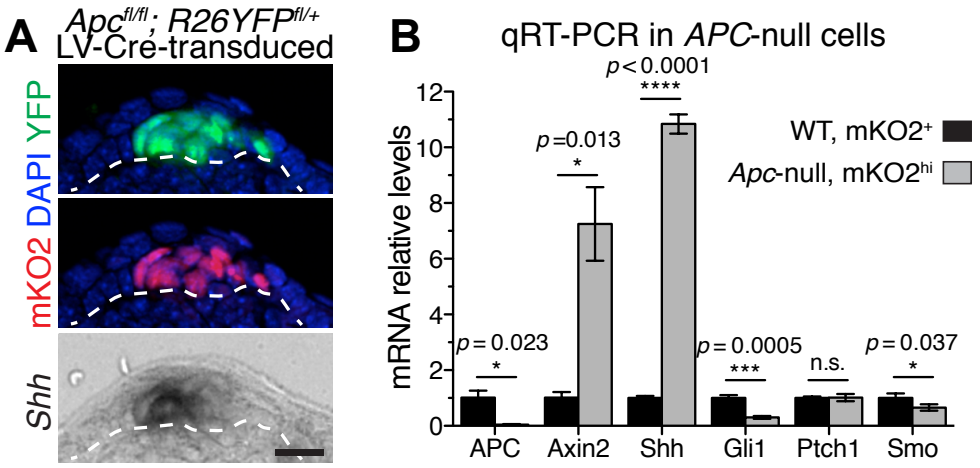

Figure 2-10. WNT^{high} cells produce, but do not respond, to SHH. (A) Sagittal section of combined *in situ* and IMF of *Apc*-null cells from *Fucci; Apc$^{fl/fl}$; R26YFP$^{fl/+}$* epidermis transduced with LV-Cre. Note *Shh* induced in ectopic WNT^{high} cells. **(B)** Quantitative real-time (qRT-)PCR in FACS-purified *Apc*-null and WT cells from n=3 litters, mean ± SD.

abundant than SOX9^{+} cells by the hair germ stage (Figure 2-11B). Moreover, the overall intensity of SOX9 immunofluorescence was reduced in the absence of SHH. Together, these findings demonstrated that although SHH signaling is not necessary for SOX9+ cell specification, it is essential to repress WNT signaling in the suprabasal placode cells, as well as to expand the SOX9+ cells and to boost their fate by suppressing WNT-signaling.

SHH-signaling plays a key role in the recruitment and assembly of the dermal condensate (Karlsson et al., 1999; St-Jacques et al., 1998). To address whether there is an additional crosstalk of epidermally-derived SHH with the dermis that is responsible for the above phenotypes, I analyzed embryos with epidermis-specific loss of *Smoothened*, which is necessary to transduce SHH signaling. WNT-signaling perturbations within *Shh*-null hair buds appeared to emanate from epithelial alterations in SHH-signaling, since they still occurred when I selectively ablated *Smoothened* in embryonic skin epithelium. Thus, in the absence of this key receptor for SHH-signaling, the population of WNT^{hi} LEF1^{+} basal cells was expanded, analogous to what I saw in *Shh*-null hair germs (Figure 2-11C).

Next, I investigated the contribution of SHH signaling to the conferral of SOX9+ status in the suprabasal cells within placode versus the basal SOX9+ cells forming the halo surrounding hair placodes. In contrast to early WT placodes and germs, the surrounding halo of SOX9^{+} IFE cells was missing in

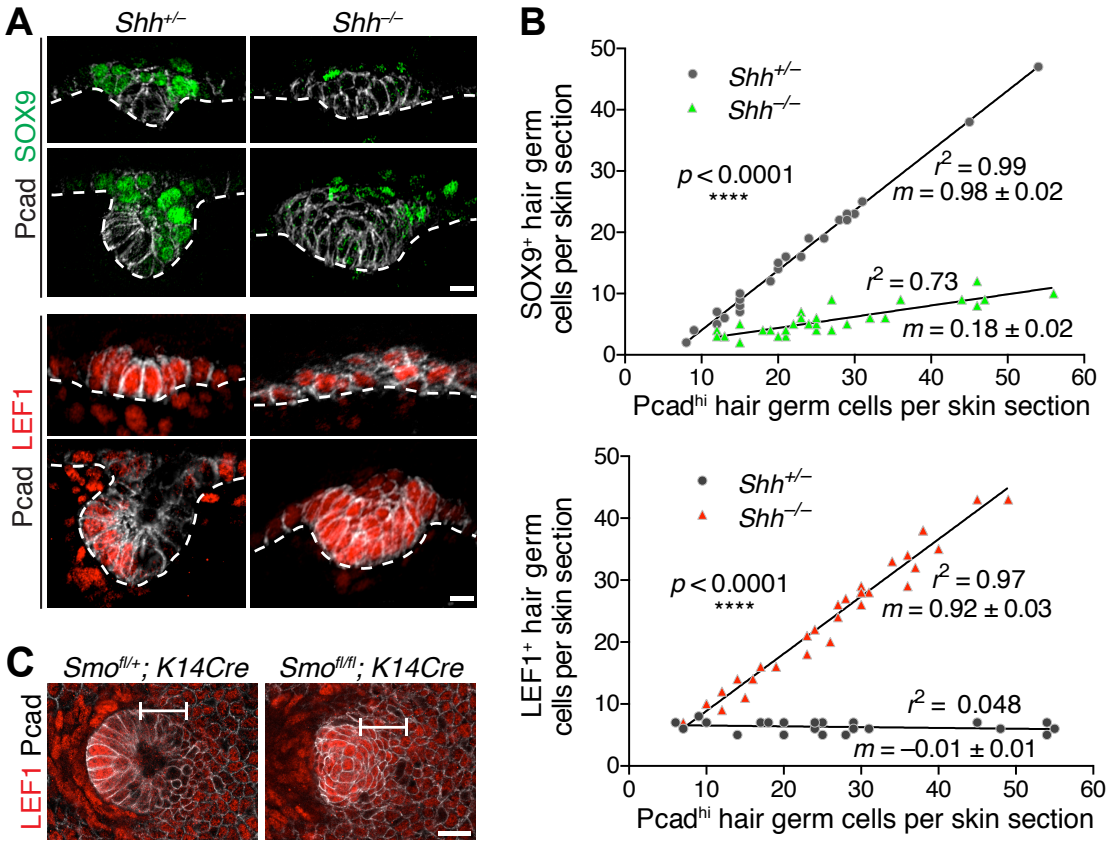

Figure 2-11. LEF1+ cells are expanded, while SOX9+ cells are reduced in *Shh* KO hair follicles. (A) IMF of sagittal sections of *Shh*$^{-/-}$ and *Shh*$^{+/-}$ hair placode and germ. **(B)** Quantifications of SOX9^{+} and LEF1^{+} cells relative to number of Pcad^{+} cells in sagittal sections of *Shh*$^{-/-}$ and *Shh*$^{+/-}$ HFs. *m* is slope ± standard error. r^2 is coefficient of determination. Epithelial buds of same stage and size were compared from n=3 embryos, 54 HFs for SOX9, 105 HFs for LEF1. **(C)** Planar confocal IMF of epithelial-specific *Smoothened* heterozygote and *Smoothened*-null hair bud showing LEF1 expanded suprabasally (brackets), as in *Shh*-null embryo.

Shh-null placodes, even though suprabasal SOX9^{+} cells were still found (Figure 2-12A). To determine whether paracrine SHH signaling is responsible for the appearance of the SOX9+ halo, I transduced *Smo*$^{fl/fl}$*; R26-YFP*$^{fl/+}$ embryos with LV-Cre to generate mosaic hair placodes, where some cells have lost Smo. Smoothened-null cells still contributed to the pool of suprabasal SOX9+ placode cells, but not to IFE halos of SOX9+ cells (Figure 2-12B).

Finally, the imbalance of SOX9^{+} and LEF1^{+} daughter cells in *Shh*-null hair buds could be caused by defect in spindle positioning during cell divisions, if they were regulated by SHH signaling. However, when I quantified the orientation of cell divisions within Shh-null hair placodes, they were still exclusively perpendicular to the underlying basement membrane (Figure 2-12C). These data further underscore the importance of WNT, but not SHH, for these divisions.

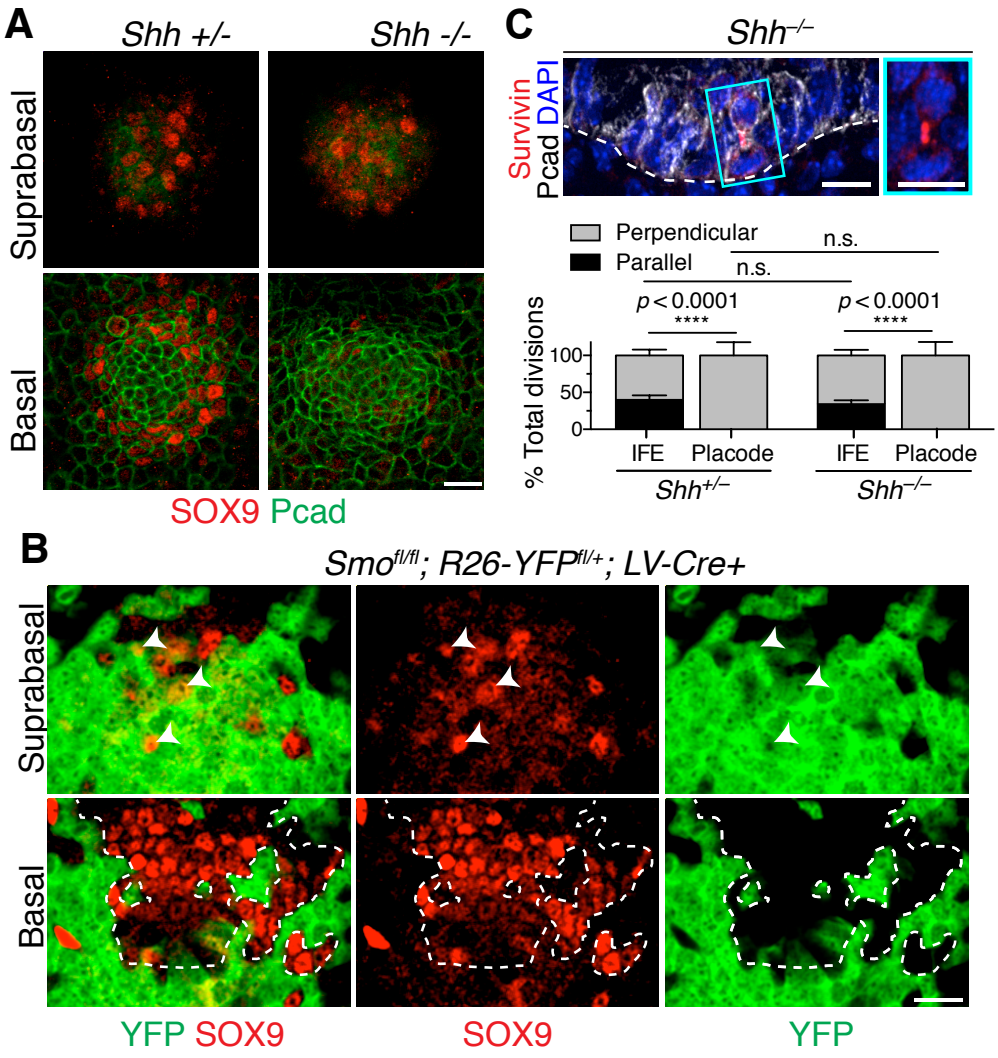

Figure 2-12. SHH signaling specifies basal SOX9+ cells surrounding developing hair placodes. (A) Planar confocal IMF of basal and suprabasal cells in a placode from E15.5 *Shh*$^{+/-}$ *and Shh*$^{-/-}$ epidermis immunolabeled for SOX9 and Pcad. Note SOX9+ suprabasal cells and their absence in the basal layer of *Shh*$^{-/-}$ placode. **(B)** Planar confocal IMF of basal and suprabasal cells in a placode from E15.5 *Smo*$^{fl/fl}$*; R26YFP*$^{fl/+}$ embryos transduced mosaically with LV-Cre, immunolabeled for SOX9 and YFP. Note the absence of SOX9+ cells in the transduced (outlined) basal, but not suprabasal, cells (arrowheads). **(C)** (Top) IMF of sagittal sections of *Shh*$^{-/-}$ hair bud showing perpendicular divisions occurring independently of SHH-signaling (boxed region magnified at right). (Bottom) Quantifications of division orientations in IFE and placodes of *Shh*$^{+/-}$ and *Shh*$^{-/-}$ placodes. Data are % ± SD (*Shh*$^{-/-}$: 30 divisions in 13 HFs, 116 divisions in IFE; *Shh*$^{+/-}$: 31 divisions in 11 HFs; 98 divisions in IFE).

Discussion

To determine how heterogeneity arises during the earliest stages of HF morphogenesis, I performed mosaic short-term lineage tracing using epidermis-specific lentiviral transduction. I found examples of single clones composed of 2-3 cells, organized perpendicular to the basement membrane. Although the clones have arisen from a single progenitor, the cells expressed different markers, with the suprabasal cell becoming SOX9+ and the basal cell remaining $Pcad^{hi}$ and SOX9-, suggesting that they have acquired differential fates shortly after the division. The perpendicular organization of the clones suggested that they have arisen from a progenitor undergoing a perpendicular asymmetric division relative to the basement membrane.

In previous studies, analyses of spindle orientations in skin were confined to either epidermis (Clayton et al., 2007; Lechler and Fuchs, 2005; Williams et al., 2011) or basal cell carcinomas (BCCs) (Larsimont et al., 2015). It is striking that, in contrast to epidermis where perpendicular spindles peak at ~50-60%, or to BCC where epidermal orientations are randomized, virtually all hair placode spindles are oriented perpendicularly.

The mechanism behind the exclusively perpendicular divisions within hair placodes remains to be elucidated. Oscar Hertwig has proposed over 100 years ago that cells preferentially divide along their long axes, suggesting that cell shape determines cell division orientation (Hertwig, 1884). More recently, computational models have been developed that can predict the division axis

based on cell shape (Minc et al., 2011). However, cell polarity and attachment to the extracellular matrix also affect the orientation of cell division (Grill et al., 2001; Thery et al., 2005). During the first steps of hair placode formation, cells undergo centripetal migration and compaction (Ahtiainen et al., 2014). This results in dramatic cell shape changes within the developing hair placode, where cells become apico-basally elongated. Both cell compaction and apico-basal elongation might in turn contribute to orienting cell division perpendicular to the basement membrane.

The relation between placode formation, asymmetric cell division, and SOX9+ cell specification became particularly intriguing when I first observed signs of asymmetric partitioning of WNT-signaling between placode daughters following the division. Growing evidence has suggested that WNTs may be a critical link between SC niche signaling and oriented cell divisions. In the early *C. elegans* embryo, WNT-signaling is coupled to spindle orientation through polarization of the β-catenin destruction complex (Cabello et al., 2010; Sugioka et al., 2011). In cultured human pluripotent SCs, a polarized bioactive WNT bead applied to one side of the cell surface results in an asymmetric division, with nuclear β-catenin confined to the daughter touching the WNT bead (Habib et al., 2013). In another study, membrane receptors for non-canonical WNT signaling antagonize canonical WNT signaling in adult hematopoietic SCs to differentially control proliferative states of daughters (Sugimura et al., 2012). Our findings now suggest a tantalizing possibility that during epithelial bud formation, the basement

membrane polarizes and restricts canonical WNT signaling, such that the pathway becomes asymmetrically partitioned in a perpendicular division.

A myriad of factors could participate in polarizing WNT signaling to the basal side of placode cells. Heparin sulfate proteoglycans, which can bind and modulate WNT ligands, are enriched within basement membranes (Astudillo and Larrain, 2014; Baeg et al., 2001). The basement membrane is known to polarize a number of surface receptors including integrins that are essential for proper spindle orientation (Lechler and Fuchs, 2005), and similar intertwined or independent interactions could also polarize WNT receptors. Preferential activation of integrins and associated FAK on the basal side of placode cells favors FAK's direct inactivation of GSK3β (Gao et al., 2015) and β-catenin stabilization basally. Conversely, since APC orients mitotic spindles of *Drosophila* germ cells relative to the hub cells (Yamashita et al., 2003) and can associate with PAR3/aPKC in mammalian cells (Etienne-Manneville and Hall, 2003; Kodama et al., 2003), the β-catenin destruction complex is favored to be apically enriched. Although the mechanism remains incompletely understood, the highly polarized placode cells and underlying basement membrane provide an environment conducive to preferentially retaining WNT-signaling in the basal daughter and reducing it in the suprabasal daughter of asymmetric cell divisions.

Suprabasal fates of asymmetrically dividing epidermal and placode cells differ markedly. Based on our findings, these differences appear to be rooted in relative levels of β-catenin/LEF activity within basal progenitors. Indeed, our

mosaic loss- and gain-of-function studies provided powerful genetic evidence that WNT-signaling and its associated SHH expression within basal progenitors are critical for reducing WNT-signaling and elevating SHH-signaling in suprabasal placode daughters to a level compatible for SOX9 induction. Our ability to genetically uncouple asymmetric cell fates from both perpendicular and asymmetric cell divisions by juxtaposing WNT^{hi} and $WNT^{neg/lo}$ cells underscores the importance of asymmetric cell divisions in establishing this condition within the native epithelial bud. Interestingly, it is not the absolute levels of WNT signaling that determine cell fates, but rather the relative levels of WNT signaling in the juxtaposed cells. For example, pairing β-catenin-null cells (WNT^{neg}) with WT cells endows the β-catenin-null cells with the SOX9+ fate. At the same time, juxtaposing APC-null (WNT^{hi}) cells with WT cells endows the WT cells with the SOX9+ fate. This uncoupling illustrates how changes in microenvironment and/or genetic mutations can alter cell fates.

The incompatibility of elevated WNT signaling and SOX9 expression in developing HFs is reminiscent of their mutually exclusive signaling in digit patterning (Raspopovic et al., 2014). Additionally, knockout of β-catenin in the limb results in the expansion of Sox9 toward the ectoderm, whereas β-catenin gain-of-function results in Sox9 down-regulation (Hill et al., 2005; Hill et al., 2006).

While juxtaposition of WNT^{hi} and WNT^{lo} cells is sufficient to induce SOX9+ fate in the WNT^{lo} cells, I also found that the levels of SOX9 and the expansion of

SOX9+ cells depends on SHH signaling. Previously, it was observed that, in E18.5 skin of *Shh*-null or *Gli2*-null embryos, SOX9 is low or absent, and when SMOOTHENED or SHH signaling are superactivated in adult epidermis, SOX9-expressing BCCs develop (Larsimont et al., 2015; Vidal et al., 2005). Interestingly, BCC formation and Sox9 expression on the background of constitutively active Smoothened still requires WNT/β-catenin (Yang et al., 2008; Youssef et al., 2012). Additionally, SOX9+ cells also seem to undergo WNT signaling, based on nuclear β-catenin staining both in early human and mouse BCCs (Yang et al., 2008). It is not clear at present what role WNT signaling has in the initiation of BCC and in the regulation of SHH signaling and Sox9 expression. While all my SHH overexpression experiments were done on WT background, it would be interesting to repeat them on WNT^{null} background, to determine whether Sox9 induction by SHH is also dependent on WNT signaling embryonically. While it is clear from the mosaic β-catenin loss-of-function data that cell autonomous WNT signaling is not required for Sox9 expression, it is possible that additional factors expressed by WNT-signaling cells are necessary for Sox9 induction.

Another long-standing mystery is why the *Shh*-expressing pocket in HFs is so small (DasGupta and Fuchs, 1999; Noramly et al., 1999; St-Jacques et al., 1998). Our genetic studies show that elevating WNT-signaling in the hair placode generates SHH, but raises the threshold for autocrine SHH-signaling. Conversely, if WNT-signaling is sufficiently low, the block in autocrine SHH-

signaling can be lifted and SHH is able to repress low-moderate levels WNT signaling.

SHH-WNT antagonism has been shown to play a role in several other developmental systems. For example, it also plays a role in taste papilla development, where Shh expression is WNT/β-catenin-dependent, but at the same time SHH antagonizes WNT signaling (Iwatsuki et al., 2007). Additionally, crosstalk between WNT and SHH signaling sets up the dorsoventral patterning of the vertebrate nervous system. In this case, WNT induces the expression of Gli3, a negative regulator of SHH signaling, thus restricting SHH response (Alvarez-Medina et al., 2008). Finally, reciprocal antagonism between WNT and SHH signaling regulates the extent of neural stem cell proliferation in the *Xenopus* retina (Borday et al., 2012). In this case, Wnt and Hedgehog signalling pathways restrain each other's activity through the transcriptional regulation of Gli3 and Sfrp-1.

The mechanisms mediating the mutual WNT-SHH antagonism in the developing HFs remain to be elucidated. It has been previously demonstrated in 293 cells that Sox9 overexpression can suppress β-catenin-induced expression of the WNT reporter TOPFLASH (Akiyama et al., 2004). This inhibition is not achieved by SOX9 binding and competing at the Tcf/Lef DNA-binding sites. On the other hand, SOX9 C-terminal transactivation domain can directly interact with the Armadillo repeats of β-catenin and compete for binding with TCF/LEF transcription factors. Additionally, binding of SOX9 and β-catenin induces β-

catenin degradation, which can be inhibited by MG132, a proteasome inhibitor (Akiyama et al., 2004; Topol et al., 2009). Therefore, it is possible that SHH-driven induction of Sox9 further dampens WNT signaling, by competing with TCF/LEF binding to β-catenin and by inducing its degradation.

Irrespective of mechanism, the outcome of this balanced antagonism between WNT and SHH signaling is that WNT^{hi} basal cells divide asymmetrically to generate WNT^{lo} daughters, which later become SCs. As our genetic analyses confirm, these features are WNT-dependent and SHH-independent. By contrast, in a SHH-dependent and WNT-independent fashion, SHH-signaling reinforces expression of the SOX9 master regulator by dampening WNT signaling and expands the SC pool. Genetic perturbation of either WNT-signaling or SHH-signaling specifically within the epithelium is sufficient to skew differential fate outcomes and behaviors.

Materials and Methods

Mouse Strains and constructs

All animals used for the experiments were generated previously: *K14-rtTA,* $Smo^{fl/fl}$*,* Shh^{neo}*,* $Gli1^{Lacz}$, $Rosa26^{Flox\text{-}Stop\text{-}Flox\text{-}YFP}$, $Ctnnb1^{fl/fl}$*, Axin2LacZ, Fucci*, and $Apc^{fl/fl}$ (Bai et al., 2002a; Brault et al., 2001; Chiang et al., 1999; Corrales et al., 2006; Dassule et al., 2000; Harfe et al., 2004; Kuraguchi et al., 2006; Litingtung et al., 1998; Long et al., 2001; Lustig et al., 2002b; Mao et al., 1999; Muzumdar et al., 2007; Nguyen et al., 2006; Sakaue-Sawano et al., 2008; Soeda et al.,

2010; Srinivas et al., 2001) were described previously. *Lhx2-EGFP* mice were from The Gene Expression Nervous System Atlas (GENSAT) Project, NINDS Contracts N01NS02331 & HHSN271200723701C to The Rockefeller University (New York, NY, USA). K14-H2BGFP transgenic mice were generated with standard pronuclear injections (Fuchs Lab). Lentiviral doxycycline-inducible Shh overexpression construct (LV-TRE-Shh-PGK-H2BGFP) has been previously described (Hsu et al., 2014b). Construct for the lentiviral CreER^{T2} has been previously described (Williams et al., 2014). Construct for the lentiviral Cre has been previously described (Beronja et al., 2010). Dkk1 from pCS2+ Dkk1-flag (gift from Xi He (Addgene plasmid # 16690)) was cloned by PCR to replace Shh in the LV-TRE-Shh-PGK-H2BGFP.

Embryo Preparation, Immunofluorescence and In Situ *Hybridization*

For immunofluorescence, embryos were fixed in 4% PFA in PBS for 1h at room temperature and washed extensively in PBS. For whole-mount or tissue sections, samples were permeabilized for 3 hours in 0.3% Triton X-100 in PBS, or embedded in OCT (Tissue Tek), cut at a thickness of 10µm and permeabilized for 10 min 0.3% in Triton X-100. Tissue samples were then blocked in Gelatin Block (2.5% fish gelatin, 5% normal donkey serum, 1% BSA, 0.3% Triton, 1× PBS). When immunolabeling with mouse antibodies, sections were incubated with the M.O.M. blocking kit according to manufacturer's instructions (Vector Laboratories). The following primary antibodies were used: P-Cadherin (goat,

1:400, R&D AF761), phospho-Tyr397 FAK (rabbit, 1:200, Cell Signaling D20B1), active β1-integrin (rat, 1:150, BD, 9EG7) Survivin (rabbit, 1:300, Cell Signaling 2808), LEF1 (rabbit, 1:300, Fuchs Lab), SOX9 (rabbit, 1:300, Fuchs Lab), LHX2 (rabbit, 1:2000, Fuchs Lab), anti-GFP/YFP (chicken, 1:2000, Abcam), β-catenin (mouse, 1:1000, BD 610154), acetylated tubulin (mouse, 1:500, Sigma T7451), Beta-Gal (rabbit, 1:10000, MP Bio). Primary antibodies were incubated at 4C overnight. After washing with 0.3% Triton X-100 in PBS, samples were incubated for 2h at room temperature with secondary antibodies conjugated with Alexa 488, RRX, or 647 (respectively, 1:1000, 1:500, and 1:100, Life Technologies). Samples were washed, counterstained with 4'6'-diamidino-2-phenilindole (DAPI) and mounted in Prolong Gold.

LacZ-derived β-galactosidase activity was assayed on frozen sections (10μm) fixed with 0.5% glutaraldehyde in PBS for 2 min, washed with PBS, and then incubated with 1 mg/ml Xgal substrates in PBS with 1.3 mM $MgCl_2$, 3 mM K3Fe(CN)6, and 3 mM K4Fe(CN)6 for 1 hr at 37C. *In situ* hybridization for *Shh* was performed as described previously (DasGupta and Fuchs, 1999).

Immunohistochemistry

Pre-fixed (4% PFA in PBS) paraffin embedded embryos were cut at 10μm. Immunohistochemistry was performed by incubating sections at 4 °C overnight with primary antibodies against mouse anti-β-catenin (mouse, 1:1000, Sigma, 15B8). For brightfield immunohistochemistry, biotinylated species-specific

secondary antibodies followed by detection using (ImmPRESS reagent kit peroxidase Universal - Vector Labs) and DAB kit (ImmPACT DAB Peroxidase (HRP) SubstrateVector Labs) were used according to the manufacturer's instructions.

Confocal and Epifluorecence Imaging

Epifluorescence images were acquired with an Axio Oberver.Z1 microscope equipped with a Hamamatsu ORCA-ER camera (Hamamatsu Photonics), and with an ApoTome.2 (Carl Zeiss) slider that reduces the light scatter in the fluorescent samples, using 20×, 40×, and 63× objectives, controlled by Zen software (Carl Zeiss). Confocal images were acquired with a Zeiss LSM780 laser-scanning microscope (Carl Zeiss MicroImaging) through a 40× or 63× oil objective. For whole mount imaging, *z* stacks of 20–40 planes (0.25mm) were acquired.

Lentiviral Lineage Tracing

LV-CreER^{T2} was used for short-term lineage tracing as previously described (Williams et al., 2014). This construct was found to have no detectable leakiness in the absence of tamoxifen both *in vitro* and *in vivo*. The *R26flox-stop-flox-YFP* mouse was used as a reporter for Cre activation and to trace progeny. The fluorescent signal was detected using a polyclonal antibody against GFP, which recognizes cytoplasmic YFP, whose progeny could then be discriminated

on the basis of their proximity. Low-titer virus containing the CreER^{T2} cassette was transduced into E9.5 embryos and clonal recombination was induced by administering a single dose of tamoxifen (4mg per dam) by oral gavage, as intraperitoneal injection of tamoxifen at doses sufficient to induce recombination frequently led to aborted litters. 48h following tamoxifen administration was empirically determined to be sufficient to allow most clones labeled to consist of 1–3 cells. Tamoxifen was administered at E15.5 to monitor peak placode formation. Although CreER^{T2} was delivered at the time when the epidermis was a single layer of basal cells, it will be expressed in all of their descendants owing to its ubiquitous PGK promoter. Only cells within early epithelial buds were counted as it is unlikely that they were present at the time of labeling given the rapid rate of HF morphogenesis at this age. Clones were imaged with Pcad and SOX9 as markers.

Spindle Orientation and Division Measurements

The method for measurement of division angles has been described previously (Williams et al., 2014). Briefly, late-stage mitotic cells were identified by the presence of survivin immunoreactivity at the midbody/cleavage furrow. Cells were scored only if both daughter nuclei surrounding the survivin staining could be unambiguously identified. Angles were measured by drawing a line through the centers of the two nuclei, and parallel to the basement membrane. To reduce any bias in data collection, all data from each group were not analyzed until all

images were collected. *n* values are indicated in the main text; each experiment was repeated with at least two replicates and data from at least 3 embryos. No statistical method was used to predetermine sample size, but data were collected from all available embryos of the indicated genotypes. All graphs and statistical analyses (Fisher's exact tests) were produced using Prism.

CHAPTER 3: SPECIFICATION AND CONTROL OF THE EARLIEST HAIR FOLLICLE STEM CELL PROGENITORS

While the heterogeneity within developing HFs can be observed very early during HF morphogenesis, the earliest time point when HFSCs are specified remains to be elucidated. Interestingly, LHX2 and SOX9 – two transcription factors critical for HFSC specification and maintenance – are expressed as early as during the placode stage of HF morphogenesis (Nowak et al., 2008; Rhee et al., 2006). Additionally, SOX9 is a pioneer transcription factor, whose expression is sufficient to dramatically change the chromatin architecture and induce the expression of previously polycomb-repressed genes (Adam et al., 2015).

As I have discussed in the previous chapter, SOX9+ cells are specified by perpendicular asymmetric divisions of SOX9- basal placode cells via WNT-SHH antagonism. To determine if the SOX9+ cells specified during early placode morphogenesis might be the HFSC progenitors and later contribute to the adult HFSC pool, I performed lineage tracing of different populations of hair placode cells. Additionally, I elucidated the mechanisms involved in the control of HFSC progenitor numbers specified via asymmetric divisions. Interestingly, basal WNT^{high} placode cells undergo slow divisions, and spend prolonged periods of time in the G1 phase of the cell cycle. On the other hand, SOX9+ HFSC progenitors undergo more rapid divisions. Finally, I also found that only early divisions within the hair placode give rise to SOX9+ HFSC progenitors, while later

divisions give rise to the differentiated lineages within the HF, further restricting the HFSC progenitor pool.

Results

SOX9+ cells specified by asymmetric cell divisions within hair placodes contribute to the adult HFSC pool

As I have discussed in Chapter 2, *Shh* is expressed exclusively by the basal WNT^{hi} placode cells, and is absent from the SOX9+ cells. Additionally, SOX9+ cells are specified by perpendicular asymmetric cell divisions of the basal WNT^{hi} Shh+ cells. Previous experiments with *R26LacZ* reporter mice showed that progeny of both *ShhCre* (Levy et al., 2005) and *Sox9Cre* (Nowak et al., 2008) label the entire HF, but they were unable to address temporal contributions of SHH+ and SOX9+ cells to various lineages within the developing HFs.

To assess whether the SOX9+ cells generated via early asymmetric cell divisions within the hair placode contribute to the adult HFSC pool, I used *ShhCreER* lineage tracing to label cells in early hair buds and trace their fate. To support our finding that SHH^+ cells divide perpendicularly and give rise to suprabasal $SOX9^+$ cells, Aaron and I labeled SHH^+ cells within early hair buds using *ShhCreER; R26mTmG*$^{fl/+}$ embryos. In this mouse model, prior to Cre-mediated recombination, all cells within the animal are Tomato+. Upon recombination, the expressed fluorescent protein switches from tomato to GFP. 30h after tamoxifen induction, we performed two-color live imaging of hair

placodes, which were the only structures with GFP^+ cells (Figure 3-1A, left). Over 18h of imaging, only a few GFP^+ (SHH^+) mitoses were observed. However, these divisions were perpendicular, generating one daughter cell atop the other (Figure 3-1A, right).

Next, I labeled a small number of cells within E14.5→E17.5 *ShhCreER; R26YFP*$^{fl/+}$ hair buds by a single tamoxifen treatment and traced their fates into adulthood. YFP^+ cells were seen within the expected domains of emerging placodes and germs (Figure 3-1B). Only basal cells were labeled at the placode stage, in agreement with Shh being expressed only in that population, also demonstrating that *ShhCreER* faithfully recapitulates endogenous Shh expression (Figure 3-1B, top left). As the HFs progressed through morphogenesis into the hair germ and hair peg stages, SOX9+ cells became YFP+, showing that they are progeny of the Shh+ basal cells (Figure 3-1B, germ and peg).

As a positive control, I used *Sox9CreER; R26YFP*$^{fl/+}$, which was expected to label SOX9+ cells, but not basal WNT^{hi} Shh+ SOX9- cells. Lineage tracing using *Sox9CreER* clearly demonstrates that the progeny of SOX9+ cells does not contribute to the basal WNT^{hi} pocket and instead remains at the upper part of invaginating HFs (Figure 3-1B). Thus, as predicted from our findings, *Shh*-expressing cells gave rise to $SOX9^+$ daughters, but *Sox9*-expressing cells at these early stages generated only $SOX9^+$ daughters and did not contribute to the WNT^{hi} *Shh*$^+$ pocket.

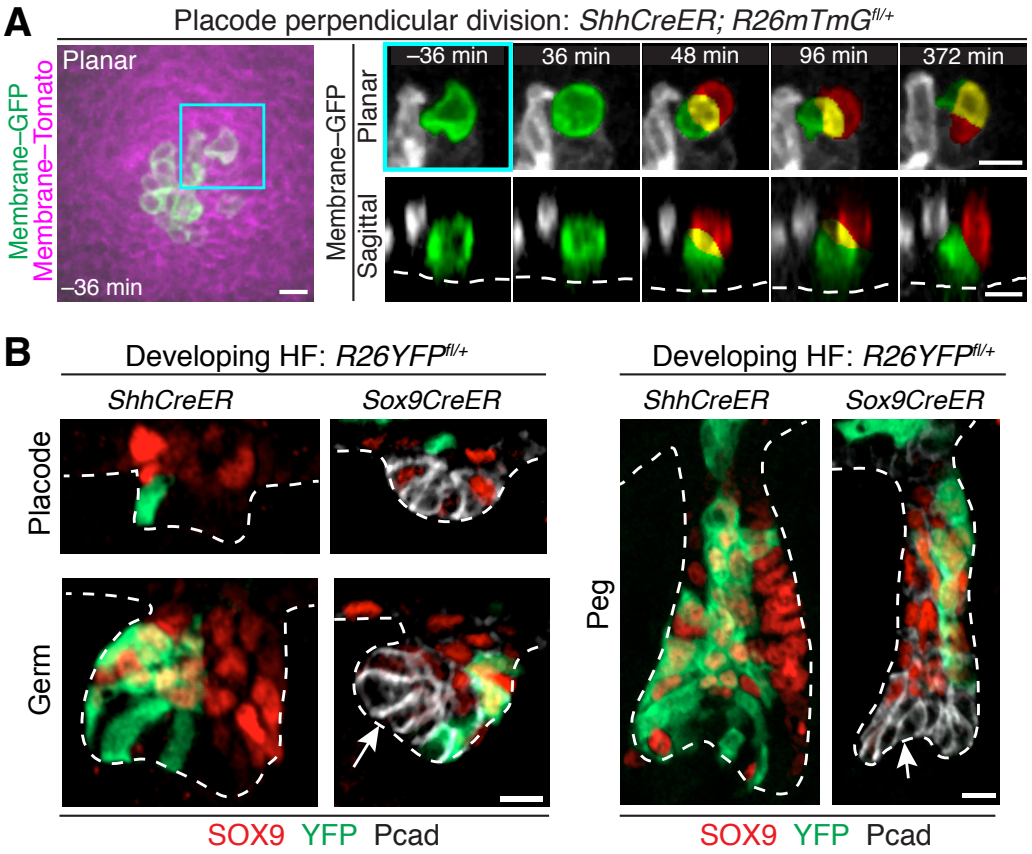

Figure 3-1. Embryonic ShhCreER and Sox9CreER lineage tracing. (A) Live imaging of perpendicular division of SHH^{+} placode cell. (Left) Labeled membrane shows SHH^{+} (GFP^{+}) cells within a placode. (Right) Time course of maximum-intensity projections of planar confocal stacks (Top) and sagittal reconstructions (Bottom) of perpendicular division of SHH^{+} placode cell (green) leading to a basal (green) and suprabasal (red) cell (overlap, yellow). *t*=0 corresponds to onset of mitosis as determined by cell rounding. **(B)** Examples of lineage tracings of SHH^{+} cells marked at early stages of HF morphogenesis. Note that SHH^{+} cells give rise to SOX9^{+} cells, but SOX9^{+} cells do not generate Pcad^{hi} SHH^{+} cells. White dashed lines indicate basement membrane. All scale bars, 10μm.

Next, I repeated the induction of *ShhCreER* and *Sox9CreER* lineage tracing during hair placode morphogenesis by a single tamoxifen treatment, and traced the labeled cells into adulthood, when the bulge HFSC niche is established. Strikingly, progeny from these early *ShhCreER*-marked cells wound up in the adult bulge, marked by keratin 24 (K24) (Figure 3-2, left). Moreover, *ShhCreER*-marked cells were functional and contributed to all SC lineages in subsequent rounds of hair cycling (Figure 3-2, right). Additionally, Sox9CreER-marked cells within the placode were also found in the adult bulge SC pool and also contributed to subsequent hair cycles (Figure 3-2, right). Together, these findings support the notion that HFSCs are born from early asymmetric cell divisions within developing hair placodes.

HF asymmetry is established during morphogenesis and is maintained into adulthood

While *ShhCreER* and *Sox9CreER* lineage tracing labeled sparse YFP^+ cells within the expected domains of emerging placodes (Figure 3-1B), strikingly *ShhCreER* often marked cells within the anterior (A) placode, while *Sox9CreER* frequently marked cells within the posterior (P) (Figure 3-3A). Such examples reflect planar cell polarity (PCP) established by the time of labeling (DasGupta and Fuchs, 1999; Devenport and Fuchs, 2008).

As the HF morphogenesis progressed, the asymmetric pattern of labeling by *ShhCreER* and *Sox9CreER* was maintained, such that if a YFP-marked *Shh*-

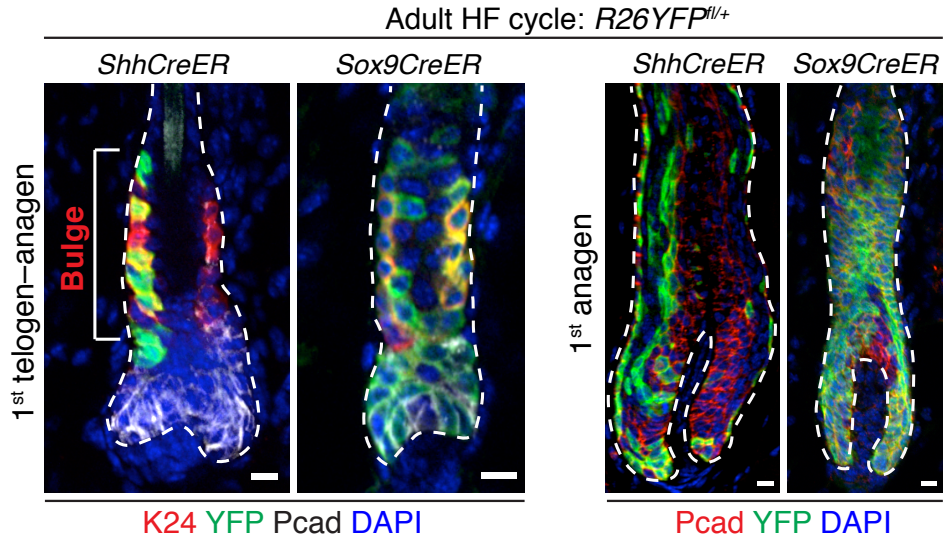

Figure 3-2. Embryonically labeled SC progenitors contribute to the adult HFSC pool. Examples of lineage tracings monitored to 1st telogen and anagen. Note *ShhCreER; R26YFP*$^{+}$ (and *Sox9CreER*) labeled cells contribute to adult SC pool (K24+) (bracket), and to all HF lineages in subsequent hair cycle (right). All scale bars, 10μm.

expressing cell was more centrally located, its progeny formed the inner layer of $SOX9^+$ cells, while if the YFP^+ *Shh*-expressing cell was at the anterior-most boundary of the pocket, it generated the anterior outer layer of $SOX9^+$ cells (Figure 3-1B, germ and peg, left). Conversely but again, in agreement with the placode's planar polarization at the invagination stage, a number of *Sox9-CreER* lineage-tracings resided along the posterior side of developing HFs (Figure 3-3A). Upon completion of morphogenesis, the A-P polarity in lineage-tracings was maintained for *Shh-CreER,* but often disappeared with *Sox9-CreER* (Figure 3-3B,C).

To determine whether the anterior-posterior asymmetry established during placode morphogenesis is maintained into adulthood, I quantified the labeling asymmetry within HFs in first and second telogen and anagen. Strikingly, even after undergoing catagen and entering first telogen, *ShhCreER* labeled cells remained anterior (Figure 3-3D,E). Upon entry into next anagen, this anterior patterning was maintained, and the marked bulge cells generated the new ORS, as well as contributed to internal differentiated lineages. When I followed the lineage tracing into the next hair cycle, anterior asymmetry was lost in the new bulge and subsequent hair cycle (Figure 3-3D,F). This loss of asymmetry was expected, given that the new bulge and hair germ are formed from the old ORS, and the ORS was already partially labeled during the previous anagen (Hsu et al., 2014a).

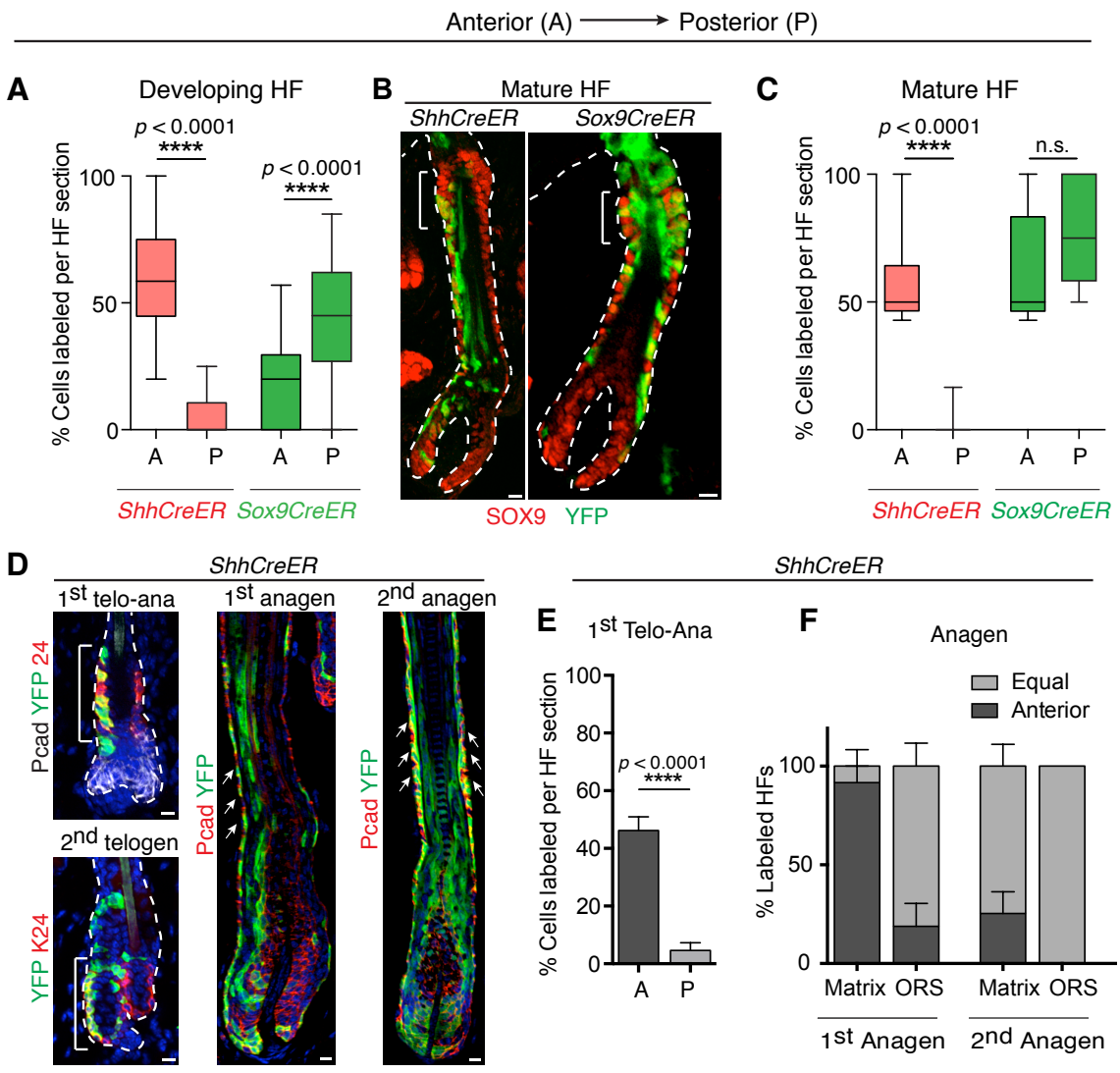

Figure 3-3. A-P asymmetry within HFs is maintained through development into adulthood. (A) Quantification of YFP$^+$ cells on anterior and posterior sides of 34 (*Shh-CreER*) and 41 (*Sox9-CreER*) developing HFs in *n*=3 embryos. **(B)** Lineage-tracings tracked to HF maturation in P0–P1 pups. **(C)** Quantification of labeled cells on anterior and posterior sides of mature HFs (*n*=12, *ShhCreER* and *n*=8 *Sox9CreER*). **(D)** *ShhCreER* lineage-tracings monitored to the 1st and 2nd adult resting (telogen) and growth (anagen) phases. Note labeling in ORS (arrows), matrix, and differentiating hair cells. **(E)** Quantification of *ShhCreER*/YFP$^+$ cells on anterior and posterior sides of bulge in first telogen→ anagen transition from n=25 HFs. **(F)** Quantification of labeled cells in matrix and ORS during 1st and 2nd anagen (34 HFs 1st anagen from *n*=3 mice; 26 HFs 2nd anagen from *n*=2 mice). Dashed white lines mark basement membrane. Bracket denotes bulge SC niche. Scale bars: all 10μm.

Controlling the number of SOX9+ stem cell progenitors

In order to understand how the number of SOX9+ SC progenitors is controlled, I analyzed the proliferation patterns of basal WNT^{hi} SOX9- placode cells, and the suprabasal WNT^{lo} SOX9+ daughter cells.

To address this question, I used *Fucci* embryos, where nuclei of G_1/G_0 cells are labeled with monomeric Kusabira-Orange 2 (mKO2) (Ahtiainen et al., 2014; Sakaue-Sawano et al., 2008). Additionally, the pregnant dams were administered a short pulse of nucleotide analogue 5'-ethynyl-2'-deoxyuridine (EdU) to label dividing cells. From analysis of both planar and saggital views of developing hair placodes, EdU showed little or no overlap with mKO2+ cells (Figure 3-4A). In the epidermis, mKO2 marked nuclei in terminally differentiating suprabasal layers (Figure 3-4A, asterisks). Within hair germs, however, mKO2 marked $LHX2^{+}$ basal cells.

Next, I used *Fucci; Lhx2EGFP* embryos to perform quantitative flow cytometry analysis to determine the relative number of mKO^{hi} cells in the hair placodes and the IFE. This analysis confirmed that, in total, ~20% of hair placode cells were $mKO2^{hi}$ (Figure 3-4B,C). This result was in stark contrast to IFE, where only 2% of $\alpha6^{hi}$ cells were $mKO2^{hi}$.

In many cell types, WNT-signaling is thought to promote self-renewal and proliferation (Clevers et al., 2014; Pei et al., 2012; Reya et al., 2003; Shin et al., 2011). In the hair placodes, however, the WNT^{hi} pocket was also the most

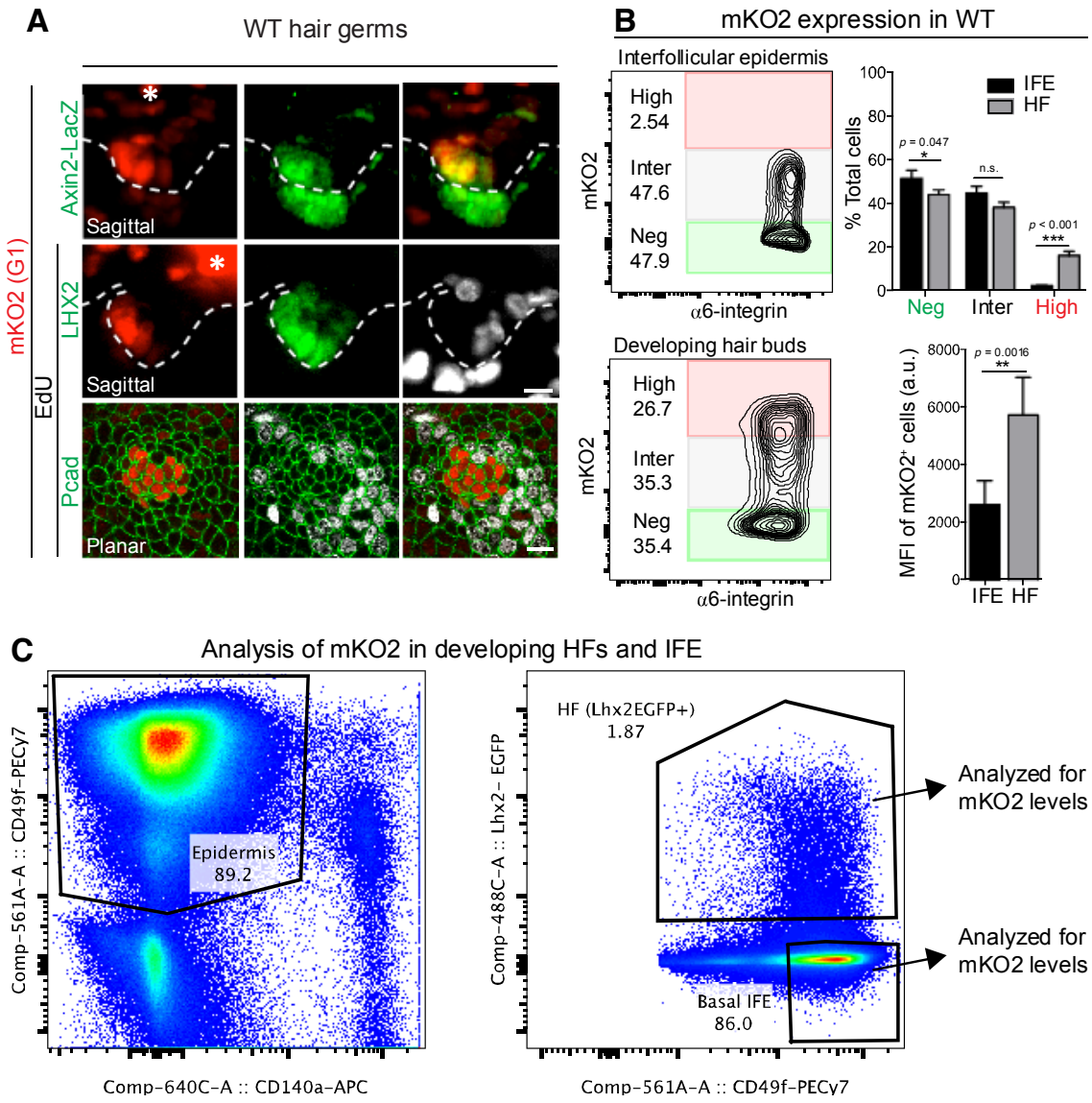

Figure 3-4. Cells in hair placodes undergo prolonged G1 phase of cell cycle. (A) mKO2 epifluorescence and immunolabeling of skin from *Fucci*; *Axin2LacZ* embryo following 4hr EdU (Axin2-LacZ=β-galactosidase). Asterisks denote terminally differentiating epidermal cells overlying the developing HF. Scale bar 10μm. **(B)** Flow-cytometry plots for α6 and mKO2 in E17.5 LHX2-EGFP embryonic HF (EGFP^{+}) and IFE (EGFP^{-}). Note that a significant fraction of α6^{hi} HF, but not IFE cells are mKO2^{bright} (red box). Mean fluorescence intensities (MFI) in IFE and HF for mKO2^{+} cells (Inter+High). Data are from 5 independent analyses and are mean ± SD. **(C)** Flow cytometry analysis scheme of developing HFs and IFE from *Lhx2-EGFP* embryos. Epidermis was identified as CD140a^{-} and α6^{+}. Hair buds are Lhx2-EGFP^{+}, while IFE is Lhx2-EGFP^{-}, α6^{hi}.

quiescent (Figure 3-4A, top), suggesting a link between WNT signaling and proliferation.

To determine whether high levels of WNT signaling in the epidermis cause cells to cycle slower, Irina and I crossed *Fucci* mice with *APC$^{fl/fl}$; R26-YFP$^{fl/+}$* transduced with low titer LV-Cre. The mKO2^{hi} population was accentuated when β-catenin stabilization was enhanced genetically (Figure 3-5A). Quantitative flow cytometry further demonstrated a dramatic increase in the number of APC-null mKO2^{hi} cells relative to uninfected controls (Figure 3-5B,C), thereby reinforcing the notion that, in developing epithelial buds *in vivo*, high WNT-signaling slows proliferation.

That said, the WNT^{hi} cells appeared to be in an extended G_1 rather than a G_0 state, since asymmetric divisions within this basal pocket were still seen at the hair germ and peg stages, and since occasional mKO2-negative and EdU^{+} cells were captured within this pocket (Figure 3-6).

From these data, I concluded that the early WNT^{hi} basal cells within the HF not only divide asymmetrically, but also do so infrequently. These coupled behaviors ensure that the pocket of WNT^{hi} cells, established during placode formation, maintains a constant position and small size throughout HF morphogenesis. At the same time, this mechanism allows for tight control of the number of the SOX9+ SC progenitors produced via the early asymmetric divisions.

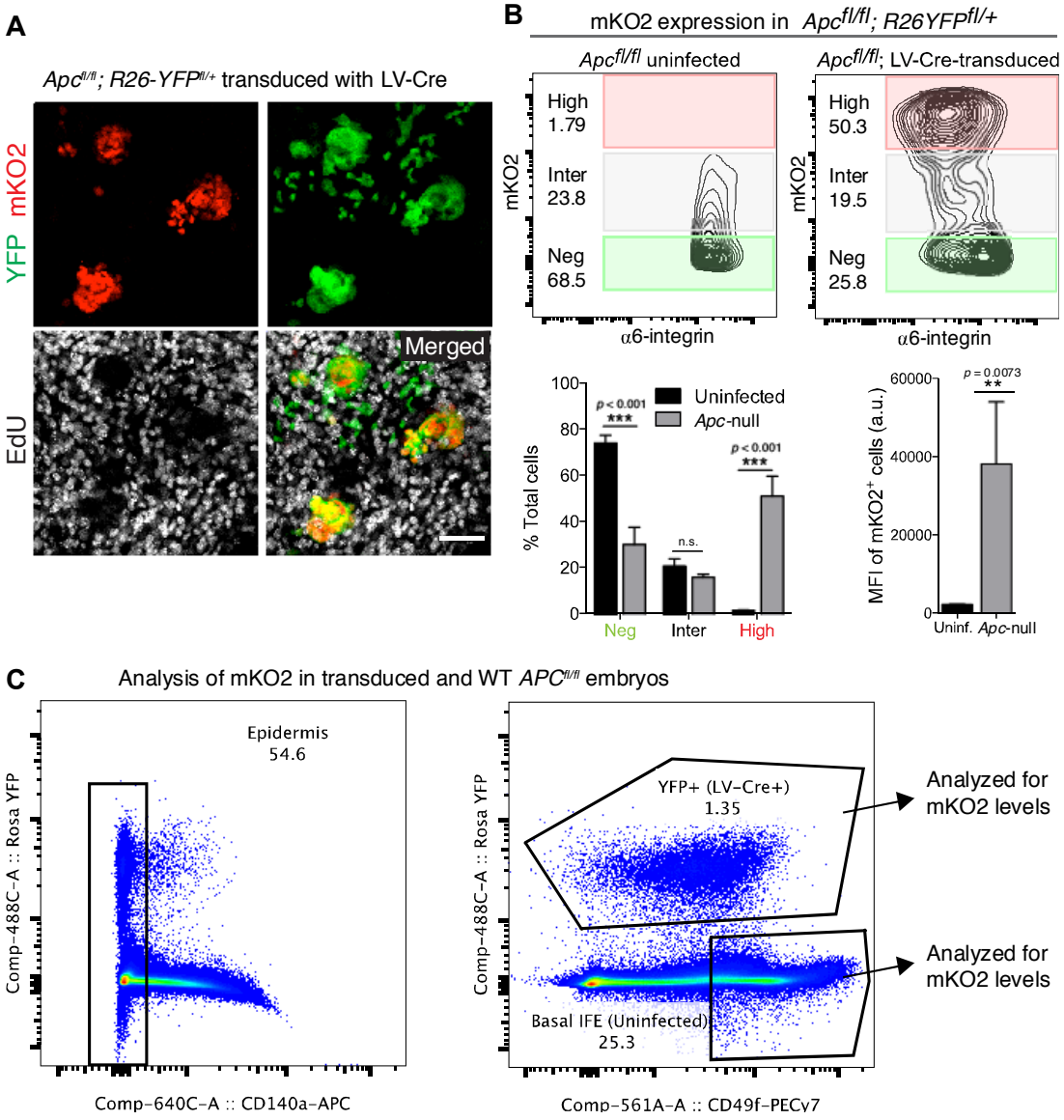

Figure 3-5. WNT Signaling Induces Prolonged G1 Phase of Cell Cycle. (A) Planar confocal IMF of epidermis from E14.5 *Fucci*;*Apc*$^{fl/fl}$;*R26YFP*$^{fl/+}$ embryo transduced mosaically with LV-Cre and labeled with EdU 4hr prior to immunolabeling as shown. Note mKO2^{bright} and EdU^{low} signals in WNT-hyperactive (YFP^{+}) regions. **(B)** Flow-cytometry plots for α6 and mKO2 in E14.5 *Fucci*;*Apc*$^{fl/fl}$;*R26YFP*$^{fl/+}$ embryos transduced with LV-Cre. Note that a significant fraction of transduced, but not WT cells are mKO2^{bright} (red box). Mean fluorescence intensities (MFI) in transduced and WT cells for mKO2 (Inter+High). Data are from 5 independent analyses and are mean ± SD. **(C)** Flow cytometry analysis scheme of *APC*-KO vs. WT cells from *APC*$^{fl/fl}$; *R26-YFP*$^{fl/+}$ embryos mosaically transduced with LV-Cre. Epidermis was identified as CD140a^{-}. *APC*-KO regions are YFP^{+}, WT cells are YFP^{-}, α6^{hi}.

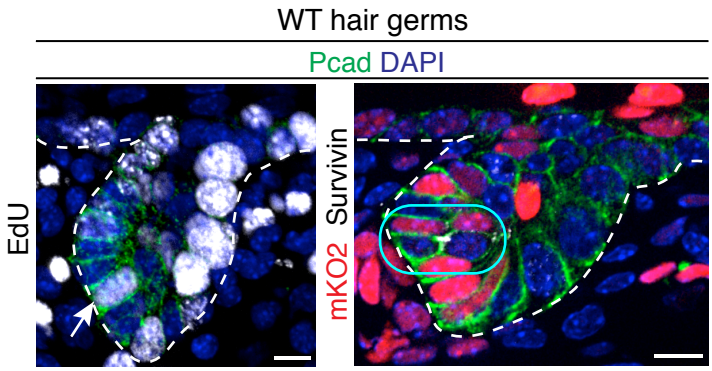

Figure 3-6. WNT^{hi} cells are in an extended G_1 rather than G_0 state. IMF of sagittal sections of hair germs showing examples of EdU^{+} cell (left, arrow) and mKO2-negative dividing cell (right, box) within Pcad^{hi} (WNT^{hi}) mKO2^{+} pocket. Scale bar 10μm.

In contrast to WNT^{hi} basal cells, SOX9^{+} suprabasal cells showed signs of rapid proliferation and expansion. From live imaging experiments, Aaron observed divisions within the suprabasal plane of the placode (Figure 3-7A). In contrast to those of the basal layer, suprabasal divisions within early placodes were exclusively parallel relative to the embryo surface.

Further evidence came from proliferation analysis of SOX9^{+} and LEF1^{+} cells following a short EdU pulse. At the placode stage, SOX9^{+} and LEF1^{+} cells were comparably proliferative, consistent with their derivation from asymmetric divisions (Figure 3-7C). However, none of the SOX9^{+} cells were mKO2^{hi}, thereby distinguishing suprabasal placode cells from mKO2^{hi} terminally differentiating epidermal cells and basal WNT^{hi} cells (Figure 3-7B). Moreover by the hair germ and peg stage, proliferation within the SOX9^{+} population clearly surpassed that in WNT^{hi} LEF1^{+} cells (Figures 3-7C,D).

The positive correlation between proliferation and SOX9 was as striking as the inverse correlation between proliferation and LEF1/WNT-signaling. This correlation was accentuated in the proliferative SOX9^{+} WT IFE halos around WNT^{hi} *Apc*-null non-proliferative patches within *Apc* mosaic skin (Figure 3-7E).

The consequence of these WNT-dependent differences became increasingly apparent as HF morphogenesis progressed. While LEF1^{+} WNT^{hi} cell numbers remained constant, SOX9^{+} WNT^{lo} cells expanded (Figure 3-7F). SOX9^{+} cell divisions appeared to be symmetric, with randomized spindle orientations (Figure 3-7G).

Figure 3-7. SOX9^{+} Cells Expand Symmetrically During HF Morphogenesis. **(A)** Time course from live imaging of parallel suprabasal division in placode. (Top) Planar views centered in suprabasal plane with dividing cell pseudo-colored green. (Bottom) Sagittal views reconstructed from confocal stacks. Dividing cell circled in cyan. *t*=0 corresponds to onset of mitosis as determined by DNA condensation. 75 suprabasal divisions imaged from *n*=3 embryos. **(B)** Sagittal endogenous fluorescence (mKO2) and IMF (SOX9) of hair bud from E17.5 *Fucci* embryo after 4h pulse of EdU. Asterisk marks terminally differentiating suprabasal cell in the epidermis. **(C)** Quantification of proliferation (4h EdU pulse) of SOX9^{+} and LEF1^{+} cells at different HF morphogenesis stages. Data from n=3 litters, 74 HFs and are mean ± SD. **(D)** Sagittal IMF (SOX9, Pcad) during different HF morphogenesis stages after 4h pulse of EdU. **(E)** Planar confocal IMF of *Apc$^{fl/fl}$; R26YFP$^{fl/+}$* epidermis transduced mosaically with *LV-Cre*, following 4h EdU pulse. **(F)** Quantification of numbers of LEF1^{+} and SOX9^{+} cells at different HF morphogenesis stages. Data from n=3 litters, 117 HFs and are mean ± SEM. **(G)** IMF of sagittal sections of HFs showing examples (arrows) of parallel, perpendicular, and suprabasal divisions in SOX9^{+} cells. White dashed lines indicate basement membrane. Scale bars in (A,B,D,G), 10μm; in (E), 20μm.

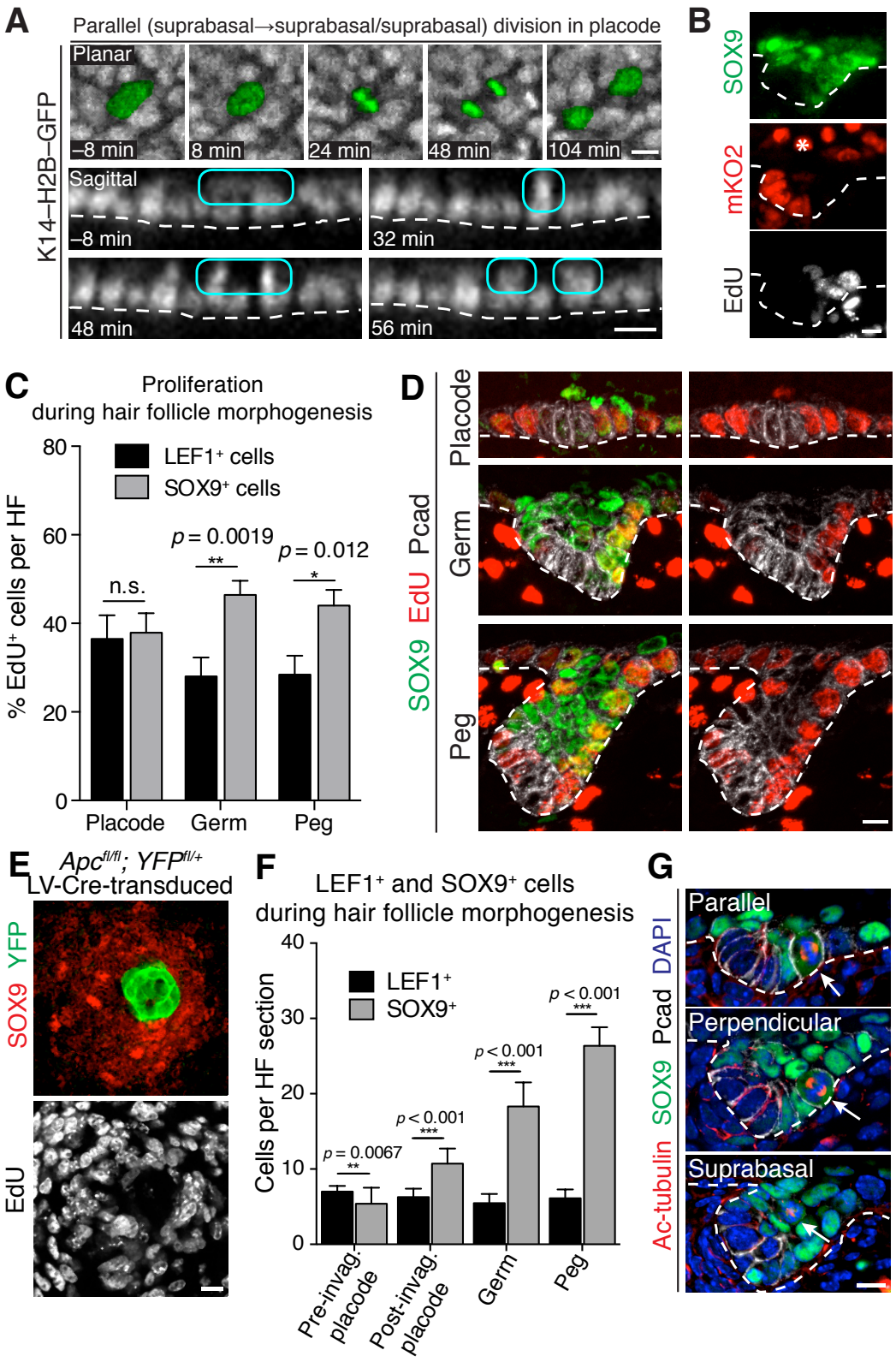
A
Parallel (suprabasal→suprabasal/suprabasal) division in placode
K14–H2B–GFP
Planar
–8 min
8 min
24 min
48 min
104 min
Sagittal
–8 min
32 min
48 min
56 min
B
SOX9
mKO2
EdU
C
Proliferation
during hair follicle morphogenesis
% EdU+ cells per HF
LEF1+ cells
SOX9+ cells
p = 0.0019
p = 0.012
n.s.
Placode
Germ
Peg
D
SOX9 EdU Pcad
Placode
Germ
Peg
E
Apcfl/fl; YFPfl/+
LV-Cre-transduced
SOX9 YFP
EdU
F
LEF1+ and SOX9+ cells
during hair follicle morphogenesis
Cells per HF section
LEF1+
SOX9+
p = 0.0067
p < 0.001
p < 0.001
p < 0.001
Pre-invag. placode
Post-invag. placode
Germ
Peg
G
Ac-tubulin SOX9 Pcad DAPI
Parallel
Perpendicular
Suprabasal

Only early asymmetric divisions within placodes produce SOX9+ HFSC progenitors

When *ShhCreER* lineage tracing was started at the hair placode stage, it resulted in the labeling of suprabasal SOX9+ HFSC progenitors (Figure 3-1B, left). However, when developing hair follicles were labeled at more advanced stages of HF morphogenesis, spatial organization was still consistent with asymmetric cell divisions, but *ShhCreER* marked progeny now consisted of inner $SOX9^-$ HF layers expressing differentiation markers for the companion layer (Cp; keratin 6) and inner root sheath (IRS; GATA3) (Figure 3-8).

These results demonstrate that only early asymmetric cell divisions by *Shh*-expressing parents give rise to $SOX9^+$ SC progenitors, while their later asymmetric cell divisions generate the differentiated cells of the hair lineages.

Along with slow asymmetric divisions of WNT^{hi} basal cells within hair placodes, this fate switch mechanism of Shh+ cells at later stages of HF morphogenesis ensures a tight control of the number of SOX9+ SC progenitors produced during HF development.

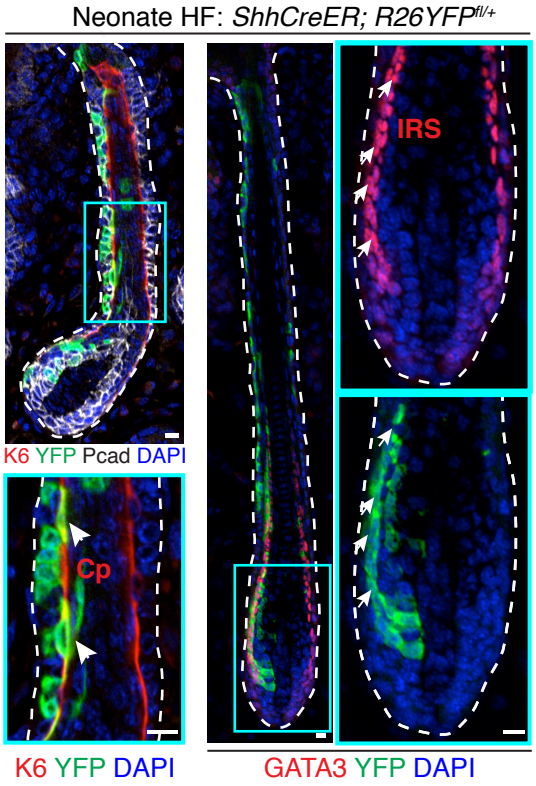

Figure 3-8. Shh+ cells give rise to differentiated lineages later in morphogenesis. Examples of lineage tracings from cells marked at later stages of HF morphogenesis and monitored to HF maturation (P1–4). Note that SHH^{+} cells marked at later times give rise to differentiated lineages: K6, companion layer (Cp, arrows); GATA3, inner root sheath (IRS, arrows). White dashed lines indicate basement membrane. All scale bars, 10μm.

Discussion

Using *ShhCreER* and *Sox9CreER* lineage tracing initiated at the earliest stages of HF morphogenesis and traced into adulthood, I demonstrate that the SOX9+ cells produced by asymmetric cell divisions of the basal WNT^{hi} cells are SC progenitors that contribute to the adult SC pool. Previously, using *Sox9Cre*, it was shown that Sox9-expressing cells give rise to the entire HF and all its lineages, however, the earliest appearance of SC progenitors remained unknown (Nowak et al., 2008). Using *ShhCreER*, I show that Shh+ cells in hair placodes undergo slow asymmetric divisions to give rise to SOX9+ HFSC progenitors. I confirm this observation by using *Sox9CreER*, where I induce labeling at the earliest stages of HF morphogenesis and demonstrate that the first SOX9+ cells in hair placodes contribute to the bulge stem cell pool.

Interestingly, the labeling patterns generated by *ShhCreER* and *Sox9CreER* lineage tracing were asymmetric, such that *ShhCreER*-labeled lineage contributed to the anterior side of the developing HFs, while *Sox9CreER*-labeled progeny contributed preferentially to the posterior side. This highlights the notion that PCP is established prior to the initiation of HF morphogenesis, and is critical to the proper HF patterning (Devenport and Fuchs, 2008). It also suggests that there is little cell mixing taking place during HF morphogenesis and even into adulthood, such that a cell labeled anteriorly tends to remain there along with its progeny. It is most striking that even after the mature HF undergoes catagen and enters first adult telogen, this asymmetry is largely maintained. During the first

adult anagen, the asymmetry is maintained preferentially in the matrix, while the ORS is now labeled on both sides. Upon entry into second adult anagen, the asymmetry is lost. These observations are consistent with the previous work showing that cells residing within the upper and middle ORS survive and give rise to the new bulge and germ, respectively (Hsu et al., 2011).

A final conundrum is how, in a system like this one, the numbers of SC progenitors and SCs are controlled. Interestingly, during early HF morphogenesis, the SOX9- WNT^{hi} pocket of cells at the invaginating tip of the HF that undergoes asymmetric divisions to give rise to SOX9+ cells spends prolonged time in the G1 phase of the cell cycle and undergoes rare divisions, thus producing few SOX9+ SC progenitors. This is likely a WNT-dependent characteristic, as *APC*-null cells are even slower cycling.

This observation contrasts with the role of WNT signaling in the intestine, where loss of *APC* results in hyperproliferation, loss of differentiation and expansion of SC-like cells (Andreu et al., 2005; Sansom et al., 2004). However, the role of WNT signaling in the intestine goes beyond regulating SC maintenance. Interestingly, the highest levels of WNT signaling in the intestine occur in Paneth cells – post-mitotic differentiated cells that are derived from intestinal SCs (Cheng and Leblond, 1974). Additionally, high levels of WNT signaling are detected in the differentiating cells of the HF that will form the hair shaft (DasGupta and Fuchs, 1999). At the same time, I have detected low-moderate levels of WNT signaling throughout the developing epidermis.

Additionally, loss of β-catenin results in decreased proliferation in developing epidermis (data not shown). Finally, LEF1 and TOPGAL activity are also detected in the proliferative hair germ at the onset of a new hair cycle, and loss of β-catenin results in the failure of HFSCs to enter anagen (DasGupta and Fuchs, 1999; Lien et al., 2014). These observations suggest that relative levels of WNT signaling determine the outcome, such that low-moderate WNT signaling is necessary for maintenance of proliferation, while high levels of WNT signaling induce differentiation.

The observations that the SOX9- WNT^{hi} basal cells in developing HFs are slow cycling were made based on the levels of EdU incorporation, as well as using Fucci embryos, where cells in G0/G1 are marked with mKO2 (Sakaue-Sawano et al., 2008). Fucci reporter hCdt1-mKO2 is a transgenic mouse model, where the reporter is expressed from a constitutively active chicken beta-actin gene promoter (CAG), such that the reporter continues to be transcribed and accumulates in a cell until the next entry into the S phase, where hCdt1 is proteolytically degraded. Therefore, the intensity of the signal correlates with the length of time a cell has spent without entering S phase. This is also supported by the brightness of the suprabasal cells of the epidermis, which are non-proliferative and therefore continue to accumulate the G0/G1 reporter. Strikingly, the SOX9- WNT^{hi} basal cells within developing HFs are marked by high levels of Cdt1-mKO2, providing another line of evidence that these cells are truly slowly cycling and produce few SOX9+ SC progenitors.

Apart from spending prolonged time in G1 and undergoing rare asymmetric divisions thus limiting the number of SOX9+ SC progenitors, only asymmetric divisions of WNT^{hi} cells within hair placodes give rise to SOX9+ cells, but not at later stages, where they give rise to differentiated cells. At the later stages of morphogenesis, WNT^{hi}, *Shh*+ cells act similar to the WNT^{hi}, *Shh*+ cells of the adult HF matrix in anagen, where they give rise to the various differentiated lineages of the adult HF (DasGupta and Fuchs, 1999; Genander et al., 2014). This is also supported by Axin2-CreER lineage tracing in developing HFs, where tracing at germ or peg stages labels much fewer HFSCs than tracing starting at the placode stage (Xu et al., 2015). The mechanisms regulating this fate switch are currently unknown. One possible hypothesis might be in the relative levels of WNT signaling, such that the intensity of WNT signaling at the leading edge of a developing HF keeps increasing throughout HF morphogenesis, possibly boosted by further signals coming from the growing dermal papilla. Eventually, the levels are high enough such that suprabasal daughter cells of the asymmetric cell divisions acquire a differentiated fate rather than SC progenitor fate.

Materials and Methods

Mouse Strains and constructs

All animals used for the experiments in this manuscript were generated previously: *ShhCreER, Sox9CreER, Rosa26*$^{Flox\text{-}Stop\text{-}Flox\text{-}YFP}$*, Fucci*, *Apc*$^{fl/fl}$, and *Rosa26mTmG*$^{fl/+}$ (Bai et al., 2002a; Brault et al., 2001; Chiang et al., 1999;

Corrales et al., 2006; Dassule et al., 2000; Harfe et al., 2004; Kuraguchi et al., 2006; Litingtung et al., 1998; Long et al., 2001; Lustig et al., 2002b; Mao et al., 1999; Muzumdar et al., 2007; Nguyen et al., 2006; Sakaue-Sawano et al., 2008; Soeda et al., 2010; Srinivas et al., 2001) were described previously. *Lhx2-EGFP* mice were from The Gene Expression Nervous System Atlas (GENSAT) Project, NINDS Contracts N01NS02331 & HHSN271200723701C to The Rockefeller University (New York, NY, USA).

Tissue Preparation and Immunofluorescence

4h prior to the desired stage of development, EdU (500 µg/g, Life Technologies) was injected intraperitonally in pregnant females and embryos were then processed. Typically, >3 embryos from independent experiments were analyzed for each condition.

For immunofluorescence, tissues were fixed in 4% PFA in PBS for 1h at room temperature and washed extensively in PBS. For whole-mount or tissue sections, samples were permeabilized for 3 hours in 0.3% Triton X-100 in PBS, or embedded in OCT (Tissue Tek), cut at a thickness of 10µm and permeabilized for 10 min 0.3% in Triton X-100. Tissue samples were then blocked in Gelatin Block (2.5% fish gelatin, 5% normal donkey serum, 1% BSA, 0.3% Triton, 1× PBS). When immunolabeling with mouse antibodies, sections were incubated with the M.O.M. blocking kit according to manufacturer's instructions (Vector Laboratories). The following primary antibodies were used: P-Cadherin (goat,

1:400, R&D AF761), Survivin (rabbit, 1:300, Cell Signaling 2808), SOX9 (rabbit, 1:300, Fuchs Lab), LHX2 (rabbit, 1:2000, Fuchs Lab), anti-GFP/YFP (chicken, 1:2000, Abcam), acetylated tubulin (mouse, 1:500, Sigma T7451), Beta-Gal (rabbit, 1:10000, MP Bio), K24 (rabbit, 1:5,000, Fuchs lab).

Primary antibodies were incubated at 4°C overnight. After washing with 0.3% Triton X-100 in PBS, samples were incubated for 2h at room temperature with secondary antibodies conjugated with Alexa 488, RRX, or 647 (respectively, 1:1000, 1:500, and 1:100, Life Technologies). Samples were washed, counterstained with 4'6'-diamidino-2-phenilindole (DAPI) and mounted in Prolong Gold, and EdU incorporation was detected by Click-It EdU AlexaFluor 647 Imaging Kit (Life Technologies).

Confocal and Epifluorescence Imaging

Epifluorescence images were acquired with an Axio Oberver.Z1 microscope equipped with a Hamamatsu ORCA-ER camera (Hamamatsu Photonics), and with an ApoTome.2 (Carl Zeiss) slider that reduces the light scatter in the fluorescent samples, using 20×, 40×, and 63× objectives, controlled by Zen software (Carl Zeiss). Confocal images were acquired with a Zeiss LSM780 laser-scanning microscope (Carl Zeiss MicroImaging) through a 40× or 63× oil objective. For whole mount imaging, *z* stacks of 20–40 planes (0.25mm) were acquired.

Fluorescence Activated Cell Sorting

Back skins from E17.5 Lhx2-EGFP/Fucci embryos were dissected and treated overnight with dispase (Gibco, 0.4mg/ml) at 4°C, which selectively removed the epidermis, hair placodes, and hair germs from the skin. This epidermal fraction was placed in a solution of 1:1 Trypsin (GIBCO):Versene (Thermo) at room temperature for 8-10 min on an orbital shaker.

Back skins from E14.5 APC/YFP/Fucci embryos were dissected and immediately placed in Trypsin at room temperature for 20 minutes. After centrifugation (300g × 10min), cells were rinsed with PBS and single cell suspensions were obtained. Antibodies and epifluorescence markers are as indicated in the text. DAPI was used to exclude dead cells. Cell isolations were performed on FACSAria sorters equipped with DIVA software (BD Biosciences), and analyzed using FlowJo.

CHAPTER 4: SUMMARY AND PERSPECTIVES

Organ morphogenesis depends on the specification of various cell types that will fulfill the function of the organ. Cell type specification needs to take place at the right time, while concurrently maintaining correct positioning within the tissue. Additionally, SCs need to be set apart that will participate in tissue homeostasis as well as in tissue repair, if need arises. Finally, proliferation needs to be tightly coordinated in order to produce enough properly positioned functional cells of the tissue, but at the same time to allow for the specification of SCs that are usually more quiescent.

In adult tissues, the niche defines SC identity and numbers. While niche signaling typically emanates from heterologous cell types, niche SCs can signal to their progeny (Pardo-Saganta et al., 2015) and SC progeny can signal back to their parents (Hsu et al., 2014b; Hsu et al., 2011). In all of these cases, however, niche vacancies are sensed and replenished to maintain a fixed SC number. Non-homeostatic vacancies can even be replenished by non-stem cells, further underscoring the importance of the niche microenvironment in dictating SC behavior (Blanpain and Fuchs, 2014). This raises a conundrum for SC specification during morphogenesis. Does SC specification require a pre-existing niche or can it occur independently?

I used HFs as a model to understand how cellular heterogeneity is established during HF morphogenesis, how proliferation is spatiotemporally regulated, and whether SC specification requires a pre-existing niche.

Establishing heterogeneity during hair follicle morphogenesis

Two distinct cell types, marked by SOX9 and LHX2, are found within the developing HFs shortly after hair placode specification (Nowak et al., 2008; Rhee et al., 2006). By performing short-term lineage tracing using lentiviral delivery of CreER into *Rosa26-YFP*$^{fl/+}$ embryonic epidermis, I found that suprabasal SOX9+ cells and basal SOX9- LHX2+ cells are derived from a common progenitor. By analyzing angles of cell division in fixed tissues as well as by live imaging, I found that in contrast to the IFE, where approximately 50% of divisions are parallel to the basement membrane and 50% are perpendicular, within developing hair placodes, virtually 100% of divisions are perpendicular to the basement membrane and asymmetric, giving rise to the suprabasal SOX9+ and basal SOX9- cells.

To understand how the two daughters of the asymmetric division acquire different fates, I looked at the patterns of WNT and SHH signaling within the developing HFs. Previous studies have demonstrated that ablation of WNT signaling abolishes hair bud specification entirely, while disruption of SHH signaling arrests HF development after specification. However, little is known about the role of these pathways in determining heterogeneity during these early stages. Previous studies on WNT- and SHH-signaling relied on their loss and gain of function in the entire epidermis, which precluded them from understanding the role of these signaling pathways in discrete cell populations within the epidermis and the HF, as they naturally arise. Therefore, I took

advantage of the *in utero* epidermis-specific lentiviral gene delivery (Beronja et al., 2010) to create juxtaposing regions of high and low WNT or SHH activity, more closely recapitulating the patterns observed naturally. Using these mosaic analyses, I demonstrated that the purpose of perpendicular divisions within the placode is to achieve differential partitioning of WNT signaling to the basal cells and to place the SOX9+ daughter cell outside of its WNT^{high} parent cell environment. Moreover, although the WNT^{high} basal daughter is the source of SHH, high levels of WNT signaling prevent it from responding to SHH, and only the suprabasal WNT^{low} daughter can respond. Additionally, I show that SHH is able to repress low-moderate levels of WNT signaling, which contributes to further repression of WNT signaling in the suprabasal SOX9+ cells, boosting the levels of SOX9 and driving their expansion (Figure 4-1).

While other signaling pathways likely intersect the circuitry, antagonism between WNT and SHH pathways is crucial not only in balancing asymmetric and symmetric cell divisions, but also in delineating cellular fates and proliferation rates. Our findings illuminate why both signaling pathways have such profound impact on cancers of the skin, where spindle orientations, cellular fates, and proliferative rates are imbalanced (Beronja et al., 2013; Blanpain and Simons, 2013; Larsimont et al., 2015). Our results also pave the way for delving further into how these two signaling pathways establish their antagonistic interplay in morphogenesis and SC establishment.

Future efforts can focus on elucidating the mechanisms behind the WNT-

SHH antagonism observed during HF morphogenesis. Understanding this process might provide novel ways to target these pathways in malignancies, where they become deregulated.

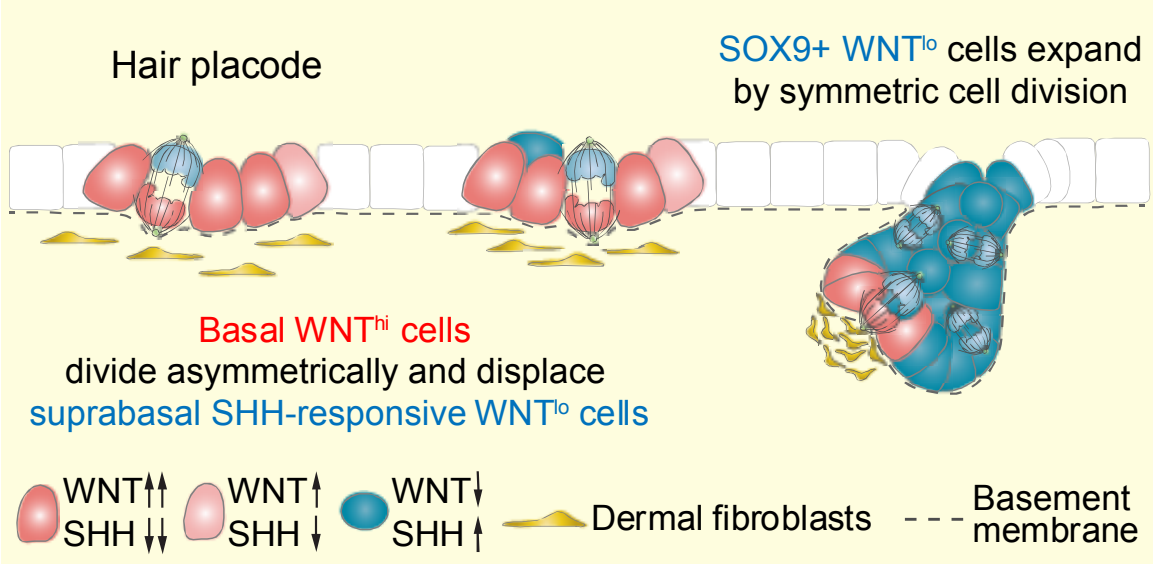

Figure 4-1. WNT-SHH antagonism drives the specification of suprabasal SOX9+ cells following basal asymmetric cell division. In response to elevated WNT-signaling, basal cells within the primitive epithelial bud undergo asymmetric cell divisions giving rise to suprabasal cells. Basal cells retain this high WNT-signaling, and express *Shh*. Suprabasal cells respond to SHH, which further decreases WNT-signaling but promotes their expansion by undergoing symmetric cell divisions. By contrast, the elevated WNT-signaling in the basal cells prevents them from responding to SHH, and drives them into a slow-cycling state, permissive for asymmetric but not symmetric divisions. Illustration provided by Irina Matos.

Specification and control of the earliest hair follicle stem cell progenitors

Recent work from our lab has shown that SOX9 is a critical transcription factor for the maintenance of HFSC fate (Adam et al., 2015; Kadaja et al., 2014). More importantly, SOX9 can act as a pioneer transcription factor, remodeling chromatin, establishing superenhancers, and turning on the expression of epigenetically-repressed genes, conferring SC properties to SOX9+ cells within the epidermis (Adam et al., 2015). SOX9 expression in a subset of cells within developing hair placodes has suggested that HFSCs might be specified much earlier than previously thought, and prior to the establishment of the niche (Nowak et al., 2008).

To address this question, I used *ShhCreER* mouse model to perform short and long-term lineage tracing. Based on my previous findings, SOX9+ cells are derived from the basal WNT^{high} *Shh*+ cells. Additionally, SOX9+ cells no longer express Shh. Therefore, *ShhCreER* lineage tracing allowed me to label the basal WNT^{high} cells and their progeny – the SOX9+ cells. By administering just one pulse of tamoxifen during hair placode formation, I was able to label SOX9+ cells in hair placodes and germs, which readily contributed to the stem cell pool that was established shortly after birth. By tracing into first telogen, when the bulge can be distinguished morphologically for the first time, it was clear that SOX9+ cells labeled at the placode stage readily contribute to the adult SC pool, and to the subsequent rounds of HF regeneration.

Performing lineage tracing with the *Sox9CreER* mouse model further

supported these results. In this case, only SOX9+ cells were labeled during hair placode morphogenesis, but not the basal SOX9- WNT^{high} *Shh*+ cells, supporting the notion that SOX9+ cells are derived from the basal WNT^{high} cells, and not vice versa. Analogous to *ShhCreER* lineage tracing, *Sox9CreER*-labeled cells contributed to the adult stem cell pool (Figure 4-2).

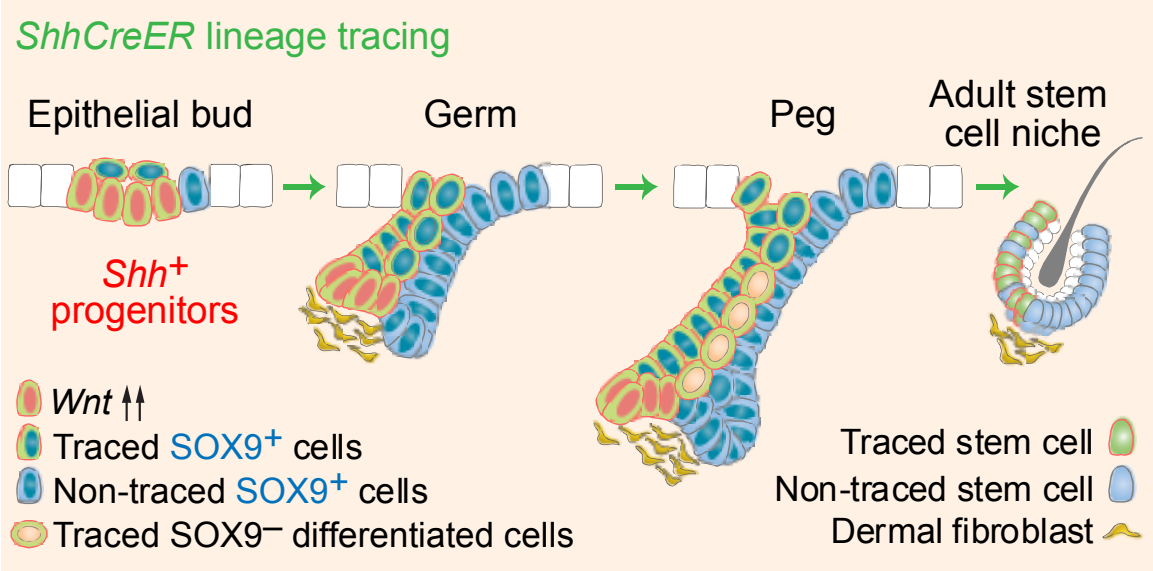

Figure 4-2. SOX9+ cells derived from asymmetric cell divisions in hair placodes contribute to the adult SC pool. *ShhCreER* lineage tracing was performed by administering a single pulse of tamoxifen during hair placode morphogenesis and chasing into adulthood. Illustration provided by Irina Matos.

A striking labeling asymmetry was observed for both *ShhCreER* and *Sox9CreER* lineage tracing. *ShhCreER* lineage tracing preferentially labeled the anterior side of the HFs, while *Sox9CreER* preferentially labeled the posterior (Figure 4-3). This supports previous findings from the lab that have demonstrated that PCP in the epidermis is established prior to HF morphogenesis and dictates

the organization of cell types within the developing hair placode right from its specification (Devenport and Fuchs, 2008). However, it also highlights that despite rapid proliferation and acquisition of the correct shape of the HF, there is little cell rearrangement within the organ, such that cells from the anterior side rarely cross over to the posterior side. This raises an interesting question of how the shape of the HF is determined, and whether cell migration plays a role. Even more strikingly, preferential anterior labeling was maintained through the first cycle of catagen and telogen, such that the anterior side of the hair matrix was still preferentially labeled in the case of *ShhCreER*. However, the ORS of most HFs was equally labeled by *ShhCreER* in first anagen, which explains why in second anagen, both matrix and ORS were mostly equally labeled.

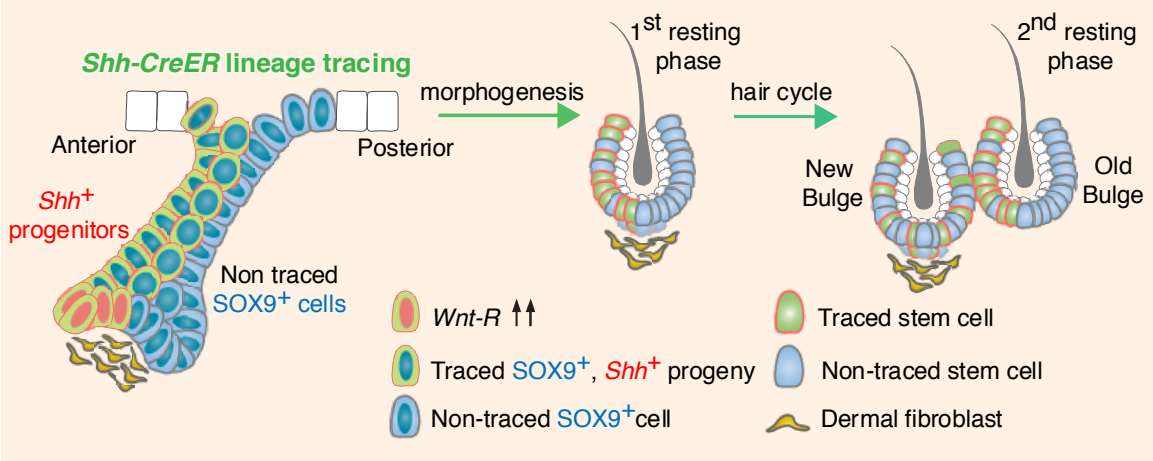

Figure 4-3. HF asymmetry is established early in HF morphogenesis and is maintained into adulthood. *Shh* is expressed by the anterior WNT^{hi} basal cells of hair buds. Upon asymmetric divisions, *Shh*-expressing progenitors produce SOX9+ cells. SOX9+ daughter cells resulting from these divisions remain on the anterior side of developing hair follicles and later contribute to the anterior side of the adult stem cell niche. This asymmetry is resolved during subsequent hair cycling, because the new stem cell niche is derived from surviving outer root sheath cells of the previous cycle. Illustration provided by Irina Matos.

In the case of *Sox9CreER* lineage tracing, the asymmetry mostly disappears by the time HFs reach maturity and can no longer be observed in subsequent hair cycles. This suggests that more cell mixing takes place in the upper HF, where SOX9+ cells reside, possibly due to the higher rates of proliferation of SOX9+ cells.

The next question that I aimed to address is how SC numbers are controlled during HF morphogenesis. First of all, I found that the basal WNT^{high} cells are slow cycling, spend prolonged time in the G1 phase of the cell cycle, and undergo rare asymmetric divisions, giving rise to few SOX9+ cells. Secondly, the fate of the daughter cells switches as morphogenesis progresses, such that asymmetric divisions of the WNT^{high} Shh+ cells within placodes give rise to SOX9+ cells, while as morphogenesis progresses, more and more asymmetric divisions give rise to differentiating SOX9- cells that will form the inner HF lineages. Therefore, the slow cycling properties of the WNT^{high} cells allow for tight control of the number of SOX9+ cells produced, while daughter cell fate switch cuts of further SOX9+ cell generation as morphogenesis progresses.

An important question that still remains to be elucidated is what determines the location of the HFSC bulge niche in the upper ORS of the developing HF? Recent work has demonstrated that when the SCs within the upper ORS of developing hair pegs are laser ablated, non-SCs enter the niche and can be reprogrammed to acquire the SC fate and contribute to the adult SC pool (Xu et al., 2015). These findings suggest that the location of the SC pool is

not determined by cell-intrinsic methods, but additional signals from the surrounding niche dictate the location of the SC pool within the upper ORS and are able to confer stemness to non-SCs that enter the niche. This is of the adult HFSCs, where non-SCs are able to enter the niche and acquire stemness if the SCs in the bulge are ablated (Rompolas et al., 2013). What are the extrinsic signals that determine the location of the bulge in the upper ORS of hair pegs? In part, the answer likely stems from the temporal distancing of uppermost, proliferating $SOX9^{+}$ SCs from their SHH-signaling center, reminiscent of what happens in the adult hair cycle (Hsu et al., 2014b). In adult HFs, upon entry in anagen, transit-amplifying cells in the matrix secrete SHH that signals to the bulge SCs to drive their proliferation. As the HF extends into the dermis, SHH-producing matrix becomes further removed from the bulge, until the signal is no longer received in sufficient quantities and the cells enter quiescence, which signals the end of anagen. Similarly, during HF morphogenesis, SHH-producing WNT^{high} cells move further into the dermis as the hair peg elongates, such that cells in the upper ORS receive progressively less signal. As I have shown, SHH is a major driver of proliferation in developing HFs, therefore it is conceivable that upon removal of SHH, upper ORS becomes more quiescent. However, removal of the SHH source is likely not the only determinant of the location of HFSCs in the upper ORS. First nerve fibers associate with developing hair placodes and hair germs as early as E15.5 (Peters et al., 2002). Interestingly, upper ORS is the site of attachment of nerve endings within the developing HFs (data not shown).

Intriguingly, peripheral nerves innervate the cells above the adult bulge and secrete SHH, which may regulate their behavior upon wounding (Brownell et al., 2011). The signals that recruit nerve fibers to the upper ORS of developing HFs remain unknown. It is also unknown whether nerve fibers secrete SHH or additional signaling molecules during HF morphogenesis, and how that influences the location of the function of the HFSCs.

Apart from becoming more quiescent, HFSCs also adopt unique cell morphology, which also distinguishes them from the rest of the ORS. Previous work in the adult HFs has implicated LHX2 in the regulation of cell morphology in the HFSC bulge (Folgueras et al., 2013). Additionally, epidermis-specific deletion of Lhx2 results in the failure of HFSC specification during morphogenesis (Folgueras et al., 2013; Rhee et al., 2006). It is tempting to speculate that LHX2 may also play a role in driving the cytoskeletal changes in the HFSCs during morphogenesis. Finally, it is unclear how the morphological changes that accompany HFSC localization within the upper ORS impact their function.

Conclusion

By studying HF morphogenesis in the embryo, I have discovered a unique mechanism of how SC identity is acquired and how SC numbers are controlled in early development. Here, I show that SCs are born through asymmetric divisions at a stage that occurs long before establishment of the HF bulge niche. Moreover, and in striking contrast to an adult niche, SC identity in early

development is acquired by the daughter that moves *away* from its parent's microenvironment. Furthermore, the paucity of WNT-signaling distributed to the SC daughter allows it to receive a paracrine SHH signal produced by its WNT^{hi} sister cell, which acts like a temporary niche. This interaction leads not only to reinforced levels of the HFSC master regulator, SOX9, but also to further suppression of *Lef1,* allowing SC progenitors to expand through symmetric and escape the WNT^{hi} slow-cycling asymmetric division status of its parent. In this model, the asymmetric cell division produces two daughter cells, such that one becomes the SC and the other – a temporary niche, producing the signal necessary for SC maintenance and expansion.

Understanding the mechanisms of lineage and SC specification during morphogenesis can guide our efforts in regenerative medicine, which aims to direct multipotent SCs into discrete lineages.

REFERENCES

Adam, R.C., Yang, H., Rockowitz, S., Larsen, S.B., Nikolova, M., Oristian, D.S., Polak, L., Kadaja, M., Asare, A., Zheng, D.*, et al.* (2015). Pioneer factors govern super-enhancer dynamics in stem cell plasticity and lineage choice. Nature *521*, 366-370.

Ahtiainen, L., Lefebvre, S., Lindfors, P.H., Renvoise, E., Shirokova, V., Vartiainen, M.K., Thesleff, I., and Mikkola, M.L. (2014). Directional cell migration, but not proliferation, drives hair placode morphogenesis. Dev Cell *28*, 588-602.

Akam, M. (1987). The molecular basis for metameric pattern in the Drosophila embryo. Development *101*, 1-22.

Akiyama, H., Lyons, J.P., Mori-Akiyama, Y., Yang, X., Zhang, R., Zhang, Z., Deng, J.M., Taketo, M.M., Nakamura, T., Behringer, R.R.*, et al.* (2004). Interactions between Sox9 and beta-catenin control chondrocyte differentiation. Genes Dev *18*, 1072-1087.

Alvarez-Medina, R., Cayuso, J., Okubo, T., Takada, S., and Marti, E. (2008). Wnt canonical pathway restricts graded Shh/Gli patterning activity through the regulation of Gli3 expression. Development *135*, 237-247.

Andl, T., Reddy, S.T., Gaddapara, T., and Millar, S.E. (2002). WNT signals are required for the initiation of hair follicle development. Dev Cell *2*, 643-653.

Andreu, P., Colnot, S., Godard, C., Gad, S., Chafey, P., Niwa-Kawakita, M., Laurent-Puig, P., Kahn, A., Robine, S., Perret, C.*, et al.* (2005). Crypt-restricted proliferation and commitment to the Paneth cell lineage following Apc loss in the mouse intestine. Development *132*, 1443-1451.

Astudillo, P., and Larrain, J. (2014). Wnt signaling and cell-matrix adhesion. Current molecular medicine *14*, 209-220.

Azzolin, L., Panciera, T., Soligo, S., Enzo, E., Bicciato, S., Dupont, S., Bresolin, S., Frasson, C., Basso, G., Guzzardo, V.*, et al.* (2014). YAP/TAZ incorporation in the beta-catenin destruction complex orchestrates the Wnt response. Cell *158*, 157-170.

Baeg, G.H., Lin, X., Khare, N., Baumgartner, S., and Perrimon, N. (2001). Heparan sulfate proteoglycans are critical for the organization of the extracellular distribution of Wingless. Development *128*, 87-94.

Bai, C.B., Auerbach, W., Lee, J.S., Stephen, D., and Joyner, A.L. (2002a). Gli2, but not Gli1, is required for initial Shh signaling and ectopic activation of the Shh pathway. Development *129*, 4753-4761.

Bai, C.B., Auerbach, W., Lee, J.S., Stephen, D., and Joyner, A.L. (2002b). Gli2, but not Gli1, is required for initial Shh signaling and ectopic activation of the Shh pathway. Development *129*, 4753-4761.

Balemans, W., and Van Hul, W. (2002). Extracellular regulation of BMP signaling in vertebrates: a cocktail of modulators. Dev Biol *250*, 231-250.

Balinsky, B.I. (1950). On the prenatal growth of the mammary gland rudiment in the mouse. J Anat *84*, 227-235.

Barker, N. (2014). Adult intestinal stem cells: critical drivers of epithelial homeostasis and regeneration. Nat Rev Mol Cell Biol *15*, 19-33.

Barker, N., van Es, J.H., Kuipers, J., Kujala, P., van den Born, M., Cozijnsen, M., Haegebarth, A., Korving, J., Begthel, H., Peters, P.J*., et al.* (2007). Identification of stem cells in small intestine and colon by marker gene Lgr5. Nature *449*, 1003-1007.

Bausek, N. (2013). JAK-STAT signaling in stem cells and their niches in Drosophila. JAKSTAT *2*, e25686.

Behrens, J., von Kries, J.P., Kuhl, M., Bruhn, L., Wedlich, D., Grosschedl, R., and Birchmeier, W. (1996). Functional interaction of beta-catenin with the transcription factor LEF-1. Nature *382*, 638-642.

Bereiter-Hahn, J., Matoltsy, A.G., Richards, K.S., and SpringerLink (Online service) (1984). Biology of the Integument Invertebrates (Berlin, Heidelberg: Springer Berlin Heidelberg : Imprint: Springer,).

Beronja, S., Janki, P., Heller, E., Lien, W.H., Keyes, B.E., Oshimori, N., and Fuchs, E. (2013). RNAi screens in mice identify physiological regulators of oncogenic growth. Nature *501*, 185-190.

Beronja, S., Livshits, G., Williams, S., and Fuchs, E. (2010). Rapid functional dissection of genetic networks via tissue-specific transduction and RNAi in mouse embryos. Nature Medicine *16*, 821-827.

Bhat, K.M., and Schedl, P. (1997). Establishment of stem cell identity in the Drosophila germline. Dev Dyn *210*, 371-382.

Blanpain, C., and Fuchs, E. (2006). Epidermal Stem Cells of the Skin. Annual Review of Cell and Developmental Biology *22*, 339-373.

Blanpain, C., and Fuchs, E. (2014). Stem cell plasticity. Plasticity of epithelial stem cells in tissue regeneration. Science *344*, 1242281.

Blanpain, C., Lowry, W.E., Geoghegan, A., Polak, L., and Fuchs, E. (2004). Self-renewal, multipotency, and the existence of two cell populations within an epithelial stem cell niche. Cell *118*, 635-648.

Blanpain, C., and Simons, B.D. (2013). Unravelling stem cell dynamics by lineage tracing. Nat Rev Mol Cell Biol *14*, 489-502.

Borday, C., Cabochette, P., Parain, K., Mazurier, N., Janssens, S., Tran, H.T., Sekkali, B., Bronchain, O., Vleminckx, K., Locker, M.*, et al.* (2012). Antagonistic cross-regulation between Wnt and Hedgehog signalling pathways controls post-embryonic retinal proliferation. Development *139*, 3499-3509.

Botchkarev, V.A., Botchkareva, N.V., Roth, W., Nakamura, M., Chen, L.H., Herzog, W., Lindner, G., McMahon, J.A., Peters, C., Lauster, R.*, et al.* (1999). Noggin is a mesenchymally derived stimulator of hair-follicle induction. Nat Cell Biol *1*, 158-164.

Bovolenta, P., Esteve, P., Ruiz, J.M., Cisneros, E., and Lopez-Rios, J. (2008). Beyond Wnt inhibition: new functions of secreted Frizzled-related proteins in development and disease. J Cell Sci *121*, 737-746.

Brault, V., Moore, R., Kutsch, S., Ishibashi, M., Rowitch, D.H., McMahon, A.P., Sommer, L., Boussadia, O., and Kemler, R. (2001). Inactivation of the beta-catenin gene by Wnt1-Cre-mediated deletion results in dramatic brain malformation and failure of craniofacial development. Development *128*, 1253-1264.

Brawley, C., and Matunis, E. (2004). Regeneration of male germline stem cells by spermatogonial dedifferentiation in vivo. Science *304*, 1331-1334.

Brownell, I., Guevara, E., Bai, C.B., Loomis, C.A., and Joyner, A.L. (2011). Nerve-derived sonic hedgehog defines a niche for hair follicle stem cells capable of becoming epidermal stem cells. Cell Stem Cell *8*, 552-565.

Cabello, J., Neukomm, L.J., Gunesdogan, U., Burkart, K., Charette, S.J., Lochnit, G., Hengartner, M.O., and Schnabel, R. (2010). The Wnt pathway controls cell death engulfment, spindle orientation, and migration through CED-10/Rac. PLoS Biol *8*, e1000297.

Cheng, H., and Leblond, C.P. (1974). Origin, differentiation and renewal of the four main epithelial cell types in the mouse small intestine. V. Unitarian Theory of the origin of the four epithelial cell types. Am J Anat *141*, 537-561.

Chiang, C., Swan, R.Z., Grachtchouk, M., Bolinger, M., Litingtung, Y., Robertson, E.K., Cooper, M.K., Gaffield, W., Westphal, H., Beachy, P.A.*, et al.* (1999). Essential role for Sonic hedgehog during hair follicle morphogenesis. Dev Biol *205*, 1-9.

Clayton, E., Doupe, D.P., Klein, A.M., Winton, D.J., Simons, B.D., and Jones, P.H. (2007). A single type of progenitor cell maintains normal epidermis. Nature *446*, 185-189.

Clements, W.K., and Traver, D. (2013). Signalling pathways that control vertebrate haematopoietic stem cell specification. Nature reviews Immunology *13*, 336-348.

Clevers, H., Loh, K.M., and Nusse, R. (2014). Stem cell signaling. An integral program for tissue renewal and regeneration: Wnt signaling and stem cell control. Science *346*, 1248012.

Clevers, H., and Nusse, R. (2012). Wnt/beta-catenin signaling and disease. Cell *149*, 1192-1205.

Corrales, J.D., Blaess, S., Mahoney, E.M., and Joyner, A.L. (2006). The level of sonic hedgehog signaling regulates the complexity of cerebellar foliation. Development *133*, 1811-1821.

Cotsarelis, G., Sun, T.T., and Lavker, R.M. (1990). Label-retaining cells reside in the bulge area of pilosebaceous unit: implications for follicular stem cells, hair cycle, and skin carcinogenesis. Cell *61*, 1329-1337.

Dansereau, D.A., and Lasko, P. (2008). The development of germline stem cells in Drosophila. Methods Mol Biol *450*, 3-26.

DasGupta, R., and Fuchs, E. (1999). Multiple roles for activated LEF/TCF transcription complexes during hair follicle development and differentiation. Development *126*, 4557-4568.

Dassule, H.R., Lewis, P., Bei, M., Maas, R., and McMahon, A.P. (2000). Sonic hedgehog regulates growth and morphogenesis of the tooth. Development *127*, 4775-4785.

Deshpande, G., Swanhart, L., Chiang, P., and Schedl, P. (2001). Hedgehog signaling in germ cell migration. Cell *106*, 759-769.

Devenport, D., and Fuchs, E. (2008). Planar polarization in embryonic epidermis orchestrates global asymmetric morphogenesis of hair follicles. Nat Cell Biol *10*, 1257-1268.

Etienne-Manneville, S., and Hall, A. (2003). Cdc42 regulates GSK-3beta and adenomatous polyposis coli to control cell polarity. Nature *421*, 753-756.

Festa, E., Fretz, J., Berry, R., Schmidt, B., Rodeheffer, M., Horowitz, M., and Horsley, V. (2011). Adipocyte lineage cells contribute to the skin stem cell niche to drive hair cycling. Cell *146*, 761-771.

Folgueras, A.R., Guo, X., Pasolli, H.A., Stokes, N., Polak, L., Zheng, D., and Fuchs, E. (2013). Architectural niche organization by LHX2 is linked to hair follicle stem cell function. Cell Stem Cell *13*, 314-327.

Fu, J., and Hsu, W. (2012). Epidermal Wnt Controls Hair Follicle Induction by Orchestrating Dynamic Signaling Crosstalk between the Epidermis and Dermis. Journal of Investigative Dermatology.

Fuchs, E. (2007). Scratching the surface of skin development. Nature *445*, 834-842.

Fukuda, K., Tanigawa, Y., Fujii, G., Yasugi, S., and Hirohashi, S. (1998). cFKBP/SMAP; a novel molecule involved in the regulation of smooth muscle differentiation. Development *125*, 3535-3542.

Fuller, M.T., and Spradling, A.C. (2007). Male and female Drosophila germline stem cells: two versions of immortality. Science *316*, 402-404.

Gao, C., Chen, G., Kuan, S.F., Zhang, D.H., Schlaepfer, D.D., and Hu, J. (2015). FAK/PYK2 promotes the Wnt/beta-catenin pathway and intestinal tumorigenesis by phosphorylating GSK3beta. eLife *4*.

Gat, U., DasGupta, R., Degenstein, L., and Fuchs, E. (1998). De Novo hair follicle morphogenesis and hair tumors in mice expressing a truncated beta-catenin in skin. Cell *95*, 605-614.

Genander, M., Cook, P.J., Ramskold, D., Keyes, B.E., Mertz, A.F., Sandberg, R., and Fuchs, E. (2014). BMP Signaling and Its pSMAD1/5 Target Genes Differentially Regulate Hair Follicle Stem Cell Lineages. Cell Stem Cell.

Glinka, A., Wu, W., Delius, H., Monaghan, A.P., Blumenstock, C., and Niehrs, C. (1998). Dickkopf-1 is a member of a new family of secreted proteins and functions in head induction. Nature *391*, 357-362.

Gomez-Orte, E., Saenz-Narciso, B., Moreno, S., and Cabello, J. (2013). Multiple functions of the noncanonical Wnt pathway. Trends Genet *29*, 545-553.

Greco, V., Chen, T., Rendl, M., Schober, M., Pasolli, H.A., Stokes, N., Dela Cruz-Racelis, J., and Fuchs, E. (2009). A two-step mechanism for stem cell activation during hair regeneration. Cell Stem Cell *4*, 155-169.

Grill, S.W., Gonczy, P., Stelzer, E.H., and Hyman, A.A. (2001). Polarity controls forces governing asymmetric spindle positioning in the Caenorhabditis elegans embryo. Nature *409*, 630-633.

Guo, N., Hawkins, C., and Nathans, J. (2004). Frizzled6 controls hair patterning in mice. Proc Natl Acad Sci U S A *101*, 9277-9281.

Habib, S.J., Chen, B.C., Tsai, F.C., Anastassiadis, K., Meyer, T., Betzig, E., and Nusse, R. (2013). A localized Wnt signal orients asymmetric stem cell division in vitro. Science *339*, 1445-1448.

Hardy, R.W., Tokuyasu, K.T., Lindsley, D.L., and Garavito, M. (1979). The germinal proliferation center in the testis of Drosophila melanogaster. J Ultrastruct Res *69*, 180-190.

Harfe, B.D., Scherz, P.J., Nissim, S., Tian, H., McMahon, A.P., and Tabin, C.J. (2004). Evidence for an expansion-based temporal Shh gradient in specifying vertebrate digit identities. Cell *118*, 517-528.

He, X.C., Zhang, J., Tong, W.G., Tawfik, O., Ross, J., Scoville, D.H., Tian, Q., Zeng, X., He, X., Wiedemann, L.M.*, et al.* (2004). BMP signaling inhibits intestinal stem cell self-renewal through suppression of Wnt-beta-catenin signaling. Nat Genet *36*, 1117-1121.

Heisenberg, C.P., Tada, M., Rauch, G.J., Saude, L., Concha, M.L., Geisler, R., Stemple, D.L., Smith, J.C., and Wilson, S.W. (2000). Silberblick/Wnt11 mediates convergent extension movements during zebrafish gastrulation. Nature *405*, 76-81.

Hertwig, O. (1884). Das Problem der Befruchtung und der Isotropie des Eies, eine Theory der Vererbung. Jenaische Zeitschrift fuer Naturwissenschaft *18*, 21-23.

Hill, T.P., Spater, D., Taketo, M.M., Birchmeier, W., and Hartmann, C. (2005). Canonical Wnt/beta-catenin signaling prevents osteoblasts from differentiating into chondrocytes. Dev Cell *8*, 727-738.

Hill, T.P., Taketo, M.M., Birchmeier, W., and Hartmann, C. (2006). Multiple roles of mesenchymal beta-catenin during murine limb patterning. Development *133*, 1219-1229.

Horsley, V., Aliprantis, A.O., Polak, L., Glimcher, L.H., and Fuchs, E. (2008). NFATc1 Balances Quiescence and Proliferation of Skin Stem Cells. Cell *132*, 299-310.

Hsu, Y.C., Li, L., and Fuchs, E. (2014a). Emerging interactions between skin stem cells and their niches. Nat Med *20*, 847-856.

Hsu, Y.C., Li, L., and Fuchs, E. (2014b). Transit-amplifying cells orchestrate stem cell activity and tissue regeneration. Cell *157*, 935-949.

Hsu, Y.C., Pasolli, H.A., and Fuchs, E. (2011). Dynamics between stem cells, niche, and progeny in the hair follicle. Cell *144*, 92-105.

Huelsken, J., Vogel, R., Erdmann, B., Cotsarelis, G., and Birchmeier, W. (2001). beta-Catenin controls hair follicle morphogenesis and stem cell differentiation in the skin. Cell *105*, 533-545.

Ingham, P.W. (1988). The molecular genetics of embryonic pattern formation in Drosophila. Nature *335*, 25-34.

Ingham, P.W., and McMahon, A.P. (2001). Hedgehog signaling in animal development: paradigms and principles. Genes Dev *15*, 3059-3087.

Iwafuchi-Doi, M., and Zaret, K.S. (2014). Pioneer transcription factors in cell reprogramming. Genes Dev *28*, 2679-2692.

Iwatsuki, K., Liu, H.X., Gronder, A., Singer, M.A., Lane, T.F., Grosschedl, R., Mistretta, C.M., and Margolskee, R.F. (2007). Wnt signaling interacts with Shh to regulate taste papilla development. Proc Natl Acad Sci U S A *104*, 2253-2258.

Jamora, C., DasGupta, R., Kocieniewski, P., and Fuchs, E. (2003). Links between signal transduction, transcription and adhesion in epithelial bud development. Nature *422*, 317-322.

Janda, C.Y., Waghray, D., Levin, A.M., Thomas, C., and Garcia, K.C. (2012). Structural basis of Wnt recognition by Frizzled. Science *337*, 59-64.

Jenkins, A.B., McCaffery, J.M., and Van Doren, M. (2003). Drosophila E-cadherin is essential for proper germ cell-soma interaction during gonad morphogenesis. Development *130*, 4417-4426.

Kadaja, M., Keyes, B.E., Lin, M., Pasolli, H.A., Genander, M., Polak, L., Stokes, N., Zheng, D., and Fuchs, E. (2014). SOX9: a stem cell transcriptional regulator of secreted niche signaling factors. Genes Dev *28*, 328-341.

Karlsson, L., Bondjers, C., and Betsholtz, C. (1999). Roles for PDGF-A and sonic hedgehog in development of mesenchymal components of the hair follicle. Development *126*, 2611-2621.

Karlsson, L., Lindahl, P., Heath, J.K., and Betsholtz, C. (2000). Abnormal gastrointestinal development in PDGF-A and PDGFR-(alpha) deficient mice implicates a novel mesenchymal structure with putative instructive properties in villus morphogenesis. Development *127*, 3457-3466.

Kawase, E., Wong, M.D., Ding, B.C., and Xie, T. (2004). Gbb/Bmp signaling is essential for maintaining germline stem cells and for repressing bam transcription in the Drosophila testis. Development *131*, 1365-1375.

Kiger, A.A., Jones, D.L., Schulz, C., Rogers, M.B., and Fuller, M.T. (2001). Stem cell self-renewal specified by JAK-STAT activation in response to a support cell cue. Science *294*, 2542-2545.

Kim, B.M., Mao, J., Taketo, M.M., and Shivdasani, R.A. (2007). Phases of canonical Wnt signaling during the development of mouse intestinal epithelium. Gastroenterology *133*, 529-538.

Kim, T.H., Escudero, S., and Shivdasani, R.A. (2012). Intact function of Lgr5 receptor-expressing intestinal stem cells in the absence of Paneth cells. Proc Natl Acad Sci U S A *109*, 3932-3937.

Knoblich, J.A. (2008). Mechanisms of asymmetric stem cell division. Cell *132*, 583-597.

Kodama, A., Karakesisoglou, I., Wong, E., Vaezi, A., and Fuchs, E. (2003). ACF7: an essential integrator of microtubule dynamics. Cell *115*, 343-354.

Koebernick, K., and Pieler, T. (2002). Gli-type zinc finger proteins as bipotential transducers of Hedgehog signaling. Differentiation *70*, 69-76.

Konno, D., Shioi, G., Shitamukai, A., Mori, A., Kiyonari, H., Miyata, T., and Matsuzaki, F. (2008). Neuroepithelial progenitors undergo LGN-dependent planar divisions to maintain self-renewability during mammalian neurogenesis. Nat Cell Biol *10*, 93-101.

Kuraguchi, M., Wang, X.P., Bronson, R.T., Rothenberg, R., Ohene-Baah, N.Y., Lund, J.J., Kucherlapati, M., Maas, R.L., and Kucherlapati, R. (2006). Adenomatous polyposis coli (APC) is required for normal development of skin and thymus. PLoS Genet *2*, e146.

Kurahashi, M., Niwa, Y., Cheng, J., Ohsaki, Y., Fujita, A., Goto, H., Fujimoto, T., and Torihashi, S. (2008). Platelet-derived growth factor signals play critical roles

in differentiation of longitudinal smooth muscle cells in mouse embryonic gut. Neurogastroenterol Motil *20*, 521-531.

Larsimont, J.C., Youssef, K.K., Sanchez-Danes, A., Sukumaran, V., Defrance, M., Delatte, B., Liagre, M., Baatsen, P., Marine, J.C., Lippens, S.*, et al.* (2015). Sox9 Controls Self-Renewal of Oncogene Targeted Cells and Links Tumor Initiation and Invasion. Cell Stem Cell *17*, 60-73.

Le Bras, S., and Van Doren, M. (2006). Development of the male germline stem cell niche in Drosophila. Dev Biol *294*, 92-103.

Lechler, T., and Fuchs, E. (2005). Asymmetric cell divisions promote stratification and differentiation of mammalian skin. Nature *437*, 275-280.

Lee, J.J., von Kessler, D.P., Parks, S., and Beachy, P.A. (1992). Secretion and localized transcription suggest a role in positional signaling for products of the segmentation gene hedgehog. Cell *71*, 33-50.

Levy, V., Lindon, C., Harfe, B.D., and Morgan, B.A. (2005). Distinct stem cell populations regenerate the follicle and interfollicular epidermis. Dev Cell *9*, 855-861.

Li, V.S., Ng, S.S., Boersema, P.J., Low, T.Y., Karthaus, W.R., Gerlach, J.P., Mohammed, S., Heck, A.J., Maurice, M.M., Mahmoudi, T.*, et al.* (2012). Wnt signaling through inhibition of beta-catenin degradation in an intact Axin1 complex. Cell *149*, 1245-1256.

Lichti, U., Weinberg, W.C., Goodman, L., Ledbetter, S., Dooley, T., Morgan, D., and Yuspa, S.H. (1993). In vivo regulation of murine hair growth: insights from grafting defined cell populations onto nude mice. J Invest Dermatol *101*, 124S-129S.

Lien, W.H., Polak, L., Lin, M., Lay, K., Zheng, D., and Fuchs, E. (2014). In vivo transcriptional governance of hair follicle stem cells by canonical Wnt regulators. Nat Cell Biol *16*, 179-190.

Litingtung, Y., Lei, L., Westphal, H., and Chiang, C. (1998). Sonic hedgehog is essential to foregut development. Nat Genet *20*, 58-61.

Long, F., Zhang, X.M., Karp, S., Yang, Y., and McMahon, A.P. (2001). Genetic manipulation of hedgehog signaling in the endochondral skeleton reveals a direct role in the regulation of chondrocyte proliferation. Development *128*, 5099-5108.

Lustig, B., Jerchow, B., Sachs, M., Weiler, S., Pietsch, T., Karsten, U., van de Wetering, M., Clevers, H., Schlag, P.M., Birchmeier, W.*, et al.* (2002a). Negative

feedback loop of Wnt signaling through upregulation of conductin/Axin2 in colorectal and liver tumors. Molecular and Cellular Biology *22*, 1184-1193.

Lustig, B., Jerchow, B., Sachs, M., Weiler, S., Pietsch, T., Karsten, U., van de Wetering, M., Clevers, H., Schlag, P.M., Birchmeier, W.*, et al.* (2002b). Negative feedback loop of Wnt signaling through upregulation of conductin/axin2 in colorectal and liver tumors. Mol Cell Biol *22*, 1184-1193.

Mao, X., Fujiwara, Y., and Orkin, S.H. (1999). Improved reporter strain for monitoring Cre recombinase-mediated DNA excisions in mice. Proc Natl Acad Sci U S A *96*, 5037-5042.

Maretto, S., Cordenonsi, M., Dupont, S., Braghetta, P., Broccoli, V., Hassan, A.B., Volpin, D., Bressan, G.M., and Piccolo, S. (2003). Mapping Wnt/beta-catenin signaling during mouse development and in colorectal tumors. Proc Natl Acad Sci U S A *100*, 3299-3304.

Mecklenburg, L., Tobin, D.J., Muller-Rover, S., Handjiski, B., Wendt, G., Peters, E.M., Pohl, S., Moll, I., and Paus, R. (2000). Active hair growth (anagen) is associated with angiogenesis. J Invest Dermatol *114*, 909-916.

Mendoza-Topaz, C., Mieszczanek, J., and Bienz, M. (2011). The Adenomatous polyposis coli tumour suppressor is essential for Axin complex assembly and function and opposes Axin's interaction with Dishevelled. Open Biol *1*, 110013.

Minc, N., Burgess, D., and Chang, F. (2011). Influence of cell geometry on division-plane positioning. Cell *144*, 414-426.

Molenaar, M., van de Wetering, M., Oosterwegel, M., Peterson-Maduro, J., Godsave, S., Korinek, V., Roose, J., Destree, O., and Clevers, H. (1996). XTcf-3 transcription factor mediates beta-catenin-induced axis formation in Xenopus embryos. Cell *86*, 391-399.

Moon, R.T., Campbell, R.M., Christian, J.L., McGrew, L.L., Shih, J., and Fraser, S. (1993). Xwnt-5A: a maternal Wnt that affects morphogenetic movements after overexpression in embryos of Xenopus laevis. Development *119*, 97-111.

Morin, X., Jaouen, F., and Durbec, P. (2007). Control of planar divisions by the G-protein regulator LGN maintains progenitors in the chick neuroepithelium. Nat Neurosci *10*, 1440-1448.

Morrison, S.J., and Spradling, A.C. (2008). Stem cells and niches: mechanisms that promote stem cell maintenance throughout life. Cell *132*, 598-611.

Muzumdar, M.D., Tasic, B., Miyamichi, K., Li, L., and Luo, L. (2007). A global double-fluorescent Cre reporter mouse. Genesis *45*, 593-605.

Nguyen, H., Rendl, M., and Fuchs, E. (2006). Tcf3 governs stem cell features and represses cell fate determination in skin. Cell *127*, 171-183.

Noramly, S., Freeman, A., and Morgan, B.A. (1999). beta-catenin signaling can initiate feather bud development. Development *126*, 3509-3521.

Nowak, J.A., Polak, L., Pasolli, H.A., and Fuchs, E. (2008). Hair follicle stem cells are specified and function in early skin morphogenesis. Cell Stem Cell *3*, 33-43.

Oshimori, N., and Fuchs, E. (2012). Paracrine TGF-beta signaling counterbalances BMP-mediated repression in hair follicle stem cell activation. Cell Stem Cell *10*, 63-75.

Pardo-Saganta, A., Tata, P.R., Law, B.M., Saez, B., Chow, R., Prabhu, M., Gridley, T., and Rajagopal, J. (2015). Parent stem cells can serve as niches for their daughter cells. Nature *523*, 597-601.

Parsons, J.T. (2003). Focal adhesion kinase: the first ten years. J Cell Sci *116*, 1409-1416.

Pei, Y., Brun, S.N., Markant, S.L., Lento, W., Gibson, P., Taketo, M.M., Giovannini, M., Gilbertson, R.J., and Wechsler-Reya, R.J. (2012). WNT signaling increases proliferation and impairs differentiation of stem cells in the developing cerebellum. Development *139*, 1724-1733.

Perinthottathil, S., and Kim, C. (2011). Bam and Bgcn in Drosophila germline stem cell differentiation. Vitam Horm *87*, 399-416.

Peters, E.M., Arck, P.C., and Paus, R. (2006). Hair growth inhibition by psychoemotional stress: a mouse model for neural mechanisms in hair growth control. Exp Dermatol *15*, 1-13.

Peters, E.M., Botchkarev, V.A., Muller-Rover, S., Moll, I., Rice, F.L., and Paus, R. (2002). Developmental timing of hair follicle and dorsal skin innervation in mice. J Comp Neurol *448*, 28-52.

Pispa, J., and Thesleff, I. (2003). Mechanisms of ectodermal organogenesis. Developmental Biology *262*, 195-205.

Plikus, M.V., Mayer, J.A., de la Cruz, D., Baker, R.E., Maini, P.K., Maxson, R., and Chuong, C.M. (2008). Cyclic dermal BMP signalling regulates stem cell activation during hair regeneration. Nature *451*, 340-344.

Qian, D., Jones, C., Rzadzinska, A., Mark, S., Zhang, X., Steel, K.P., Dai, X., and Chen, P. (2007). Wnt5a functions in planar cell polarity regulation in mice. Dev Biol *306*, 121-133.

Raspopovic, J., Marcon, L., Russo, L., and Sharpe, J. (2014). Modeling digits. Digit patterning is controlled by a Bmp-Sox9-Wnt Turing network modulated by morphogen gradients. Science *345*, 566-570.

Reddy, S., Andl, T., Bagasra, A., Lu, M.M., Epstein, D.J., Morrisey, E.E., and Millar, S.E. (2001). Characterization of Wnt gene expression in developing and postnatal hair follicles and identification of Wnt5a as a target of Sonic hedgehog in hair follicle morphogenesis. Mech Dev *107*, 69-82.

Renault, A.D., Sigal, Y.J., Morris, A.J., and Lehmann, R. (2004). Soma-germ line competition for lipid phosphate uptake regulates germ cell migration and survival. Science *305*, 1963-1966.

Rendl, M., Lewis, L., and Fuchs, E. (2005). Molecular dissection of mesenchymal-epithelial interactions in the hair follicle. PLoS Biol *3*, e331.

Rendl, M., Polak, L., and Fuchs, E. (2008). BMP signaling in dermal papilla cells is required for their hair follicle-inductive properties. Genes Dev *22*, 543-557.

Reya, T., and Clevers, H. (2005). Wnt signalling in stem cells and cancer. Nature *434*, 843-850.

Reya, T., Duncan, A.W., Ailles, L., Domen, J., Scherer, D.C., Willert, K., Hintz, L., Nusse, R., and Weissman, I.L. (2003). A role for Wnt signalling in self-renewal of haematopoietic stem cells. Nature *423*, 409-414.

Rhee, H., Polak, L., and Fuchs, E. (2006). Lhx2 maintains stem cell character in hair follicles. Science *312*, 1946-1949.

Rompolas, P., Deschene, E.R., Zito, G., Gonzalez, D.G., Saotome, I., Haberman, A.M., and Greco, V. (2012). Live imaging of stem cell and progeny behaviour in physiological hair-follicle regeneration. Nature *487*, 496-499.

Rompolas, P., Mesa, K.R., and Greco, V. (2013). Spatial organization within a niche as a determinant of stem-cell fate. Nature *502*, 513-518.

Rosenquist, T.A., and Martin, G.R. (1996). Fibroblast growth factor signalling in the hair growth cycle: expression of the fibroblast growth factor receptor and ligand genes in the murine hair follicle. Dev Dyn *205*, 379-386.

Sakaue-Sawano, A., Kurokawa, H., Morimura, T., Hanyu, A., Hama, H., Osawa, H., Kashiwagi, S., Fukami, K., Miyata, T., and Miyoshi, H. (2008). Visualizing Spatiotemporal Dynamics of Multicellular Cell-Cycle Progression. Cell *132*, 487-498.

Sansom, O.J., Reed, K.R., Hayes, A.J., Ireland, H., Brinkmann, H., Newton, I.P., Batlle, E., Simon-Assmann, P., Clevers, H., Nathke, I.S.*, et al.* (2004). Loss of Apc in vivo immediately perturbs Wnt signaling, differentiation, and migration. Genes Dev *18*, 1385-1390.

Sato, T., van Es, J.H., Snippert, H.J., Stange, D.E., Vries, R.G., van den Born, M., Barker, N., Shroyer, N.F., van de Wetering, M., and Clevers, H. (2011). Paneth cells constitute the niche for Lgr5 stem cells in intestinal crypts. Nature *469*, 415-418.

Scadden, D.T. (2014). Nice neighborhood: emerging concepts of the stem cell niche. Cell *157*, 41-50.

Schmierer, B., and Hill, C.S. (2007). TGFβ–SMAD signal transduction: molecular specificity and functional flexibility. Nature Reviews Molecular Cell Biology *8*, 970-982.

Schofield, R. (1978). The relationship between the spleen colony-forming cell and the haemopoietic stem cell. Blood cells *4*, 7-25.

Schulz, C., Kiger, A.A., Tazuke, S.I., Yamashita, Y.M., Pantalena-Filho, L.C., Jones, D.L., Wood, C.G., and Fuller, M.T. (2004). A misexpression screen reveals effects of bag-of-marbles and TGF beta class signaling on the Drosophila male germ-line stem cell lineage. Genetics *167*, 707-723.

Sengel, P. (1976). Morphogenesis of skin (Cambridge, Eng. ; New York: Cambridge University Press).

Sheng, X.R., Posenau, T., Gumulak-Smith, J.J., Matunis, E., Van Doren, M., and Wawersik, M. (2009). Jak-STAT regulation of male germline stem cell establishment during Drosophila embryogenesis. Dev Biol *334*, 335-344.

Shimomura, Y., Agalliu, D., Vonica, A., Luria, V., Wajid, M., Baumer, A., Belli, S., Petukhova, L., Schinzel, A., Brivanlou, A.H.*, et al.* (2010). APCDD1 is a novel Wnt inhibitor mutated in hereditary hypotrichosis simplex. Nature *464*, 1043-1047.

Shin, K., Lee, J., Guo, N., Kim, J., Lim, A., Qu, L., Mysorekar, I.U., and Beachy, P.A. (2011). Hedgehog/Wnt feedback supports regenerative proliferation of epithelial stem cells in bladder. Nature *472*, 110-114.

Shyer, A.E., Huycke, T.R., Lee, C., Mahadevan, L., and Tabin, C.J. (2015). Bending gradients: how the intestinal stem cell gets its home. Cell *161*, 569-580.

Shyer, A.E., Tallinen, T., Nerurkar, N.L., Wei, Z., Gil, E.S., Kaplan, D.L., Tabin, C.J., and Mahadevan, L. (2013). Villification: how the gut gets its villi. Science *342*, 212-218.

Sick, S., Reinker, S., Timmer, J., and Schlake, T. (2006). WNT and DKK determine hair follicle spacing through a reaction-diffusion mechanism. Science *314*, 1447-1450.

Siller, K.H., and Doe, C.Q. (2009). Spindle orientation during asymmetric cell division. Nat Cell Biol *11*, 365-374.

Soeda, T., Deng, J.M., de Crombrugghe, B., Behringer, R.R., Nakamura, T., and Akiyama, H. (2010). Sox9-expressing precursors are the cellular origin of the cruciate ligament of the knee joint and the limb tendons. Genesis.

Song, X., Wong, M.D., Kawase, E., Xi, R., Ding, B.C., McCarthy, J.J., and Xie, T. (2004). Bmp signals from niche cells directly repress transcription of a differentiation-promoting gene, bag of marbles, in germline stem cells in the Drosophila ovary. Development *131*, 1353-1364.

Song, X., Zhu, C.H., Doan, C., and Xie, T. (2002). Germline stem cells anchored by adherens junctions in the Drosophila ovary niches. Science *296*, 1855-1857.

Spradling, A., Drummond-Barbosa, D., and Kai, T. (2001). Stem cells find their niche. Nature *414*, 98-104.

Spradling, A.C., de Cuevas, M., Drummond-Barbosa, D., Keyes, L., Lilly, M., Pepling, M., and Xie, T. (1997). The Drosophila germarium: stem cells, germ line cysts, and oocytes. Cold Spring Harb Symp Quant Biol *62*, 25-34.

Srinivas, S., Watanabe, T., Lin, C.S., William, C.M., Tanabe, Y., Jessell, T.M., and Costantini, F. (2001). Cre reporter strains produced by targeted insertion of EYFP and ECFP into the ROSA26 locus. BMC Dev Biol *1*, 4.

St-Jacques, B., Dassule, H.R., Karavanova, I., Botchkarev, V.A., Li, J., Danielian, P.S., McMahon, J.A., Lewis, P.M., Paus, R., and McMahon, A.P. (1998). Sonic hedgehog signaling is essential for hair development. Curr Biol *8*, 1058-1068.

Sugimura, R., He, X.C., Venkatraman, A., Arai, F., Box, A., Semerad, C., Haug, J.S., Peng, L., Zhong, X.B., Suda, T.*, et al.* (2012). Noncanonical Wnt signaling maintains hematopoietic stem cells in the niche. Cell *150*, 351-365.

Sugioka, K., Mizumoto, K., and Sawa, H. (2011). Wnt regulates spindle asymmetry to generate asymmetric nuclear beta-catenin in C. elegans. Cell *146*, 942-954.

Tabata, T., Eaton, S., and Kornberg, T.B. (1992). The Drosophila hedgehog gene is expressed specifically in posterior compartment cells and is a target of engrailed regulation. Genes Dev *6*, 2635-2645.

Takahashi, K., and Yamanaka, S. (2006). Induction of pluripotent stem cells from mouse embryonic and adult fibroblast cultures by defined factors. Cell *126*, 663-676.

Tata, P.R., Mou, H., Pardo-Saganta, A., Zhao, R., Prabhu, M., Law, B.M., Vinarsky, V., Cho, J.L., Breton, S., Sahay, A.*, et al.* (2013). Dedifferentiation of committed epithelial cells into stem cells in vivo. Nature *503*, 218-223.

Taylor, G., Lehrer, M.S., Jensen, P.J., Sun, T.T., and Lavker, R.M. (2000). Involvement of follicular stem cells in forming not only the follicle but also the epidermis. Cell *102*, 451-461.

Thery, M., Racine, V., Pepin, A., Piel, M., Chen, Y., Sibarita, J.B., and Bornens, M. (2005). The extracellular matrix guides the orientation of the cell division axis. Nat Cell Biol *7*, 947-953.

Thompson, T.B., Lerch, T.F., Cook, R.W., Woodruff, T.K., and Jardetzky, T.S. (2005). The structure of the follistatin:activin complex reveals antagonism of both type I and type II receptor binding. Dev Cell *9*, 535-543.

Topol, L., Chen, W., Song, H., Day, T.F., and Yang, Y. (2009). Sox9 inhibits Wnt signaling by promoting beta-catenin phosphorylation in the nucleus. J Biol Chem *284*, 3323-3333.

Tulina, N., and Matunis, E. (2001). Control of stem cell self-renewal in Drosophila spermatogenesis by JAK-STAT signaling. Science *294*, 2546-2549.

Tumbar, T., Guasch, G., Greco, V., Blanpain, C., Lowry, W.E., Rendl, M., and Fuchs, E. (2004). Defining the epithelial stem cell niche in skin. Science *303*, 359-363.

Van Doren, M., Broihier, H.T., Moore, L.A., and Lehmann, R. (1998). HMG-CoA reductase guides migrating primordial germ cells. Nature *396*, 466-469.

Van Doren, M., Mathews, W.R., Samuels, M., Moore, L.A., Broihier, H.T., and Lehmann, R. (2003). fear of intimacy encodes a novel transmembrane protein required for gonad morphogenesis in Drosophila. Development *130*, 2355-2364.

van Es, J.H., Sato, T., van de Wetering, M., Lyubimova, A., Nee, A.N., Gregorieff, A., Sasaki, N., Zeinstra, L., van den Born, M., Korving, J.*, et al.* (2012). Dll1+ secretory progenitor cells revert to stem cells upon crypt damage. Nat Cell Biol *14*, 1099-1104.

van Genderen, C., Okamura, R.M., Farinas, I., Quo, R.G., Parslow, T.G., Bruhn, L., and Grosschedl, R. (1994). Development of several organs that require inductive epithelial-mesenchymal interactions is impaired in LEF-1-deficient mice. Genes Dev *8*, 2691-2703.

Vidal, V.P., Chaboissier, M.C., Lutzkendorf, S., Cotsarelis, G., Mill, P., Hui, C.C., Ortonne, N., Ortonne, J.P., and Schedl, A. (2005). Sox9 is essential for outer root sheath differentiation and the formation of the hair stem cell compartment. Curr Biol *15*, 1340-1351.

Vinson, C.R., Conover, S., and Adler, P.N. (1989). A Drosophila tissue polarity locus encodes a protein containing seven potential transmembrane domains. Nature *338*, 263-264.

Walton, K.D., Whidden, M., Kolterud, A., S, K.S., Czerwinski, M.J., Kushwaha, J., Parmar, N., Chandhrasekhar, D., Freddo, A.M., Schnell, S.*, et al.* (2016). Villification in the mouse: Bmp signals control intestinal villus patterning. Development *143*, 427-436.

Ward, E.J., Shcherbata, H.R., Reynolds, S.H., Fischer, K.A., Hatfield, S.D., and Ruohola-Baker, H. (2006). Stem cells signal to the niche through the Notch pathway in the Drosophila ovary. Curr Biol *16*, 2352-2358.

Weinberg, W.C., Goodman, L.V., George, C., Morgan, D.L., Ledbetter, S., Yuspa, S.H., and Lichti, U. (1993). Reconstitution of hair follicle development in vivo: determination of follicle formation, hair growth, and hair quality by dermal cells. J Invest Dermatol *100*, 229-236.

Wessells, N.K. (1965). Morphology and proliferation during early feather development. Dev Biol *12*, 131-153.

Williams, S.E., Beronja, S., Pasolli, H.A., and Fuchs, E. (2011). Asymmetric cell divisions promote Notch-dependent epidermal differentiation. Nature *470*, 353-358.

Williams, S.E., Ratliff, L.A., Postiglione, M.P., Knoblich, J.A., and Fuchs, E. (2014). Par3-mInsc and Galphai3 cooperate to promote oriented epidermal cell divisions through LGN. Nat Cell Biol *16*, 758-769.

Woo, W.M., Zhen, H.H., and Oro, A.E. (2012). Shh maintains dermal papilla identity and hair morphogenesis via a Noggin-Shh regulatory loop. Genes Dev *26*, 1235-1246.

Wu, D., and Pan, W. (2010). GSK3: a multifaceted kinase in Wnt signaling. Trends Biochem Sci *35*, 161-168.

Xie, T., and Spradling, A.C. (2000). A niche maintaining germ line stem cells in the Drosophila ovary. Science *290*, 328-330.

Xu, Z., Wang, W., Jiang, K., Yu, Z., Huang, H., Wang, F., Zhou, B., and Chen, T. (2015). Embryonic attenuated Wnt/beta-catenin signaling defines niche location and long-term stem cell fate in hair follicle. eLife *4*.

Yamashita, Y.M., Jones, D.L., and Fuller, M.T. (2003). Orientation of asymmetric stem cell division by the APC tumor suppressor and centrosome. Science *301*, 1547-1550.

Yang, S.H., Andl, T., Grachtchouk, V., Wang, A., Liu, J., Syu, L.J., Ferris, J., Wang, T.S., Glick, A.B., Millar, S.E.*, et al.* (2008). Pathological responses to oncogenic Hedgehog signaling in skin are dependent on canonical Wnt/beta3-catenin signaling. Nat Genet *40*, 1130-1135.

Yano, K., Brown, L.F., and Detmar, M. (2001). Control of hair growth and follicle size by VEGF-mediated angiogenesis. J Clin Invest *107*, 409-417.

Youssef, K.K., Lapouge, G., Bouvrée, K., Rorive, S., Brohée, S., Appelstein, O., Larsimont, J.-C., Sukumaran, V., Van de Sande, B., Pucci, D.*, et al.* (2012). Adult interfollicular tumour-initiating cells are reprogrammed into an embryonic hair follicle progenitor-like fate during basal cell carcinoma initiation. Nature Cell Biology.

Zeng, X., Goetz, J.A., Suber, L.M., Scott, W.J., Jr., Schreiner, C.M., and Robbins, D.J. (2001). A freely diffusible form of Sonic hedgehog mediates long-range signalling. Nature *411*, 716-720.

Zhang, N., Zhang, J., Purcell, K.J., Cheng, Y., and Howard, K. (1997). The Drosophila protein Wunen repels migrating germ cells. Nature *385*, 64-67.

Zhang, Y., Tomann, P., Andl, T., Gallant, N.M., Huelsken, J., Jerchow, B., Birchmeier, W., Paus, R., Piccolo, S., Mikkola, M.L.*, et al.* (2009). Reciprocal requirements for EDA/EDAR/NF-kappaB and Wnt/beta-catenin signaling pathways in hair follicle induction. Dev Cell *17*, 49-61.

Zhou, P., Byrne, C., Jacobs, J., and Fuchs, E. (1995). Lymphoid enhancer factor 1 directs hair follicle patterning and epithelial cell fate. Genes Dev *9*, 700-713.

Zhu, C.H., and Xie, T. (2003). Clonal expansion of ovarian germline stem cells during niche formation in Drosophila. Development *130*, 2579-2588.